Laser Medicine and Biomedical Imaging

Academic and Research Staff
Professor James G. Fujimoto

Visiting Scientists and Research Affiliates
Dr. Yu Chen, Mariana Carvalho, Dr. Robert Huber, Dr. Norihiko Nishizawa (Nagoya University, Japan), Adelina L. Paunescu (New England Eye Center), Dr. Alphan Sennaroglu (Koc University, Turkey), Dr. Kenji Taira, Dr. Maciej Wojtkowski, Dr. Rebecca Younkin

Graduate Students
Desmond C. Adler, Aaron D. Aguirre, Paul R. Herz, Pei-Lin Hsiung, Tony H. Ko, Andrew M. Kowalevicz, Vikas Sharma, Vivek J. Srinivasan, Aurea Zare

Technical and Support Staff
Dorothy A. Fleischer, Donna L. Gale

Research Areas and Projects

1. Optical Coherence Tomography (OCT)

2. OCT Technology

2.1 Ultrahigh Resolution OCT imaging
- 2.1.1 Broadband Superluminescent Diode for Ultrahigh Resolution Optical Coherence Tomography
- 2.1.2 All-Fiber Continuous-Wave (CW) Raman Continuum Light Source for High Resolution OCT
- 2.1.3 Real-Time High Resolution OCT using All-Fiber Femtosecond Fiber Laser Continuum at 1.5 μm
- 2.1.4 Compact Cr^{4+}:Forsterite Laser for High Resolution Endoscopic OCT Imaging

2.2 Ultrahigh Resolution High Speed Spectral Domain OCT for Ophthalmology
2.3 Digital Signal Processing Techniques for Optical Coherence Tomography
2.4 OCT Delivery Devices
- 2.4.1 Micromotor Catheter Probe for Endoscopic Imaging
- 2.4.2 MEMS Scanner for Endoscopic OCT

3. Optical Coherence Microscopy Development

4. Optical Biopsy using OCT

4.1 Ultrahigh Resolution OCT in Ophthalmology
4.2 Ultrahigh Resolution OCT Imaging in the Pathology Laboratory
4.3 Endoscopic Imaging of Barrett's Esophagus and Gastrointestinal Cancer

1. Optical Coherence Tomography (OCT)

Optical coherence tomography (OCT) is an emerging diagnostic technology, developed by our research group and collaborators in 1991 [1], and it has been investigated for applications in several medical fields [2]. OCT enables the visualization of tissue microstructure *in situ* and in real time with resolutions in the 1-10 μm range, and previous studies have demonstrated that changes in tissue architectural morphology associated with neoplasia can be identified [3-6]. Clinical OCT systems often use superluminescent diodes (SLDs) that enable imaging with 10-15 μm axial resolution. These resolutions are typically insufficient for identifying neoplastic changes for cancer detection or tissue morphological and structural features for the visualization of other pathologies. Advances in solid-state lasers and nonlinear fiber technology have enabled the development of ultrahigh resolution and spectroscopic OCT techniques that promise to improve tissue differentiation and image contrast. The recent development of spectral domain OCT techniques enables high speed *in vivo* imaging of biological tissues, which has strong potential for imaging large tissue volumes in three dimensions for clinical diagnosis.

References

1. D. Huang, E.A. Swanson, C.P. Lin, J.S. Schuman, W.G. Stinson, W. Chang, M.R. Hee, T. Flotte, K. Gregory, C.A. Puliafito, and J.G. Fujimoto, "Optical coherence tomography," *Science* 254(5035): 1178-81 (1991).
2. J.G. Fujimoto, "Optical coherence tomography for ultrahigh resolution in vivo imaging," *Nat Biotechnol* 21(11): 1361-7 (2003).
3. J.G. Fujimoto, M.E. Brezinski, G.J. Tearney, S.A. Boppart, B. Bouma, M.R. Hee, J.F. Southern, and E.A. Swanson, "Optical biopsy and imaging using optical coherence tomography," *Nat Med* 1(9): 970-2 (1995).
4. M. Brezinski, G. Tearney, B. Bouma, J. Izatt, M. Hee, E. Swanson, J. Southern, and J. Fujimoto, "Optical coherence tomography for optical biopsy: properties and demonstration of vascular pathology," *Circulation* 93: 1206-13 (1996).
5. J.G. Fujimoto, C. Pitris, S.A. Boppart, and M.E. Brezinski, "Optical coherence tomography: an emerging technology for biomedical imaging and optical biopsy," *Neoplasia* 2(1-2): 9-25 (2000).
6. W. Drexler, U. Morgner, R.K. Ghanta, F.X. Kaertner, J.S. Schuman, and J.G. Fujimoto, "Ultrahigh resolution ophthalmic optical coherence tomography," *Nat Med* 7: 502-507 (2001).

2. OCT Technology

2.1 Ultrahigh Resolution OCT imaging

The longitudinal resolution in OCT images is inversely proportional to the optical bandwidth and proportional to the square of the center wavelength of the light source. Enhancing the resolution of OCT images continues to be a very active field of research [1,2]. Ultrahigh resolution OCT requires extremely broad bandwidths because of the $\lambda^2/\Delta\lambda$ dependence on longitudinal resolution. This is particularly the case for the spectral region between 1.0 μm and 1.5 μm. This spectral region is of great interest for OCT research because of the high penetration depth in biological tissue and the possibility to perform spectroscopic OCT imaging of functional parameters such as water content and tissue oxygenation [3]. Previously, we demonstrated OCT imaging with resolutions of 1 μm at 800 nm and 5.1 μm at 1300 nm in biological tissue by using solid-state mode-locked lasers as well as nonlinear fiber sources [4-6]. We recently investigated compact, portable light sources for ultrahigh resolution OCT imaging at wavelengths of 890 nm, 1300 nm, and 1500 nm. The portable sources will enable more widespread ultrahigh resolution and spectroscopic OCT imaging to be performed in clinical settings.

References

1. J.G. Fujimoto, "Optical coherence tomography for ultrahigh resolution in vivo imaging," *Nat. Biotechnol.* 21(11): 1361-7 (2003).
2. W. Drexler, "Ultrahigh resolution optical coherence tomography," *Journal of Biomedical Optics* 9(1): 47-74 (2004).
3. U. Morgner, W. Drexler, F.X. Kartner, X.D. Li, C. Pitris, E.P. Ippen, and J.G. Fujimoto, "Spectroscopic optical coherence tomography," *Optics Letters* 25(2): 111-13 (2000).
4. B. Bouma, G.J. Tearney, S.A. Boppart, M.R. Hee, M.E. Brezinski, and J.G. Fujimoto, "High-resolution optical coherence tomographic imaging using a mode-locked Ti:Al_2O_3 laser source," *Optics Letters* 20(13): 1486-1488 (1995).
5. W. Drexler, U. Morgner, F.X. Kartner, C. Pitris, S.A. Boppart, X.D. Li, E.P. Ippen, and J.G. Fujimoto, "In vivo ultrahigh-resolution optical coherence tomography," *Optics Letters* 24(17): 1221-3 (1999).
6. I. Hartl, X.D. Li, C. Chudoba, R.K. Ghanta, T.H. Ko, J.G. Fujimoto, J.K. Ranka, and R.S. Windeler, "Ultrahigh-resolution optical coherence tomography using continuum generation in an air-silica microstructure optical fiber," *Optics Letters* 26(9): 608-610 (2001).

2.1.1 Broadband Superluminescent Diode for Ultrahigh Resolution Optical Coherence Tomography

Sponsors
National Institutes of Health – R01-CA75289-06, R01-EY11289-18
National Science Foundation – ECS-01-19452, BES-0119494
Air Force Office of Scientific Research – F49620-01-1-0186, F49620-01-01-0084
The Whitaker Foundation

Project Staff
Tony H. Ko, Desmond C. Adler, Dr. Maciej Wojtkowski, Professor James G. Fujimoto, Vladimir Shidlovski (Superlum Diodes Ltd.), Sergei Yakubovich (Superlum Diodes Ltd.), Dr. Jay S. Duker (New England Eye Center), Dr. Joel Schuman (University of Pittsburg Medical Center)

Standard resolution optical coherence tomography (OCT) with 10-15 μm axial resolution has been applied extensively to image tissue microstructure in several medical specialties, ranging from ophthalmology to gastroenterology. Recently, ultrahigh resolution optical coherence tomography (UHR-OCT) with axial resolution of 1-3 μm was demonstrated by using either femtosecond solid-state lasers or femtosecond lasers in combination with nonlinear optical fibers [1-5]. UHR-OCT imaging with 3 μm axial resolution has also been demonstrated in ophthalmology, thus enabling an improved visualization of intraretinal architecture when compared to standard resolution OCT [6,7]. However, femtosecond lasers are expensive and can be difficult to operate, thus presenting a major challenge to the widespread adoption of UHR-OCT imaging technology in the clinical setting. Superluminescent diode (SLD) sources are compact, robust, easy to operate, and much less expensive than femtosecond solid-state lasers. Until recently, the bandwidths of commercial SLD sources were relatively limited. Consequently, OCT axial resolutions were limited to ~10 μm when SLD sources were used. The development of a broadband SLD light source for ultrahigh resolution OCT will greatly enhance the clinical utility of UHR-OCT imaging.

Broadband superluminescent sources for OCT imaging were previously investigated, but *in vivo* ultrahigh resolution OCT imaging has not been possible. Broadband superluminescence generated from a Ti:Sapphire crystal pumped with high-power lasers can provide ~2 μm OCT axial resolution [8,9]. However, the power that can be coupled into a single mode fiber (in the μW range) is too low for high-speed *in vivo* imaging [8,9]. Ti:Sapphire waveguides can be used to improve the coupling efficiency of the superluminescence into a single-mode fiber, but the power is still not sufficient for *in vivo* imaging [10-12]. Superluminescent diodes (SLD) are high-gain semiconductor optical amplifiers that generate amplified spontaneous emission. Early superluminescent diodes had a structure similar to diode lasers, except that antireflection coatings were applied to the diode facets to reduce feedback and inhibit lasing. However, spectral modulation of the diode output and the lasing from parasitic feedback limited the output power of these designs to a few milliwatts. The use of angled waveguide structures further reduced feedback that would enable higher power operation without spectral modulation or lasing [13-15]. The use of quantum well structures enabled broad gain bandwidths to be achieved at lower current densities than what had been possible with “bulk” heterostructure devices [13].

To further increase the optical output bandwidth while maintaining high output power, wavelength division multiplexing (WDM) of spectrally shifted SLDs can be performed. Early work demonstrated improvement in axial resolution from 10 μm to 6 μm by using two wavelength-division-multiplexed SLDs [16]. In another study, using a dual-beam OCT approach, two spectrally displaced SLD beams were combined to achieve an effective bandwidth of 50 nm, which corresponds to an OCT axial resolution of 6-7 μm [17]. However the output powers of these sources were low and, thus, it limited signal-to-noise performance for *in vivo* OCT imaging applications. Furthermore, the total optical bandwidth was not sufficient enough to achieve ultrahigh axial resolutions of 2-3 μm, which is possible with femtosecond solid-state laser light sources.

In this project, we demonstrate *in vivo* ultrahigh resolution OCT imaging by using a new broadband superluminescent diode light source. The broadband source consists of two independent SLD diodes, where the two optical outputs are multiplexed in order to achieve a total bandwidth of 155 nm and >4 mW

total CW output power. An axial resolution of ~2.3 μm was obtained in scattering tissue and an axial resolution of ~3.2 μm was obtained in the retina. The image quality and resolution in both scattering tissue and the retina are comparable to those obtained by using femtosecond solid-state laser sources. This result demonstrates the ability to achieve *in vivo* ultrahigh resolution OCT imaging without femtosecond solid-state lasers.

The broadband SLD source is a new prototype developed by Superlum Diodes, Ltd., and consists of two spectrally multiplexed, independently driven SLD diodes operating at 840 nm and 920 nm, respectively. An SLD diode based on a SQW (GaAl)As heterostructure [18] and a recently developed SLD diode based on a SQW (InGa)As/(AlGa)As heterostructure with graded-index (GRIN) waveguides [19] were used. The SLDs have optical outputs with overlapping spectral bands that can be combined with a broadband fiber coupler. A custom-built, broadband, single-mode fiber Y-coupler based on fiber GRIN microlenses and partially transmitting miniature mirrors with dielectric multilayer coatings was developed to spectrally multiplex the SLD outputs. In the spectral range of 750-1100 nm, a coupling ratio of ~50% and an insertion loss of <1 dB were achieved with this coupler. The combined SLD output provides 155 nm of bandwidth at a center wavelength of 890 nm with >4 mW of CW output power. When compared to a solid-state laser, this broadband SLD source is quite compact and has a total footprint of only 31 x 26 x 15 cm, including the power supply; or 31 x 15 x 5 cm for the SLD and multiplexer package alone. The total cost of this light source is approximately an order of magnitude less than that of a typical commercial Ti:Sapphire femtosecond laser.

Figure 1a shows the individual output spectra of the two superluminescent diodes. Figure 1b shows the fiber-coupled spectrum of the broadband SLD source, demonstrating a full-width-half-maximum bandwidth of 155 nm. A maximum of 1.6 mW power was available at the sample arm. The interferometric point spread function (PSF) was measured by using an attenuated isolated reflection from a mirror. The coherence PSF of the broadband SLD source was measured by placing a mirror behind the imaging microscope in the sample arm. The interferometric PSF from a mirror with an optical density (OD) 3.0 filter was measured (Fig. 1c) and showed a 3.0 μm OCT axial resolution in air, which corresponded to ~2.3 μm in tissue. Figure 1d shows the PSF after logarithmic demodulation, demonstrating a sensitivity of 102 dB. For *in vivo* ultrahigh resolution OCT ophthalmic imaging, the water in the vitreous absorbs strongly at wavelengths above 920 nm and limits the bandwidth that can be used for retinal imaging [20]. Since wavelengths longer than 920 nm are absorbed in the vitreous, the light incident on the eye was filtered to remove long wavelengths that would be absorbed, and a bandwidth of 120 nm for ophthalmic imaging was used. The interferometric axial PSF measured by using an isolated, attenuated reflection from a mirror was 4.3 μm in air, which corresponds to 3.2 μm in tissue. By using 750 μW of incident power at the slitlamp output, which is well below the ANSI safety limit for retinal exposure, a sensitivity of 94 dB was obtained.

To demonstrate *in vivo* ultrahigh resolution OCT imaging in scattering tissue, an everted hamster cheek pouch was imaged by using a microscope for beam delivery. The broadband SLD had ~4 mW total CW power output, of which 1.6 mW was incident on the hamster cheek pouch. The image taken from the *in vivo* sample had a total scan depth of 1.5 mm in tissue and a transverse scan length of 2 mm. The total imaging time needed to acquire 1000 axial scans was ~40 seconds. For these imaging measurements, axial scanning was performed at a velocity of 82 mm/sec with a Doppler frequency of 205 kHz and a detection bandwidth of 54 kHz. Figure 2 shows an example of *in vivo* ultrahigh resolution OCT imaging in the hamster cheek pouch using the broadband SLD light source. This image has an axial resolution of ~2.3 μm in tissue and a transverse resolution of ~5 μm. A glass coverslip was used on the surface of the exposed cheek pouch epithelium in order to reduce the high specular reflection caused by the large index mismatch from air to tissue. This OCT image taken with the broadband SLD light source has image resolution and quality comparable to that of ultrahigh resolution OCT images of the hamster cheek pouch taken with a solid-state laser light source [3]. The stratum cornium is seen as a highly backscattering layer at the top of the cheek pouch, followed by the low backscattering epithelium layer. The muscularis layers and connective tissues below the epithelium layer can also be clearly seen in this image. Blood vessels are clearly visible, which causes a characteristic shadowing of the OCT signal below the level of the vessels.

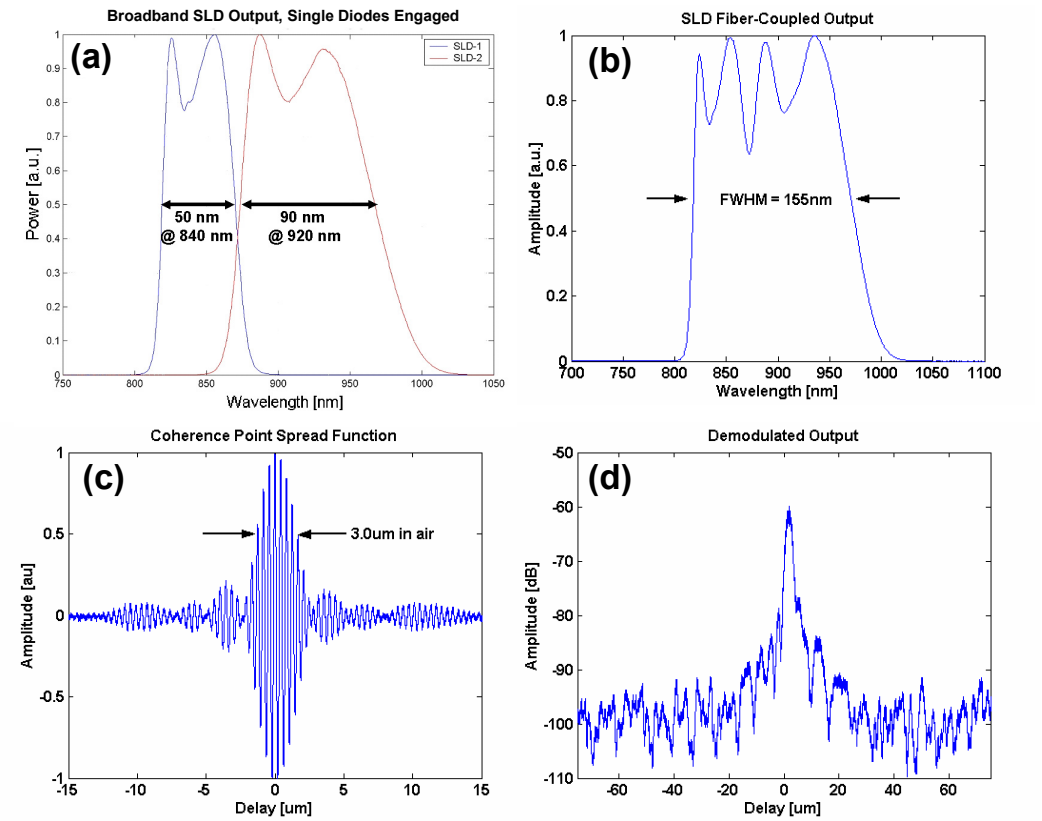

Figure 1. (a) Individual output spectra of two superluminescent diodes. (b) Fiber-coupled multiplexed spectrum of the broadband superluminescent diode (SLD) source. (c) Coherence point spread function (PSF) of the broadband SLD source. (d) Logarithmic demodulated coherence PSF. A 3.0 optical density (OD) filter was used to prevent detector saturation.

Figure 3 shows an example of *in vivo* ultrahigh resolution OCT imaging in the human retina by using a broadband SLD light source. This image is 6 mm long in the transverse direction and centered on the fovea of the retina. The OCT axial resolution was ~3.2 μm in the retina and transverse resolution was 15-20 μm. For ophthalmic imaging, axial scanning was performed at a velocity of 410 mm/sec with 1 MHz Doppler frequency and 170 kHz detection bandwidth. The axial scan length was 1.5 mm in tissue and the scan repetition rate was ~140 scans per second. Each ophthalmic image consists of 600 A-scans with an imaging scan time of ~4 seconds. This acquisition time was identical to that using a femtosecond solid-state laser light source and was sufficiently short for the subject to keep the eye open and maintain fixation. A false-color mapping similar to that used in the commercial ophthalmic OCT system (StratusOCT, Carl Zeiss Meditec, Dublin, CA) was used in order to better highlight individual intraretinal layers [21]. This ultrahigh resolution ophthalmic OCT image taken with the broadband SLD has image resolution and quality similar to that of ultrahigh resolution ophthalmic OCT images previously reported [6,7].

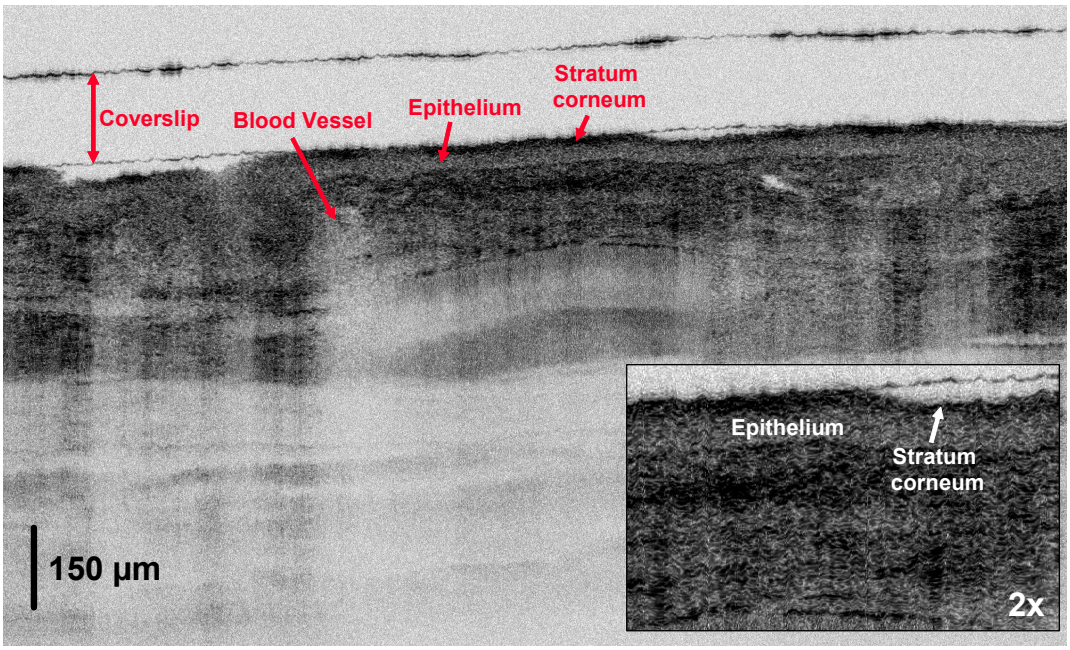

Figure 2. *In vivo* ultrahigh resolution OCT image of the Syrian golden hamster cheek pouch taken with the broadband SLD light source. Image axial resolution is 2.3 µm in tissue and transverse resolution is 5 µm. Ultrahigh resolution OCT imaging using a broadband SLD light source is capable of visualizing the stratum cornium, epithelium, muscularis, connective tissue, and blood vessels in the hamster cheek pouch.

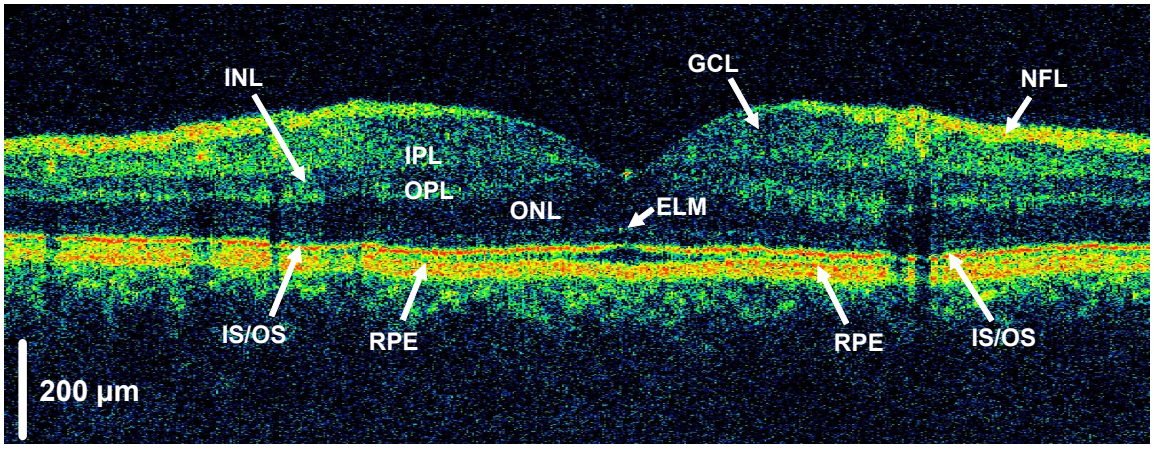

Figure 3. *In vivo* ultrahigh resolution OCT image of the human retina taken with the broadband SLD light source. Image axial resolution in the retina was about 3.2 µm and transverse resolution was about 15-20 µm. All the major intraretinal layers can be clearly seen in this ultrahigh resolution OCT image.

We have demonstrated *in vivo* ultrahigh resolution imaging using a broadband superluminescent diode (SLD) light source. A broadband optical output was achieved by multiplexing the outputs from two SLDs operating at 840 nm and 920 nm. This light source generated a 155 nm bandwidth with a 4 mW output power. Ultrahigh resolution OCT imaging with 2.3 µm axial resolution in scattering tissue and 3.2 µm resolution in the retina was demonstrated. The image resolution for retinal imaging was limited by water absorption in the eye. The development of SLD devices at shorter wavelengths, which do not overlap the

onset of water absorption at 920 nm, should improve resolution for retinal imaging in the future [20]. Although output powers are limited, the broadband SLD light source produces ultrahigh resolution OCT images that are comparable to those obtained by using femtosecond solid-state lasers [1-7]. These results demonstrate the ability to achieve *in vivo* ultrahigh resolution OCT imaging by using a compact, easy to operate, and relatively inexpensive SLD light source. The development of these new light sources should greatly enhance the availability of ultrahigh resolution OCT technology, especially in clinical applications such as ophthalmology.

References

1. B. Bouma, G.J. Tearney, S.A. Boppart, M.R. Hee, M.E. Brezinski, and J.G. Fujimoto, "High-resolution optical coherence tomographic imaging using a mode-locked Ti:Al_2O_3 laser source," *Optics Letters* 20(13): 1486-8 (1995).
2. W. Drexler, U. Morgner, F.X. Kartner, C. Pitris, S.A. Boppart, X.D. Li, E.P. Ippen, and J.G. Fujimoto, "In vivo ultrahigh-resolution optical coherence tomography," *Optics Letters* 24(17): 1221-3 (1999).
3. I. Hartl, X.D. Li, C. Chudoba, R.K. Hganta, T.H. Ko, J.G. Fujimoto, J.K. Ranka, and R.S. Windeler, "Ultrahigh-resolution optical coherence tomography using continuum generation in an air-silica microstructure optical fiber," *Optics Letters* 26(9): 608-10 (2001).
4. Y.M. Wang, Y.H. Zhao, J.S. Nelson, Z.P. Chen, and R.S. Windeler, "Ultrahigh-resolution optical coherence tomography by broadband continuum generation from a photonic crystal fiber," *Optics Letters* 28(3): 182-4 (2003).
5. D.L. Marks, A.L. Oldenburg, J.J. Reynolds, and S.A. Boppart, "Study of an ultrahigh-numerical-aperture fiber continuum generation source for optical coherence tomography," *Optics Letters* 27(22): 2010-12 (2002).
6. W. Drexler, U. Morgner, R.K. Ghanta, F.X. Kaertner, J.S. Schuman, and J.G. Fujimoto, "Ultrahigh resolution ophthalmic optical coherence tomography," *Nat. Med.* 7: 502-507 (2001).
7. W. Drexler, H. Sattmann, B. Hermann, T.H. Ko, M. Stur, A. Unterhuber, C. Scholda, O. Findl, M. Wirtitsch, J.G. Fujimoto, and A.F. Fercher, "Enhanced visualization of macular pathology with the use of ultrahigh-resolution optical coherence tomography," *Arch. Ophthalmol.* 121(5): 695-706 (2003).
8. X. Clivaz, F. Marquis-Weible, and R.P. Salathe, "Optical low coherence reflectometry with 1.9 μm spatial resolution," *Electronics Letters* 28(16): 1553-1554 (1992).
9. A.M. Kowalevicz, T. Ko, I. Hartl, J.G. Fujimoto, M. Pollnau, and R.P. Salathe, "Ultrahigh resolution optical coherence tomography using a superluminescent light source," *Optics Express* 10(7) (2002).
10. M. Pollnau, R.P. Salathe, T. Bhutta, D.P. Shepherd, and R.W. Eason, "Continuous-wave broadband emitter based on a transition-metal-ion-doped waveguide," *Optics Letters* 26(5): 283-285 (2001).
11. A. Crunteanu, M. Pollnau, G. Janchen, C. Hibert, P. Hoffmann, R.P. Salathe, R.W. Eason, C. Grivas, and D.P. Shepherd, "Ti:sapphire rib channel waveguide fabricated by reactive ion etching of a planar waveguide," *Applied Physics B (Lasers and Optics)* B75(1): 15-17 (2002).
12. M. Pollnau, "Broadband luminescent materials in waveguide geometry," *Journal of Luminescence* 102-103: 797-801 (2003).
13. G.A. Alphonse. "*Design of high-power superluminescent diodes with low spectral modulation*," paper presented at the *Test and Measurement Applications of Optoelectric Devices, Jan 21-22 2002*, San Jose, CA, United States, 2002.
14. G.A. Alphonse and M. Toda, "Mode coupling in angled facet semiconductor optical amplifiers and superluminescent diodes," *Journal of Lightwave Technology* 10(2): 215-19 (1992).
15. V. Shidlovski and J. Wei. "*Superluminescent diodes for optical coherence tomography*," paper presented at the *Test and Measurement Applications of Optoelectric Devices, Jan 21-22 2002*, San Jose, CA, United States, 2002.
16. E.A. Swanson, S.R. Chinn, S.A. Boppart, B. Bouma, M.R. Hee, G.J. Teary, J.G. Fujimoto, and M.B. Brezinski. "*Optical coherence tomography: principles, instrumentation, and applications*," paper presented at the *Proceedings of 21st Australian Conference on Optical Fibre Technology (ACOFT'96), 1-4 Dec. 1996*, Gold Coast, Qld., Australia, 1996.
17. A. Baumgartner, C.K. Hitzenberger, H. Sattmann, W. Dresler, and A.F. Fercher, "Signal and resolution enhancements in dual beam optical coherence tomography of the human eye," *Journal of Biomedical Optics* 3(1): 45-54 (1998).

18. A.T. Semenov, V.R. Shidlovski, D.A. Jackson, R. Willsch, and W. Ecke, "Spectral control in multisection AlGaAs SQW superluminescent diodes at 800 nm," *Electronics Letters* 32(3): 255-256 (1996).
19. D.S. Mamedov, V.V. Prokhorov, and S.D. Yakubovich, "Superbroadband high-power superluminescent diode emitting at 920 nm," *Quantum Electron.* 33(6): 471-473 (2003).
20. G.M. Hale and M.R. Query, "Optical constants of water in the 200-nm to 200-μm wavelength region," *Applied Optics* 12(3): 555-563 (1973).
21. M.R. Hee, J.A. Izatt, E.A. Swanson, D. Huang, J.S. Schuman, C.P. Lin, C.A. Puliafito, and J.G. Fujimoto, "Optical coherence tomography of the human retina," *Arch. Ophthalmol.* 113(3): 325-32 (1995).

2.1.2 All-Fiber Continuous-Wave (CW) Raman Continuum Light Source for High Resolution OCT

Sponsors
National Institutes of Health – R01-CA75289-06, R01-EY11289-18
National Science Foundation – ECS-01-19452, BES-0119494
Air Force Office of Scientific Research – F49620-01-1-0186, F49620-01-01-0084
Poduska Family Foundation Fund for Innovative Research in Cancer
Philanthropy of Mr. Gerhard Andlinger

Project Staff
Pei-Lin Hsiung, Dr. Yu Chen, Tony H. Ko, Professor James G. Fujimoto (MIT)
Christiano J.S. de Matos, Sergei V. Popov, Professor James R. Taylor (Imperial College, United Kingdom)
Valentin P. Gapontsev (IPG Photonics Corporation, MA)

High-performance, short-coherence-length light sources with broad bandwidths and high output powers are critical for high speed, ultrahigh resolution OCT imaging. The lack of compact and portable high-performance broadband light sources with sufficient power and bandwidths has been a limitation to achieving ultrahigh resolution, high speed OCT imaging outside the laboratory setting. Standard OCT systems use superluminescent diode light sources, which achieve a resolution of 10-15 μm. Femtosecond solid-state lasers have been demonstrated to directly generate broad bandwidths that can be used for OCT imaging, but they are difficult to operate outside the laboratory [1,2]. Nonlinear and microstructure fibers pumped by femtosecond bulk and fiber systems have also enabled imaging with unprecedented resolutions, but they require the use of femtosecond lasers [3-5]. Reductions in cost can be achieved by using low-threshold femtosecond lasers, which use inexpensive low-power pump lasers [6,7]. Femtosecond fiber-laser-based sources promise to be compact and robust, but they still require adjustment [8]. The 1300 nm wavelength region is of particular interest for biomedical applications, because it permits improved imaging depth when compared with shorter wavelengths due to reduced scattering in biological tissue [9]. The development of broadband light sources for OCT imaging in scattering tissue has, therefore, focused on this wavelength range [3,5,8,10]. Recent work has also investigated light source development and imaging at center wavelengths closer to 1000 nm, which provide a compromise of higher resolution for a given bandwidth at the expense of reduced image penetration [5,11]. A portable source suitable for *in vivo* clinical applications has been demonstrated in this wavelength range by using a femtosecond diode-pumped Nd:Glass laser with a highly nonlinear fiber [11].

A novel approach to broadband continuum generation in photonic crystal fibers has become possible due to the development of high-power, all-fiber pump sources. These new light sources promise ultrahigh resolution, high speed OCT imaging with lower cost and complexity than what is possible with femtosecond laser-based light sources. Microstructure and photonic crystal fibers typically have been pumped with femtosecond lasers in order to provide the peak powers necessary to initiate self-phase modulation and four-wave-mixing-supported continuum generation under conditions of anomalous or near-zero dispersion. However, the use of high intensity femtosecond sources for continuum generation in holey fibers leads to severe spectral modulation of the continuum in the vicinity of the pump wavelength. This spectral modulation produces side lobes and reduced contrast in the interferometric point spread function. Femtosecond quasi-CW-pulsed pumping of holey fibers also may result in excessive temporal instability (up to 50% in amplitude) of the continuum and nonlinearly amplified quantum noise, which can lead to dramatic >20 dB relative intensity noise fluctuations [12]. An alternative to using high peak powers is to increase the effective nonlinear interaction length of the Raman interaction, which is governed by optical losses in the fiber and dispersive walk-off between the pump and continuum pulses. The use of longer pump pulses reduces this dispersive walk-off effect. Stimulated Raman scattering has been shown to be the principle nonlinearity for continuum generation by using nanosecond-scale pump pulses [13,14]. Recently, the possibility of low peak power and even continuous-wave, multiwatt Raman continuum generation in highly nonlinear fibers was demonstrated [15]. Continuous-wave pumping of nonlinear fibers can enable the development of robust and turnkey continuum light sources that require no optical alignment, thus enabling high speed, ultrahigh resolution OCT imaging in a wide range of applications outside the laboratory.

In collaboration with Professor James R. Taylor's group at Imperial College, we have demonstrated a continuous-wave-pumped, all-fiber Raman continuum light source with 330 mW power for high speed, ultrahigh resolution OCT imaging in scattering tissue. This source is robust, compact, turnkey, and suitable for clinical applications. The broadband fiber light source was based on a 10 W continuous-wave, nonpolarized, multimode diode-pumped, single-mode Yb-fiber laser (IPG Photonics) directly spliced to an anomalously dispersive holey fiber (Crystal Fiber). The Raman-soliton continuum produced in this fiber had 3.8 W of power and a spectral width of 324 nm (20dB) with a flatness of ±3.5 dB in the spectral range from 1090 nm to 1375 nm [15]. The output was filtered using a special wavelength division multiplex (WDM) coupler to remove the pump wavelength. Figure 1 shows the continuum produced by the Raman continuum source, and typical spectra before and after spectral shaping by the WDM coupler. The output power after the coupler was ~330 mW and the spectrum was Gaussian-shaped with a bandwidth of ~140 nm, which corresponds to a theoretical resolution of 5 μm in free space. The complete light source contains no bulk optical components, requires no alignment, and is turnkey, compact (25 x 25 x 20 cm) and robust.

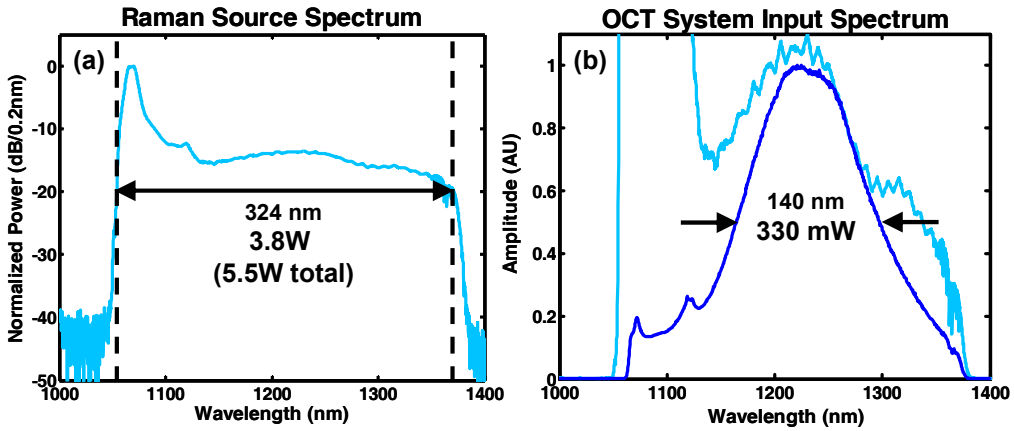

Figure 1. (a) Continuum produced by Raman source. (b) Typical output spectrum before and after spectral shaping.

Figure 2 shows the schematic of the experimental setup. The OCT system consists of broadband 80/20 and 50/50 fiber couplers to optimize power coupled back to the detectors. The reference arm was scanned using a reflective delay scanner. Polarization controllers were used in both the sample arm and the reference arms. *In vivo* imaging was performed using an X-Y galvanometer scanning probe. Near-infrared achromatic lenses were used to minimize chromatic aberration. Dual-balanced detection with two InGaAs photodiodes was used to reduce excess intensity noise. The interference signal was electronically band-pass filtered, logarithmically demodulated, low-pass filtered, and digitized. The performance of the OCT system using the Raman continuum light source was measured by using an isolated reflection from a single mirror. To maintain axial resolution, the dispersion in the interferometer sample and reference arms was carefully matched. Appropriate-thickness glass blanks of fused silica, SFL6 and LakN22 were inserted into the reference arm to balance the dispersion of the achromatic lenses in the imaging probe. The measured axial resolution was 6.3 μm in air, which corresponds to 4.8 μm in tissue. The detected optical spectrum was measured to be 110 nm by Fourier transformation of the interferometric signal. This reduction in bandwidth may be the result of wavelength dependence of the fiber couplers, as well as wavelength variations in the sensitivity of the InGaAs photodiodes.

We demonstrated high speed, ultrahigh resolution *in vivo* OCT imaging in the hamster cheek pouch, which is a well-established model for studies of cancer progression. To minimize the effect of wavefront aberration and dehydration, and to achieve better index matching, the cheek pouch was irrigated with saline and covered with a thin cover glass. Figure 3 shows a high speed, ultrahigh resolution *in vivo* image of the hamster cheek pouch with <5 μm axial resolution. The image had 500 transverse pixels and 1000 axial pixels, and it measured 2.5 mm by 1.8 mm. The axial dimension was scaled by 1.3 to account for the approximate index of refraction. The epithelial layer, muscular layers, and two prominent vessels are clearly visible in the hamster cheek pouch.

In conclusion, we have demonstrated an all-fiber, continuous-wave-pumped, broadband Raman continuum fiber light source at a center wavelength of ~1.3 μm for high speed, ultrahigh resolution *in vivo* OCT imaging. We achieved an axial resolution of <5 μm in tissue, which is a factor of 2-3 times finer than what is possible using conventional superluminescent diode light sources. This fiber Raman light source requires no alignment; it is compact, turnkey, and promising for clinical OCT imaging applications. Broader output spectra and lower excess noise may be obtained using higher power Yb lasers and different fiber geometries. Although the cost of the light source is rather high, because of the cost of the photonic crystal fiber, these fibers are expected to be available at significantly lower cost in the future. The future cost should be significantly lower than that of femtosecond laser-based light sources. The high performance and ease of use of this light source promises high speed, ultrahigh resolution OCT imaging in a wide range of applications.

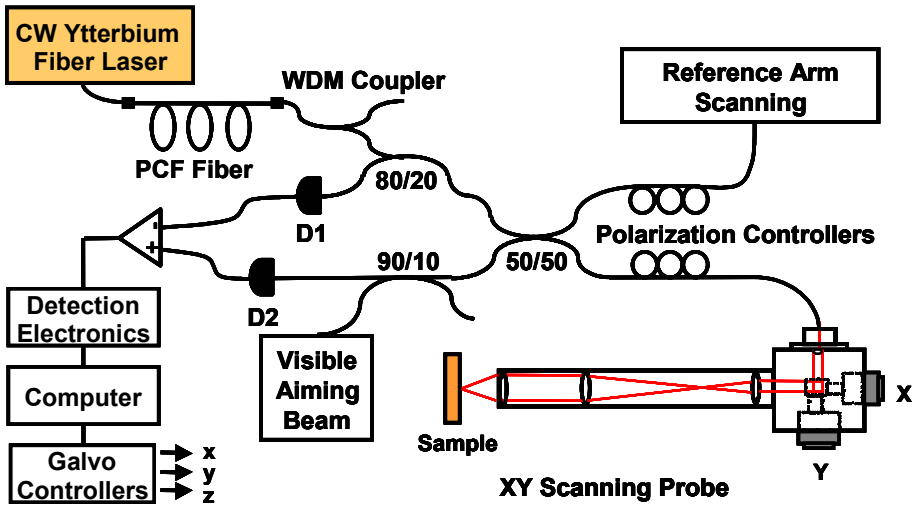

Figure 2. Schematic of a high speed, ultrahigh resolution OCT system using an all-fiber Raman continuum light source. The system uses broadband 80/20 and 50/50 couplers to optimize the power on the sample and is coupled back to the detectors. Dispersion was matched in the sample and reference arms of the interferometer in order to maintain high axial resolution.

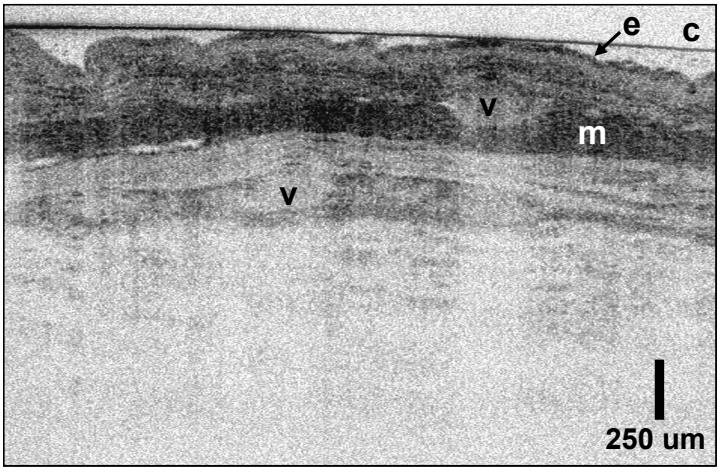

Figure 3. High speed, ultrahigh resolution *in vivo* OCT image of a Syrian hamster cheek pouch. The epithelial layer (e), muscular layers (m), and two prominent vessels (v) are clearly visible. A microscope cover glass (c) was placed over the top of the cheek pouch (~18 μm x 4.8 μm transverse x axial resolution, 500 x 1000 pixels, 2.5 x 1.8 mm).

References

1. B.E. Bouma, G.J. Tearney, S.A. Boppart, M.R. Hee, M.E. Brezinski, and J.G. Fujimoto, "High-resolution optical coherence tomographic imaging using a mode-locked Ti:Al_2O_3 laser source," *Optics Letters* 20(13): 1486-1488 (1995).
2. W. Drexler, U. Morgner, F.X. Kartner, C. Pitris, S.A. Boppart, X.D. Li, E.P. Ippen, and J.G. Fujimoto, "In vivo ultrahigh-resolution optical coherence tomography," *Optics Letters* 24(17): 1221-3 (1999).
3. I. Hartl, X.D. Li, C. Chudoba, R.K. Ghanta, T.H. Ko, J.G. Fujimoto, J.K. Ranka, and R.S. Windeler, "Ultrahigh-resolution optical coherence tomography using continuum generation in an air-silica microstructure optical fiber," *Optics Letters* 26(9): 608-610 (2001).
4. B. Povazay, K. Bizheva, A. Unterhuber, B. Hermann, H. Sattmann, A.F. Fercher, W. Drexler, A. Apolonski, W.J. Wadsworth, J.C. Knight, P.S.J. Russell, M. Vetterlein, and E. Scherzer, "Submicrometer axial resolution optical coherence tomography," *Optics Letters* 27(20): 1800-2 (2002).
5. Y. Wang, Y. Zhao, J.S. Nelson, Z. Chen, and R.S. Windeler, "Ultrahigh-resolution optical coherence tomography by broadband continuum generation from a photonic crystal fiber," *Optics Letters* 28(3): 182-4 (2003).
6. A.M. Kowalevicz, T.R. Schibli, F.X. Kartner, and J.G. Fujimoto, "Ultralow-threshold Kerr-lens mode-locked Ti:Al_2O_3 laser," *Optics Letters* 27(22): 2037-2039 (2002).
7. A. Unterhuber, B. Povazay, B. Hermann, H. Sattmann, W. Drexler, V. Yakovlev, G. Tempea, C. Schubert, E.M. Anger, P.K. Ahnelt, M. Stur, J.E. Morgan, A. Cowey, G. Jung, T. Le, and A. Stingl, "Compact, low-cost Ti:Al_2O_3 laser for in vivo ultrahigh-resolution optical coherence tomography," *Optics Letters* 28(11): 905-7 (2003).
8. K. Bizheva, B. Povazay, B. Hermann, H. Sattmann, W. Drexler, M. Mei, R. Holzwarth, T. Hoelzenbein, V. Wacheck, and H. Pehamberger, "Compact, broad-bandwidth fiber laser for sub-2-microm axial resolution optical coherence tomography in the 1300-nm wavelength region," *Optics Letters* 28(9): 707-9 (2003).
9. J.M. Schmitt, A. Knuttel, M. Yadlowsky, and M.A. Eckhaus, "Optical coherence tomography of a dense tissue - statistics of attenuation and backscattering," *Physics in Medicine and Biology* 39(10): 1705-1720 (1994).
10. B.E. Bouma, G.J. Tearney, I.P. Bilinsky, B. Golubovic, and J.G. Fujimoto, "Self-phase-modulated Kerr-lens mode-locked Cr:forsterite laser source for optical coherence tomography," *Optics Letters* 21(22): 1839-41 (1996).
11. S. Bourquin, A.D. Aguirre, I. Hartl, P. Hsiung, T.H. Ko, and J.G. Fujimoto, "Compact broadband light source for ultra high resolution optical coherence tomography imaging using a femtosecond Nd:Glass laser and a nonlinear fiber," *Optics Express* 11(24): 3290-3297 (2003).
12. K.L. Corwin, N.R. Newbury, J.M. Dudley, S. Coen, S.A. Diddams, K. Weber, and R.S. Windeler, "Fundamental noise limitations to supercontinuum generation in microstructure fiber," *Physical Review Letters* 90(11): 113904-1 (2003).
13. P.A. Champert, S.V. Popov, and J.R. Taylor, "Generation of multiwatt, broadband continua in holey fibers," *Optics Letters* 27(2): 122-4 (2002).
14. L. Provino, J.M. Dudley, H. Maillotte, N. Grossard, R.S. Windeler, and B.J. Eggleton, "Compact broadband continuum source based on microchip laser pumped microstructured fibre," *Electronics Letters* 37(9): 558-60 (2001).
15. A.V. Avdokhin, S.V. Popov, and J.R. Taylor, "Continuous-wave, high-power, in Raman continuum generation holey fibers," *Optics Letters* 28(15): 1353-1355 (2003).

2.1.3 Real-Time High Resolution OCT using All-Fiber Femtosecond Fiber Laser Continuum at 1.5 μm

Sponsors
National Institute of Health – NIH-5-R01-CA75289-06, NIH-2-R01-EY11289-18
National Science Foundation – ECS-0119452, BES-0119494
Air Force Office of Scientific Research – F49620-01-01-0084, F49620-01-1-0186

Project Staff
Dr. Norihiko Nishizawa, Dr. Yu Chen, Pei-Lin Hsiung, Vikas Sharma, Paul R. Herz, Tony H. Ko, Professor Erich P. Ippen, Professor James G. Fujimoto

Optical coherence tomography (OCT) is an emerging technology for micron-scale cross-sectional imaging of biological tissues and materials [1]. One of the key limitations to achieving ultrahigh resolution OCT imaging outside of the laboratory setting has been the lack of compact, high-performance broadband light sources with sufficient power and stability to enable practical real-time imaging. Sources using femtosecond solid-state lasers were demonstrated to directly generate broad bandwidths that can be used for OCT imaging, but they are difficult to use for general applications outside the laboratory [2]. Broadband supercontinuum (SC) generated using nonlinear and microstructure fibers pumped by femtosecond laser systems have enabled imaging with unprecedented resolutions, but they require femtosecond solid-state lasers [3-6].

Compact, broad bandwidth supercontinuum sources were recently demonstrated by using femtosecond fiber lasers in combination with nonlinear fibers [7,8]. Fiber lasers can provide a more compact and robust approach for ultrahigh resolution imaging when compared to bulk solid-state lasers. Fiber-based light sources have achieved sub-2-μm high-resolution OCT in the 1300 nm wavelength region [9]. Because the optical scattering in tissues is reduced and the penetration depth is increased at longer wavelengths, the wavelength region around 1.4-1.6 μm is of interest for OCT imaging [10,11]. This wavelength region is also attractive for the characterization of optical devices or for spectroscopic applications using water absorption [12].

In this study, we have developed an all-fiber scheme for real-time high-resolution OCT imaging in the 1.4-1.7 μm wavelength region. A low-noise supercontinuum with 38 mW power and 180 nm bandwidth was generated using a high-power, stretched-pulse, passively modelocked fiber laser and highly nonlinear fiber. The details of this laser were reported earlier. *In vivo* imaging of human skin is demonstrated using the SC source and a high-speed OCT imaging system.

Figure 1 shows the experimental setup of OCT imaging using the high-power stretched-pulse passively modelocked Er-doped fiber laser. The generated supercontinuum was coupled into a high-speed OCT system. The OCT system consists of an optical circulator and a broadband 50/50 fiber coupler to optimize power coupled back to the detectors. The reference arm was scanned using a reflective scanner with a scan speed of 7.6 m/s and a repetition rate of 1900 Hz. Polarization controllers were used in both the sample arm and the reference arm to match the polarizations in the two interferometer arms. *In vivo* imaging was performed using an XY galvanometer scanning probe. A dual-balanced detection configuration was performed with two InGaAs photodiodes. The detected interference signal was band-pass filtered, logarithmically demodulated, low-pass filtered, and acquired by the computer.

The performance of the OCT system was measured by using an attenuated isolated reflection from a single mirror. To maintain high axial resolution, the dispersion in the two arms of the interferometer was carefully matched and glass blanks of fused silica, SFL6 and LaKN22 were used to balance the dispersion of the achromatic lenses in the imaging probe. Figures 2(a) and 2(b) show the interference signal and the logarithmic demodulated signal after band-pass and low-pass filtering. Since the spectral shape is almost Gaussian, the magnitude of side lobes was small on a linear scale. On a log scale, there are several small side lobes at –40 to –50 dB below the main peak, which is caused by small residual modulation in the spectrum. The measured axial resolution was 7.4 μm full-width-at-half-maximum

(FWHM) in air, which corresponds to 5.6 μm in tissue. The detected optical spectrum was measured to be 151 nm by Fourier transforming the interferometric signal. This reduction in bandwidth may be due to the wavelength dependence of the circulator, couplers, and optical lenses, as well as wavelength variations in the sensitivity of the InGaAs photodiodes.

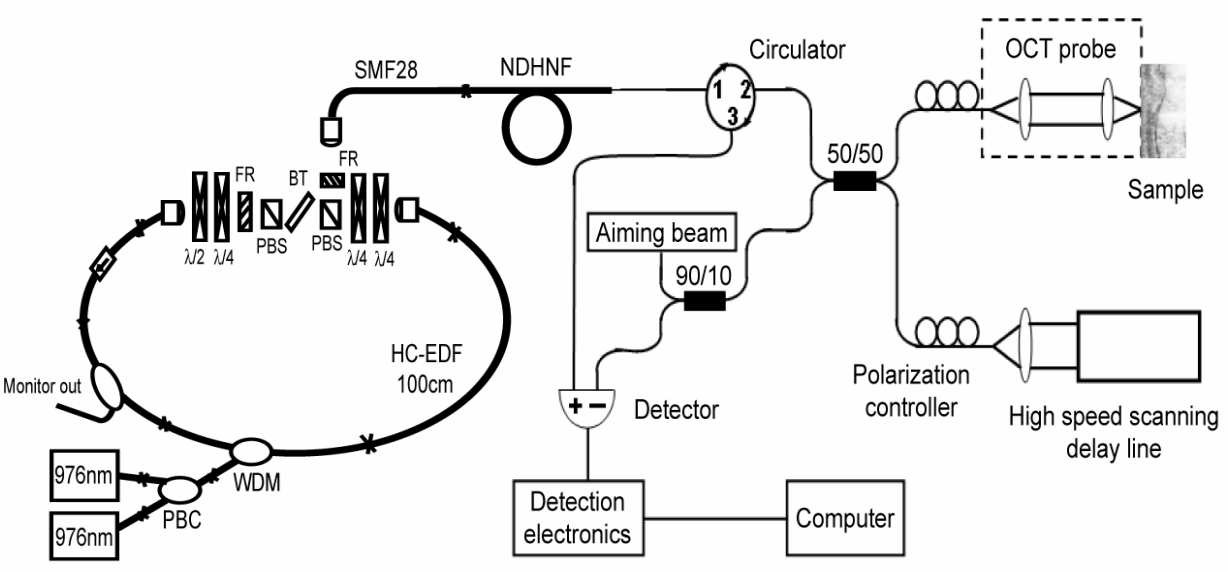

Figure 1. Experimental setup of an all fiber, real-time, ultrahigh resolution OCT system at 1.55 μm wavelength. (PBC: polarization beam combiner; WDM: wavelength division multiplexed coupler; HC-EDF: high concentration Er doped fiber; PBS: polarization beam splitter; FR: Faraday rotator; BT: birefringent plate).

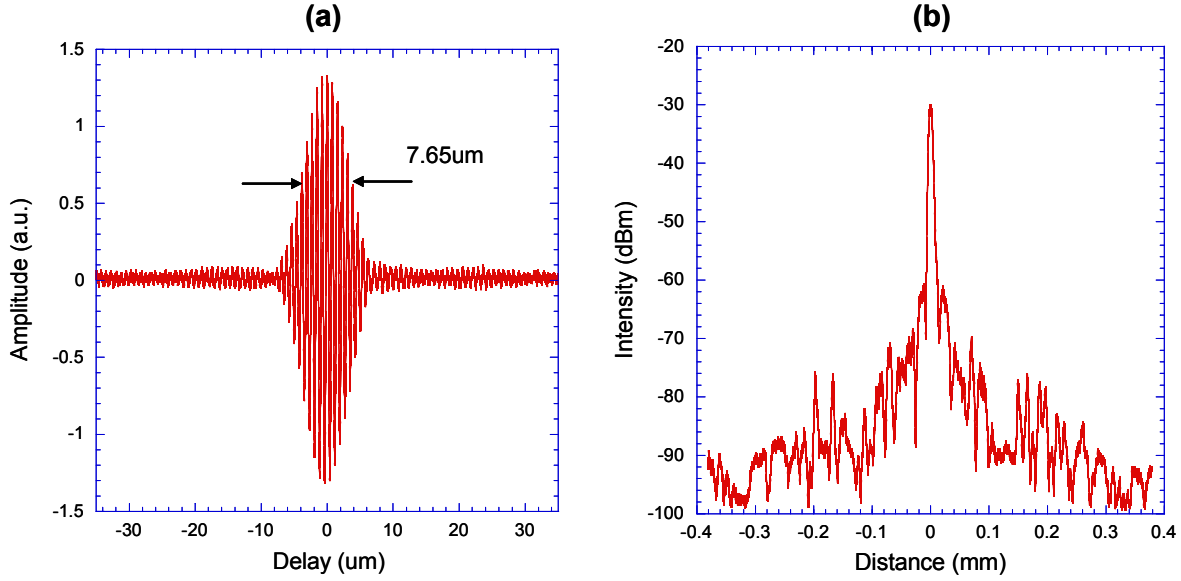

Figure 2. (a) Interference signal point spread function and (b) logarithmically demodulated signal showing an axial resolution of 7.4 μm in air, which corresponds to 5.6 μm in tissue.

The system sensitivity was measured by the placement of calibrated attenuators in the sample arm. The signal-to-noise ratio, consistent with the minimum visible isolated mirror reflection on the screen, corresponds to a system sensitivity of 98.7 dB with a power of 12 mW incident on the sample. This sensitivity is near the theoretical sensitivity for this incident power and detection bandwidth.

We demonstrated the feasibility of using this light source for high-speed *in vivo* OCT by imaging the human skin. To minimize the effect of wavefront aberration, and tissue dehydration, and to achieve better index matching, a transparent gel was applied. Figure 3 shows an *in vivo* image of human skin. The image consists of 500 transverse scans with 1000 pixels per scan, which covers an area of 2.5 mm by 1.8 mm. The image was scaled by 1.3 times in the axial dimension in order to compensate for the approximate index of refraction. The epidermis, sweat duct, and junction of epidermis and dermis are clearly visible.

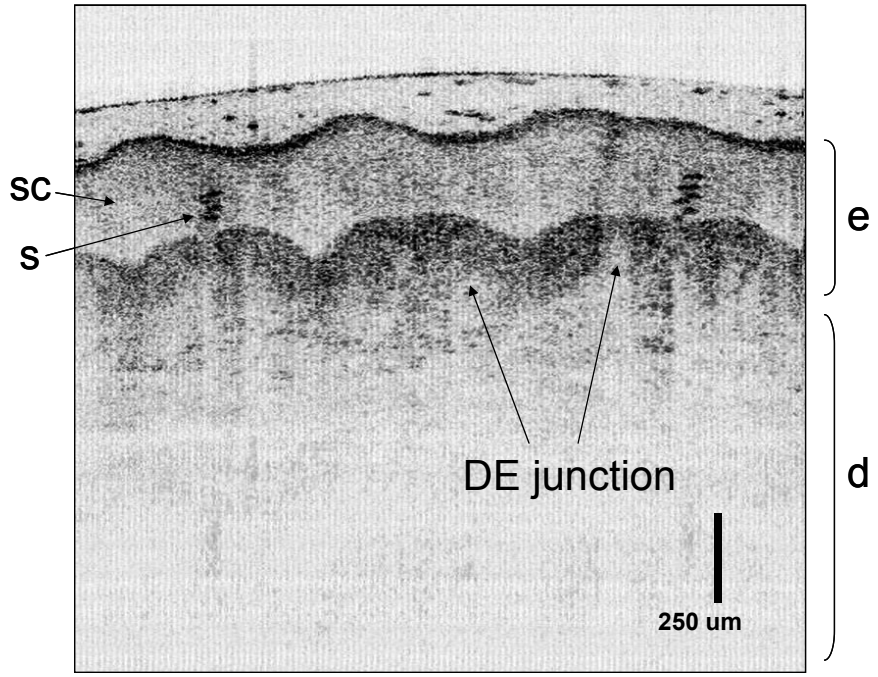

Figure 3. High-speed *in vivo* OCT image of human skin. The stratum corneum (sc), epidermis (e), sweat duct (s), and dermis (d) are clearly visible (~18 μm x 4.8 μm transverse x axial resolution; 500 x 1000 pixels; 2.5 x 1.8 mm).

In conclusion, we have demonstrated an all-fiber, real-time, high resolution OCT imaging system by using a high-power, broadband, supercontinuum fiber laser light source in the 1.55 μm wavelength region. Fiber lasers can provide a more compact and robust approach to ultrahigh resolution imaging than what is possible with bulk solid-state lasers. Low-noise supercontinua with 180 nm bandwidth and 38 mW output power was generated using a stretched-pulse, passively modelocked high-power femtosecond fiber laser and normal dispersive highly nonlinear fiber. We achieved an axial resolution of ~7.4 μm in air and ~5.6 μm in tissue at a center wavelength of ~1.5 μm. This light source is stable, compact, and self-starting, and it should be useful for a wide range of high resolution high-speed OCT imaging applications.

References

1. D. Huang, E.A. Swanson, C.P. Lin, J.S. Schuman, W.G. Stinson, W. Chang, M.R. Hee, T. Flotte, K. Gregory, C.A. Puliafito, and J.G. Fujimoto, "Optical coherence tomography," *Science* 254(5035): 1178-81 (1991).
2. W. Drexler, U. Morgner, F.X. Kartner, C. Pitris, S.A. Boppart, X.D. Li, E.P. Ippen, and J.G. Fujimoto, "In vivo ultrahigh-resolution optical coherence tomography," *Optics Letters* 24(17): 1221-3 (1999).

3. I. Hartl, X.D. Li, C. Chudoba, R.K. Ghanta, T.H. Ko, J.G. Fujimoto, J.K. Ranka, and R.S. Windeler, "Ultrahigh-resolution optical coherence tomography using continuum generation in an air-silica microstructure optical fiber," *Optics Letters* 26(9): 608-610 (2001).
4. B. Povazay, K. Bizheva, A. Unterhuber, B. Hermann, H. Sattmann, A.F. Fercher, W. Drexler, A. Apolonski, W.J. Wadsworth, J.C. Knight, P.S.J. Russell, M. Vetterlein, and E. Scherzer, "Submicrometer axial resolution optical coherence tomography," *Optics Letters* 27(20): 1800-2 (2002).
5. Y. Wang, Y. Zhao, J.S. Nelson, Z. Chen, and R.S. Windeler, "Ultrahigh-resolution optical coherence tomography by broadband continuum generation from a photonic crystal fiber," *Optics Letters* 28(3): 182-4 (2003).
6. S. Bourquin, A.D. Aguirre, I. Hartl, P. Hsiung, T.H. Ko, J.G. Fujimoto, T.A. Birks, W.J. Wadsworth, U. Bunting, and D. Kopf, "Ultrahigh resolution real time OCT imaging using a compact femtosecond Nd:Glass laser and nonlinear fiber," *Optics Express* 11(24): 3290-3297 (2003).
7. N. Nishizawa and T. Goto, "Widely broadened supercontinuum generation using highly nonlinear dispersion shifted fibers and femtosecond fiber laser," *Jpn. J. Appl. Phys.* 40: 365-367 (2001).
8. J.W. Nicholson, M.F. Yan, P. Wisk, J. Fleming, F. DiMarcello, E. Monberg, A. Yablon, C. Jorgensen, and T. Veng, "All-fiber, octave-spanning supercontinuum," *Optics Letters* 28(8): 643-645 (2003).
9. K. Bizheva, B. Povazay, B. Hermann, H. Sattmann, W. Drexler, M. Mei, R. Holzwarth, T. Hoelzenbein, V. Wacheck, and H. Pehamberger, "Compact, broad-bandwidth fiber laser for sub-2-μm axial resolution optical coherence tomography in the 1300-nm wavelength region," *Optics Letters* 28(9): 707-9 (2003).
10. B.E. Bouma, L.E. Nelson, G.J. Tearney, D.J. Jones, M.E. Brezinski, and J.G. Fujimoto, "Optical coherence tomographic imaging of human tissue at 1.55 μm and 1.81 μm using Er and Tm-doped fiber sources," *Journal of Biomedical Optics* 3(1): 76-9 (1998).
11. J.M. Schmitt, A. Knuttel, M. Yadlowsky, and M.A. Eckhaus, "Optical coherence tomography of a dense tissue - statistics of attenuation and backscattering," *Physics in Medicine and Biology* 39(10): 1705-1720 (1994).
12. J.M. Schmitt, S.H. Xiang, and K.M. Yung, "Differential absorption imaging with optical coherence tomography," *Journal of the Optical Society of America A* 15(9): 2288-96 (1998).

2.1.4 Compact Cr^{4+}:Forsterite Laser for High Resolution Endoscopic OCT Imaging

Sponsors
National Institute of Health – NIH-5-R01-CA75289-06, NIH-2-R01-EY11289-18
National Science Foundation – ECS-0119452, BES-0119494
Air Force Office of Scientific Research – F49620-01-01-0084, F49620-01-01-0186

Project Staff
Paul Herz, Dr. Yu Chen, Pei-Lin Hsiung, Aaron D. Aguirre, Tony H. Ko, Karl Schneider, Amanda Koski (LightLab Imaging), Dr. Joseph Schmitt (LightLab Imaging), Professor James G. Fujimoto

One of the medical areas where high resolution OCT imaging could significantly impact the detection and diagnosis of disease is endoscopic imaging [1]. Gastrointestinal (GI) endoscopy has received increased attention due to the prevalence of esophageal, stomach, and colonic cancers. In the early stages of development, these cancers manifest as cellular and architectural changes in the epithelium or mucosal layers located inside the wall of the gastrointestinal tract. In contrast to conventional video endoscopy, which can only visualize the surface alterations, OCT can detect changes in tissue morphology beneath the tissue surface. Therefore, endoscopic imaging with high resolution OCT could potentially improve the detection, visualization, and diagnosis of gastrointestinal diseases.

Previous studies of endoscopic OCT imaging have documented the capability of OCT to differentiate abnormal GI pathologies such as the Barrett's esophagus, adnomatous polyps, and adenocarcinoma from normal tissues [2-8], while the resolution of these previous OCT systems is typically 10-15 μm. Higher resolution OCT systems may enable the identification of early neoplastic changes in gastrointestinal tissue. This advance could enable image-guided biopsy at high resolution, with the prospect of improving the sensitivity of biopsy by reducing false-negative rates caused by sampling errors.

In this study, we have developed high resolution endoscopic OCT imaging system by using a compact, broadband $Cr4^{+}$:Forsterite laser as the light source. Prismless operation within the laser cavity was achieved by using double-chirped mirrors for intracavity dispersion compensation [9]. Combined with a dispersion-shifted highly non-linear fiber, a spectral bandwidth of >200 nm at center wavelength of 1250 nm and an output power of 50 mW was generated, as shown in Figure 1. The compact Cr^{4+}:Forsterite laser has a footprint of 40 cm by 60 cm, and its portability makes it accessible to clinical settings.

Figure 2 depicts the schematic of the OCT imaging system. Light was coupled into a broadband optical circulator and a 90/10 fiber optic coupler, which transmits 90% of the incident light to the sample arm. A rapid scanning delay line in the reference arm provided real-time imaging up to 3125 axial scans per second. Polarization controllers were used in both the sample and reference arms to optimize signal strength and interference. To match the optical dispersion within the system, SFL6 and LaKN22 dispersion-compensating glass (DCG) was inserted in the reference arm, and an air-gap coupling (AGC) was used in the sample arm. The use of the air coupling allowed precise dispersion compensation and enabled broadband operation for high resolution imaging performance. The OCT signal after interference was split into two orthogonal polarization dependent channels by a polarizing beam splitter (PBS), and the two detector outputs were digitally demodulated. A polarization diversity signal was calculated using the square root of the sum of the squared signal intensities from the two channels. Due to the bandwidth limitations in the optical circulator and other optical components in the sample and reference arms, the back-coupled spectrum on the detector has a bandwidth of 150 nm, which corresponds to a theoretical axial resolution of 4.6 μm in air. The width of the measured axial point spread function is 5 μm, which is a two- to three-fold improvement over standard OCT systems. This corresponds to a 3.6 μm resolution in the tissue, assuming a 1.4 mean index of refraction. With improvements in the bandwidth support of the optical components, higher axial resolutions could be achieved.

The light was delivered through a 1.5-mm-diameter imaging catheter with a 15 μm focal spot size and a 0.5 mm focal distance from the outer wall of the catheter sheath. The catheter was driven by a magnetic

actuator in order to create a linear cross-sectional imaging scan through the tissue surface. A 4 Hz frame rate was implemented in the *in vivo* imaging to reduce the movement artifacts.

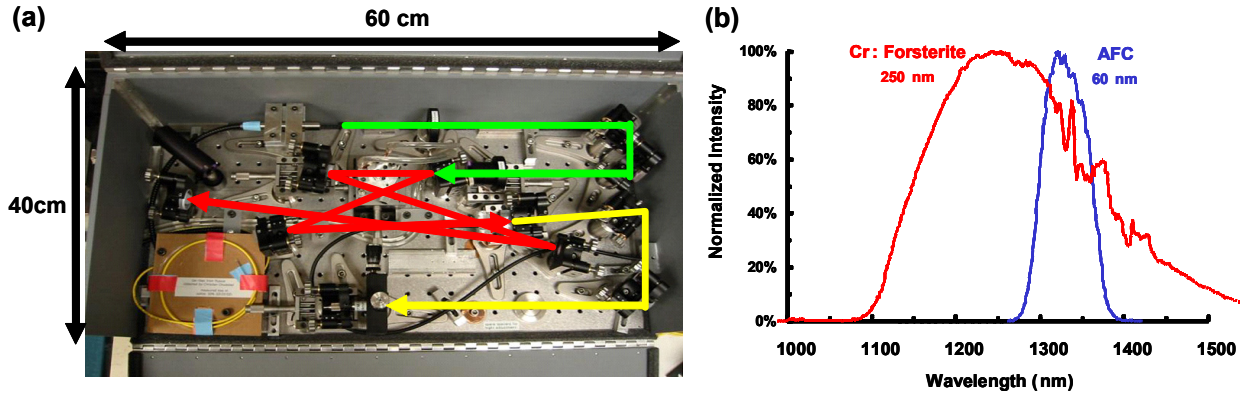

Figure 1. (a) The photo of the compact Cr^{4+}:Forsterite laser with the optical beam highlighted (top: pump light; middle: laser cavity; bottom: output coupling). (b) The output spectrum of the Cr^{4+}:Forsterite laser, compared with the spectrum of standard SLD source.

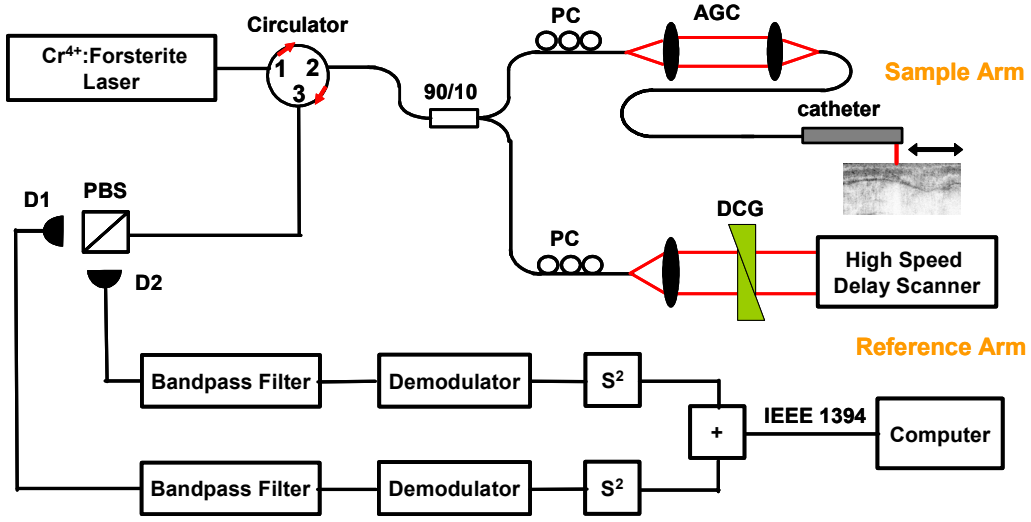

Figure 2. Schematic of an endoscopic OCT imaging system using a broadband Cr^{4+}:Forsterite light source. Accurate dispersion matching is achieved through the use of an air-gap coupling (AGC) and dispersion-compensating prisms (DCG), which enables broadband, high resolution operation.

The feasibility of endoscopic OCT imaging was demonstrated on the animal model. The gastrointestinal tracts of New Zealand White rabbit were imaged by using the linear scanning catheter. All imaging procedures were performed at MIT facilities with protocols approved by the MIT Committee on Animal Care (CAC). The rabbit was anesthetized, and the OCT imaging catheter was manually introduced into the upper gastrointestinal (esophagus) and lower gastrointestinal (colon) tracts respectively.

Figure 3(a) shows an *in vivo* OCT image of the rabbit esophagus taken with the linear scanning catheter. The corresponding histology is shown in Figure 3(b). The structure of the esophagus is delineated clearly, with well-organized layers of the squamous epithelium (ep), lamina propria (lp), muscularis mucosa (mm), submucosa (sm), and inner (im) and outer muscular (om) layers. The OCT image correlates well with the histology in both the order of layers and the layer thickness. This result is in agreement with previous OCT imaging studies of the esophagus [10], while higher resolution provides more refined details of

tissue morphology. Imaging of a larger tissue area was achieved by mechanically pulling back the imaging catheters and acquiring a series of images. Figure 4 shows a composite image of five OCT linear scans acquired sequentially as the catheter was withdrawn during imaging. Images were acquired over a 12 mm scanning range from the inner esophagus to the epiglottis. This image illustrates the capability of surveying tissue morphology over a large field at high resolution using endoscopic OCT system.

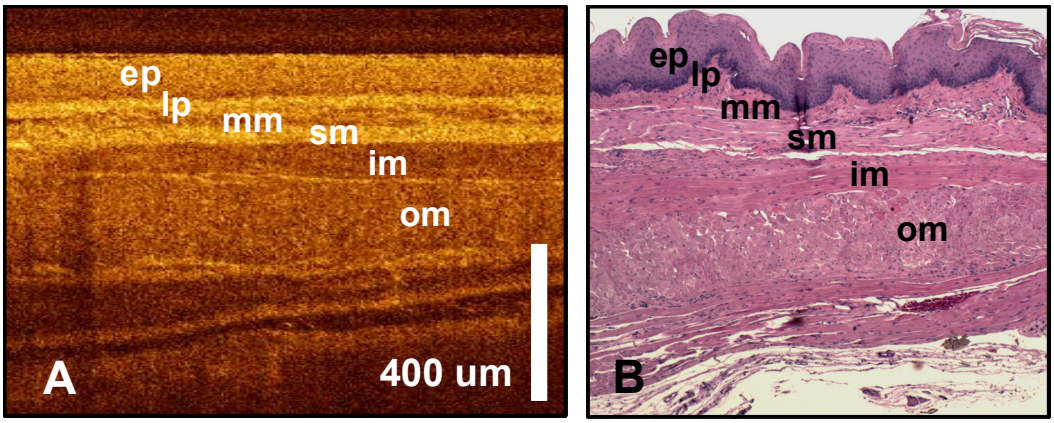

Figure 3. (A) *In* vivo endoscopic OCT image of rabbit esophagus with corresponding histology (B). Good correlation is seen between the OCT and histological cross sections for epithelium (ep), lamina propria (lp), muscularis mucosa (mm), submucosa (sm), and inner (im) and outer muscular (om) layers.

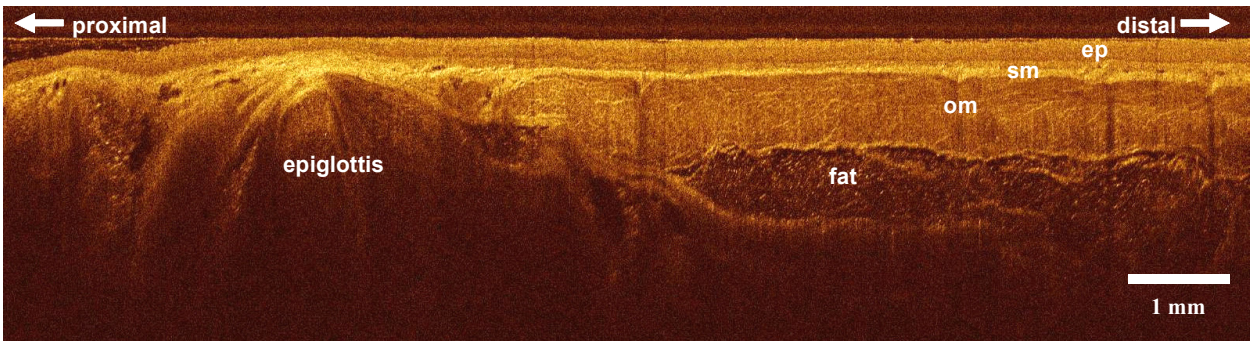

Figure 4. *In* vivo OCT image of sequential scans that span from the rabbit epiglottis to the inner esophagus. High resolution imaging capability is maintained over a large tissue field, thus allowing detailed discrimination of tissue structure.

In Figure 5, an *in vivo* OCT image and a corresponding histology of the rabbit colon are shown. The OCT image shows a highly scattering and multistructured layer at the surface that correlates with the colonic mucosa. Individual crypts can be seen in the OCT image and they correlate well with the histology. The crypt features within the mucosa are visualized at greater detail in the 3x magnification images at the right side. Crypt boundaries within the lamina exhibit high scattering intensity in the OCT image, thereby increasing the contrast between individual crypts. This allows the colonic crypt structure to be visualized clearly. The capability to resolve crypt features within the colon is important in the clinical diagnosis of conditions such as inflammatory bowel disease and colon cancer.

In summary, we have developed a high resolution endoscopic OCT imaging system and have obtained high resolution OCT images of the rabbit gastrointestinal tract with minimally invasive catheter devices. Using a compact, broadband Cr^{4+}:Forsterite laser, we demonstrated endoscopic OCT imaging *in vivo* at the highest resolution attained to date. A linear scanning protocol was used to generate high pixel

density images at a real-time imaging rate of 4 frames per second. Histological cross sections were obtained from *in vivo* imaging sites and an excellent correspondence of architectural detail was seen between histopathology and OCT scans. Identification of clinically relevant tissue layers was possible at high resolution and is in agreement with histological findings.

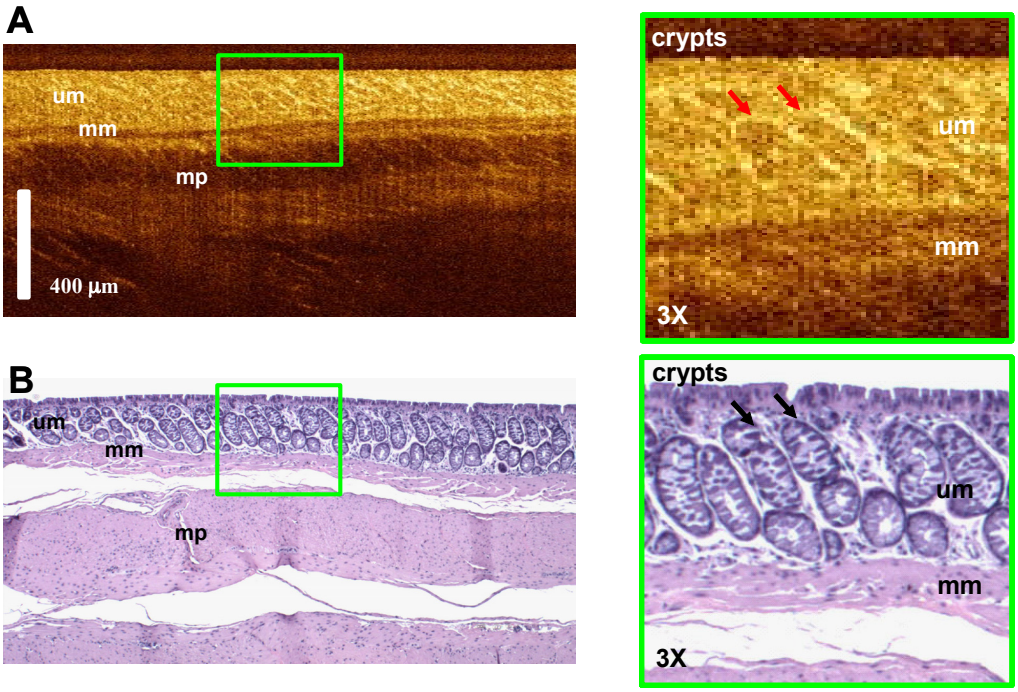

Figure 5. *In* vivo endoscopic OCT image of rabbit colon (A) with corresponding histology (B). Delineation of colon upper mucosa (um), muscular mucosa (mm), and muscularis propria (me) is possible. Enlarged images show the capability to visualize crypt structures in finer details.

These results demonstrate the feasibility of using high resolution endoscopic OCT for the identification of clinically significant architectural features in the gastrointestinal tract. We are currently applying the high resolution endoscopic OCT system in the clinical studies. Ongoing advances in the development of turnkey and portable broadband optical light sources promise greater access to high resolution OCT imaging capability for investigators.

References

1. J.G. Fujimoto, "Optical coherence tomography for ultrahigh resolution in vivo imaging," *Nat Biotechnol* 21(11): 1361-7 (2003).
2. A.M. Sergeev, V.M. Gelikonov, G.V. Gelikonov, F.I. Feldchtein, R.V. Kuranov, N.D. Gladkova, N.M. Shakhova, L.B. Snopova, A.V. Shakov, I.A. Kuznetzova, A.N. Denisenko, V.V. Pochinko, Y.P. Chumakov, and O.S. Streltzova, "In vivo endoscopic OCT imaging of precancer and cancer states of human mucosa," *Optics Express* 1(13): 432 (1997).
3. S. Jäckle, N. Gladkova, F. Feldchtein, A. Terentieva, B. Brand, G. Gelikonov, V. Gelikonov, A. Sergeev, A. Fritscher-Ravens, J. Freund, U. Seitz, S. Schröder, and N. Soehendra, "In vivo endoscopic optical coherence tomography of esophagitis, Barrett's esophagus, and adenocarcinoma of the esophagus," *Endoscopy* 32(10): 750-5 (2000).
4. M.V. Sivak, K. Kobayashi, J.A. Izatt, A.M. Rollins, R. Ung-runyawee, A. Chak, R.C.K. Wong, G.A. Isenberg, and J. Willis, "High-resolution endoscopic imaging of the GI tract using optical coherence tomography," *Gastrointest. Endosc.* 51(4): 474-479 (2000).

5. B.E. Bouma, G.J. Tearney, C.C. Compton, and N.S. Nishioka, "High-resolution imaging of the human esophagus and stomach in vivo using optical coherence tomography," *Gastrointest. Endosc.* 51(4) Pt 1: 467-74 (2000).
6. X.D. Li, S.A. Boppart, J. Van Dam, H. Mashimo, M. Mutinga, W. Drexler, M. Klein, C. Pitris, M.L. Krinsky, M.E. Brezinski, and J.G. Fujimoto, "Optical coherence tomography: advanced technology for the endoscopic imaging of Barrett's esophagus," *Endoscopy* 32(12): 921-30 (2000).
7. J.M. Poneros, S. Brand, B.E. Bouma, G.J. Tearney, C.C. Compton, and N.S. Nishioka, "Diagnosis of specialized intestinal metaplasia by optical coherence tomography," *Gastroenterology* 120(1): 7-12 (2001).
8. P.R. Pfau, M.V. Sivak, A. Chak, M. Kinnard, R.C.K. Wong, G.A. Isenberg, J.A. Izatt, A. Rollins, and V. Westphal, "Criteria for the diagnosis of dysplasia by endoscopic optical coherence tomography," *Gastrointest. Endosc.* 58(2): 196-202 (2003).
9. F.X. Kartner, N. Matuschek, T. Schibli, U. Keller, H.A. Haus, C. Heine, R. Morf, V. Scheuer, M. Tilsch, and T. Tschudi, "Design and fabrication of double-chirped mirrors," *Optics Letters* 22: 831-833 (1997).
10. G.J. Tearney, M.E. Brezinski, B.E. Bouma, S.A. Boppart, C. Pitvis, J.F. Southern, and J.G. Fujimoto, "In vivo endoscopic optical biopsy with optical coherence tomography," *Science* 276(5321): 2037-9 (1997).

2.2 Ultrahigh Resolution High Speed Spectral Domain OCT for Ophthalmology

Sponsors
National Institutes of Health – R01-EY11289-18, R01-CA75289-06
National Science Foundation – ECS-01-19452, BES-0119494
Air Force Office of Scientific Research – MFEL F49620-01-1-0186, F49620-01-01-0084

Project Staff
Dr. Maciej Wojtkowski, Vivek J. Srinivasan, Tony H. Ko, Professor James G. Fujimoto, Dr. Jay S. Duker (NEEC)

Ultrahigh resolution optical coherence tomography (OCT) has improved the differentiation of architectural morphology in the retina and can visualize subtle changes associated with early disease [1,2]. One limitation of standard OCT using time domain detection is that high resolution imaging requires a decrease in imaging speed. Because light exposure levels in the eye are limited, the imaging speed possible with a time domain detection system is limited by the minimum sensitivity required for good image quality. Fourier domain techniques such as spectral domain OCT do not have this limitation, thus making it possible to image with ultrahigh resolution and high speed. With the higher speeds enabled by spectral domain OCT, it is possible to form three-dimensional maps of the macula and optic disk *in vivo*. This enables cross-registration of three-dimensional data sets with fundus photographs for a more accurate diagnosis of disease and evaluation of treatment outcomes. Video-rate movies of dynamic processes in the eye are also possible. High-quality images can be generated by oversampling in the transverse direction and by averaging data, which allows for the enhanced visualization of intraretinal layers and better segmentation. Furthermore, spectral domain OCT has the advantage of providing direct access to the spectral fringe pattern, thus enabling a wide range of novel applications in Doppler flow imaging [3], absorption measurement [4], dispersion compensation [5], and complex spectral analysis [6].

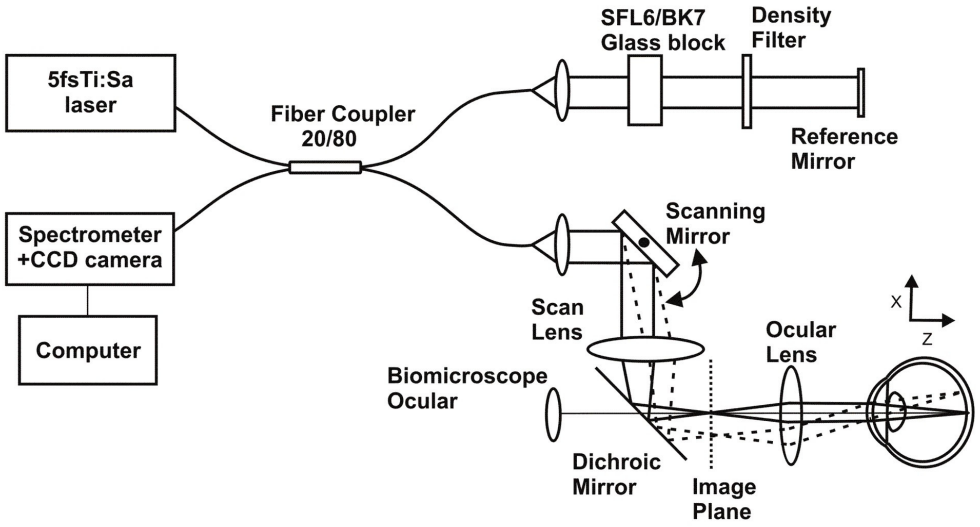

Figure 1. Schematic diagram of the ultrahigh resolution spectral domain OCT system. Retinal imaging was performed using a slitlamp biomicroscope. Optical materials were used in the reference arm to compensate dispersion mismatch between the reference and sample arm optical components. The spectrometer consisted of a collimating lens, a transmission grating, and a lens that imaged the spectrum onto a 2048-element-line-scan CCD.

In spectral domain OCT, a spectrometer with a multichannel analyzer is used to acquire and process the spectral components of the optical signal. Backreflected or backscattered light from all axial depths in the sample is acquired simultaneously as an interferometric spectrum and is processed in software in order to obtain the axial or depth scan. This method is different than time domain detection, where a reference

arm with a variable delay is scanned and data from different axial depths is sequentially acquired. A schematic of the spectral domain ultrahigh resolution ophthalmic system is shown in Figure 1. Note that it differs from the time domain system: the reference arm is stationary, a spectrometer and CCD camera are used in place of time domain electronics, and the software processing is computationally more intensive. Because of its detection method, spectral domain OCT has an inherent sensitivity and/or speed advantage over time domain OCT. In time domain OCT, the signal noise increases with increasing detection bandwidth. Since ultrahigh resolution requires broadband sources and high optical bandwidths, the imaging speed must be reduced so that the electronic detection bandwidth decreases and the image quality is maintained. Alternatively, the imaging speed may be increased if a reduction in sensitivity can be tolerated. With spectral domain OCT, no such penalty in sensitivity is incurred by increasing the imaging speed and/or source bandwidth.

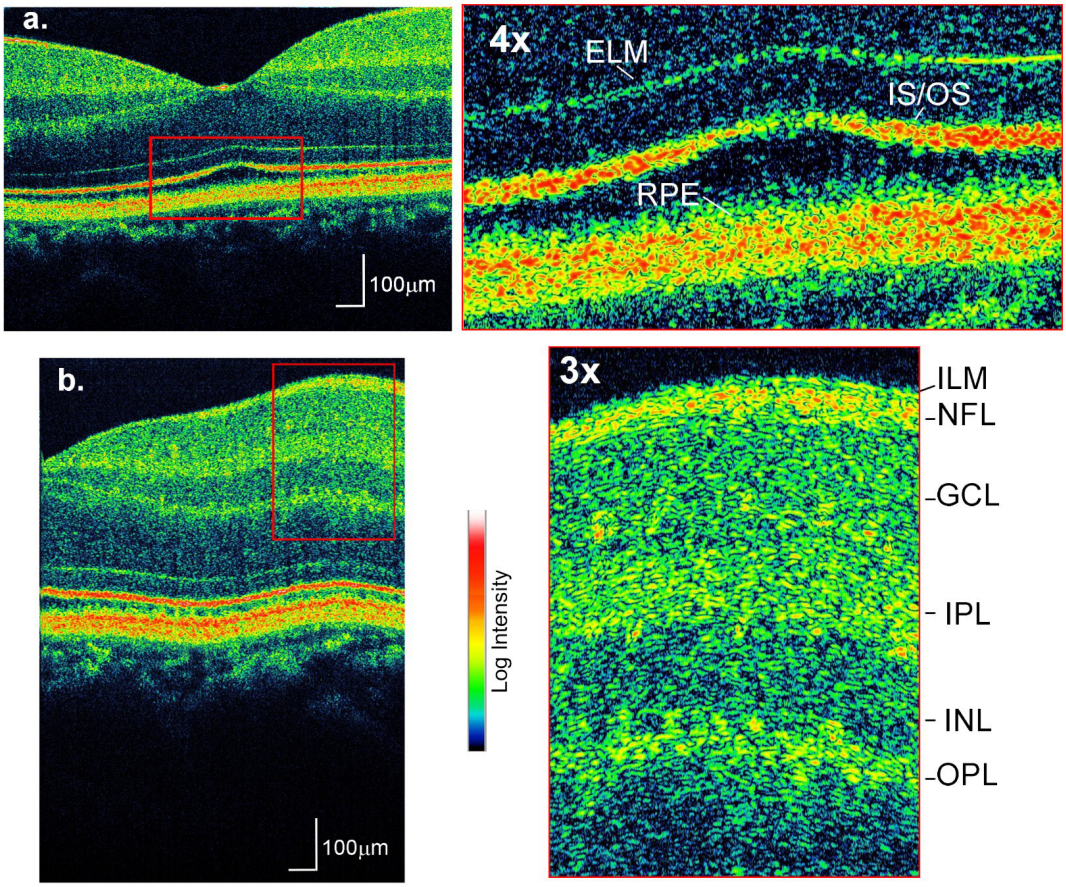

Figure 2. Spectral domain OCT images of the human retina *in vivo*. Scans was taken along the papillomacular axis, with 3000 axial scans acquired in 150 ms. a) The high transverse pixel density and high sensitivity allow a better discrimination of thin retinal layers, including the external limiting membrane (ELM), the photoreceptor inner and outer segment junction (IS/OS), and the retinal pigment epithelium (RPE). b) The inner limiting membrane (ILM) can also be discriminated from the nerve fiber layer (NFL) in the 3x image. Note that the image quality is maintained in the zoomed images due to the high transverse pixel density.

Spectral domain OCT was recently applied to retinal imaging [7] and has been shown to achieve better imaging speed and sensitivity than time domain OCT [8,9]. Recently, video-rate retinal *in vivo* imaging was demonstrated by using spectral domain OCT [10]. Our group was first to demonstrate ultrahigh resolution high speed retinal imaging by using spectral domain OCT [5]. Acquisition of 16,000 axial scans per second with 1024 pixels per axial scan was demonstrated by using a 12-bit, 2048-pixel-line-scan

camera. 2.1 μm resolution was achieved with a 5 fs Ti:Sapphire laser [11] and a broadband spectrometer design. The system sensitivity was 98 dB, thus yielding excellent image quality as shown in Figure 2. In addition, we have demonstrated that spectral domain OCT enables an increase of 100x in imaging speed improvement over time domain OCT in ultrahigh resolution imaging. A comparison of spectral and time domain ultrahigh resolution images is shown in Figure 3. We have also developed an efficient software procedure for automatic dispersion compensation, an important factor in achieving ultrahigh resolution [5]. We have built a clinical spectral domain OCT system using a low-threshold, compact Ti:Sapphire laser[12], and have demonstrated three-dimensional imaging of retinal pathologies in collaboration with the New England Eye Center at the Tufts-New England Medical Center, as shown in Figure 4. We will continue to research the applications of spectral domain OCT through clinical studies, as well as conduct basic research on system design and imaging techniques.

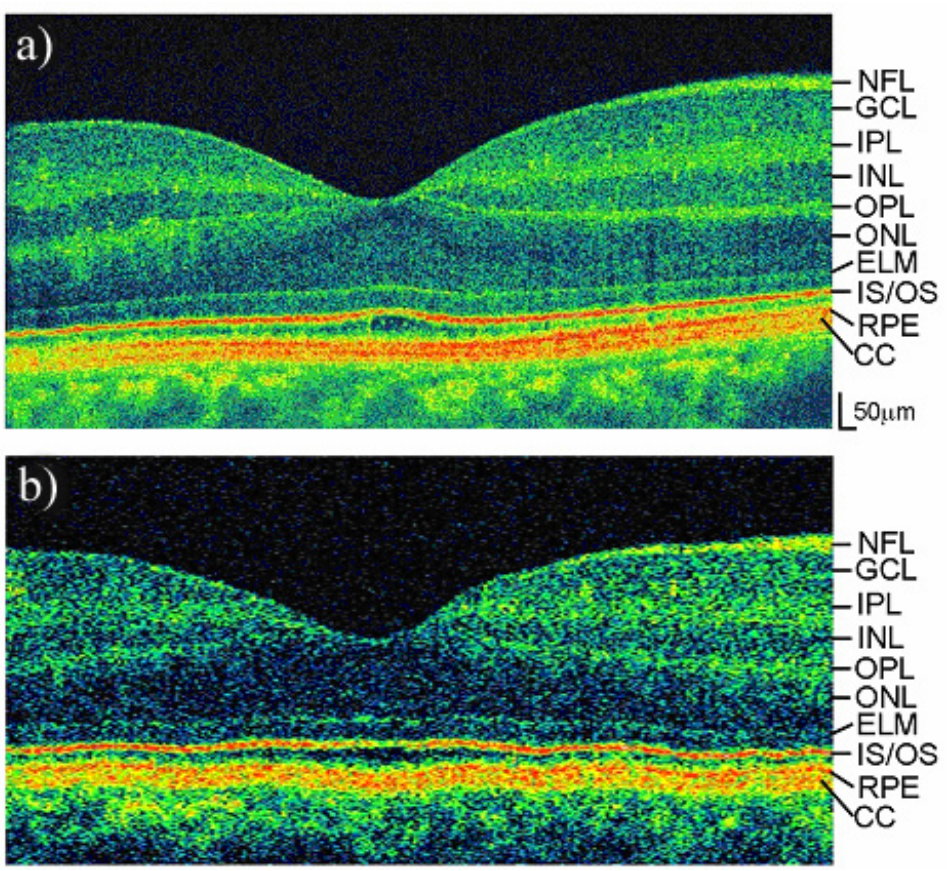

Figure 3. Comparison of ultrahigh resolution spectral domain OCT (a) and ultrahigh resolution time domain OCT (b). The spectral OCT image consists of 3000 axial scans and was acquired in 150 ms. The time domain image consists of 300 axial scans and was acquired in two seconds.

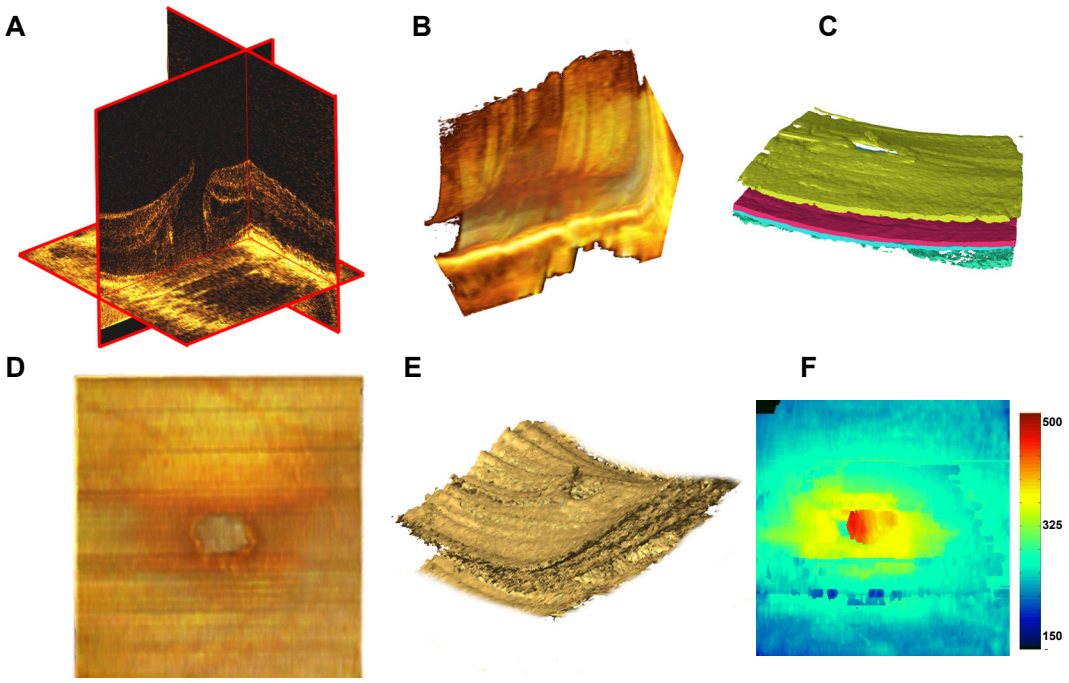

Figure 4. Three-dimensional reconstructions of full thickness macular hole: (A) ortho-slices; (B) virtual rendering; (C) retinal segmentation; (D) en-face view; (E) surface topographic view; (F) full thickness mapping.

References

1. W. Drexler, U. Morgner, R.K. Ghanta, F.X. Kaertner, J.S. Schuman, and J.G. Fujimoto, "Ultrahigh resolution ophthalmic optical coherence tomography," *Nat. Med.* 7: 502-507 (2001).
2. W. Drexler, H. Sattmann, B. Hermann, T.H. Ko, M. Stur, A. Unterhuber, C. Scholda, O. Findl, M. Wirtitsch, J.G. Fujimoto, and A.F. Fercher, "Enhanced visualization of macular pathology with the use of ultrahigh-resolution optical coherence tomography," *Arch. Ophthalmol.* 121(5): 695-706 (2003).
3. R.A. Leitgeb, L. Schmetterer, W. Drexler, A.F. Fercher, R.J. Zawadzki, and T. Bajraszewski, "Real-time assessment of retinal blood flow with ultrafast acquisition by color Doppler Fourier domain optical coherence tomography," *Optics Express* 11(23): 3116-3121 (2003).
4. R. Leitgeb, M. Wojtkowski, A. Kowalczyk, C.K. Hitzenberger, M. Sticker, and A.F. Fercher, "Spectral measurement of absorption by spectroscopic frequency-domain optical coherence tomography," *Optics Letters* 25(11): 820-2 (2000).
5. M. Wojtkowski, V.J. Srinivasan, T.H. Ko, J.G. Fujimoto, A. Kowalczyk, and J.S. Duker, "Ultrahigh resolution, high speed, Fourier domain optical coherence tomography and methods for dispersion compensation," *Optics Express*, forthcoming.
6. M. Wojtkowski, A. Kowalczyk, R. Leitgeb, and A.F. Fercher, "Full range complex spectral optical coherence tomography technique in eye imaging," *Optics Letters* 27(16): 1415-17 (2002).
7. M. Wojtkowski, R. Leitgeb, A. Kowalczyk, T. Bajraszewski, and A.F. Fercher, "In vivo human retinal imaging by Fourier domain optical coherence tomography," *Journal of Biomedical Optics* 7(3): 457-63 (2002).
8. R. Leitgeb, C.K. Hitzenberger, and A.F. Fercher, "Performance of Fourier domain vs. time domain optical coherence tomography," *Optics Express* 11(8) (2003).
9. M. Wojtkowski, T. Bajraszewski, P. Targowski, and A. Kowalczyk, "Real-time in vivo imaging by high-speed spectral optical coherence tomography," *Opt Lett* 28(19): 1745-7 (2003).

10. N. Nassif, B. Cense, B.H. Park, S.H. Yun, T.C. Chen, B.E. Bouma, G.J. Tearney, and J.F. de Boer, "In vivo human retinal imaging by ultrahigh-speed spectral domain optical coherence tomography," *Optics Letters* 29(5): 480-482 (2004).
11. U. Morgner, F.X. Kartner, S.H. Cho, Y. Chen, H.A. Haus, J.G. Fujimoto, E.P. Ippen, V. Scheuer, G. Angelow, and T. Tschudi, "Sub-two-cycle pulses from a Kerr-lens mode-locked Ti:Sapphire laser," *Optics Letters* 24(6): 411-413 (1999).
12. A.M. Kowalevicz, T.R. Schibli, F.X. Kartner, and J.G. Fujimoto, "Ultralow-threshold Kerr-lens mode-locked Ti:Al_2O_3 laser," *Optics Letters* 27(22): 2037-2039 (2002).

2.3 Digital Signal Processing Techniques for Optical Coherence Tomography

Sponsors
U.S. Army Medical Research Material Command – DAMD 17-01-1-156
National Institutes of Health – R01-CA75289-05
National Science Foundation – ECS-01-19452
Air Force Office of Scientific Research – F49620-01-1-0186
Poduska Family Foundation Fund for Innovative Research in Cancer
Philanthropy of Mr. Gerhard Andlinger
National Science and Engineering Research Council of Canada

Project Staff
Desmond C. Adler, Tony H. Ko, Paul R. Herz, Professor James G. Fujimoto

Digital signal processing (DSP) represents a diverse group of hardware and software technologies that can be used to improve the flexibility, functionality, and image quality of ultrahigh resolution OCT systems. The field of digital signal processing is quite mature and has found many applications in other medical imaging fields such as magnetic resonance imaging, computed tomography, and positron emission tomography. In the specific area of coherent imaging, DSP technology is used in many aspects of synthetic aperture radar and medical ultrasound. To date, however, OCT systems have used very little of this technology.

Two specific areas were identified where DSP technology could fundamentally improve OCT imaging through the application of DSP: the investigation of spectroscopic OCT, where the entire spectrum of the backscattered light is analyzed and used to provide alternative contrast modalities to traditional intensity-based OCT; and development of wavelet-based image enhancement techniques to remove speckle noise and improve signal-to-noise performance of OCT systems, specifically those using low-cost, low-power superluminescent diode light sources.

Spectroscopic Optical Coherence Tomography

Traditional OCT systems analyze the envelope of the demodulated interference signal to produce two-dimensional maps of back-reflected/backscattered light intensity. These maps provide information on tissue microstructure by looking at the amount of light backscattered by the tissue at each point in the sample. However, there is much information encoded in the spectrum of the backscattered light that is not available with intensity-based OCT imaging. For example, different types of tissue will have different scattering and absorption spectra, depending on the cell sizes, blood content, water content, and whether the area is oxygenated or deoxygenated. Although multiple biological structures may scatter the same amount of light (therefore be indistinguishable with intensity-based OCT), the spectrum of the detected light may be different, thus providing an alternative contrast modality. Spectroscopic OCT may have application in functional imaging (by detecting local variations in blood oxygenation), the early detection of cancer (by detecting local variations in cell size or nuclear density), and enhanced tissue differentiation for the detection of other pathologies (by detecting changes in spectroscopic properties of tissue types not normally visible with OCT). A related technique, Doppler flow OCT, is well developed and capable of high-accuracy quantization of blood flow to an accuracy of a few microns of flow per second [1,2]. This method measures the Doppler shift of local spectra to produce quantitative maps of fluid flow *in vivo*. Earlier work on spectroscopic OCT took a similar approach, creating 2D maps of variations in center wavelength to "spectroscopically stain" standard-intensity images [3]. However, this method has drawbacks that make it unsuitable for many applications, which will be discussed later.

The technique for spectroscopic OCT imaging is based on short time Fourier transform (STFT) analysis. By applying sequential shifts of a local one-dimensional windowing function to each A-scan, and calculating the Fourier transform of the windowed data, an approximate local spectrum can be calculated for every pixel in the image. This requires the complete interference fringe to be acquired and processed using DSP technology. If the sample being imaged were a perfect mirror, the calculated spectra would be identical to the laser spectrum. Spectroscopic analysis produces a four-dimensional data set consisting

of *x* and *y* spatial coordinates, an RF frequency equivalent to an optical wavelength, and a spectral amplitude. To create an interpretable image, it is necessary to condense this information into three dimensions. This forms the critical step in spectroscopic OCT analysis, since the metric chosen to describe the spectrum at each pixel strongly affects the contrast enhancement of the system as well as the types of spectroscopic properties that will be visible. Metrics based on spectral modulation, which constitute an indirect measurement of scattering particle size, were developed and applied to developmental biology specimens. Traditional center wavelength analyses were also carried out on scattering tissue samples, such as the hamster cheek pouch, thus demonstrating the ability to detect deeply buried blood vessels *in vivo*.

Figure 1 shows a standard intensity-based OCT image of a Syrian golden hamster cheek pouch, acquired *in vivo*. Figure 2 shows the same image after spectroscopic analysis, where the color indicates variations in the center wavelength of the detected spectra. Red colors indicate red-shifting of the spectra, while green colors indicate blue-shifting of the spectra. Blood vessels are clearly visible in Figure 2 as areas of significant red- and blue-shifting, including one deeply buried vessel not visible under standard OCT analysis.

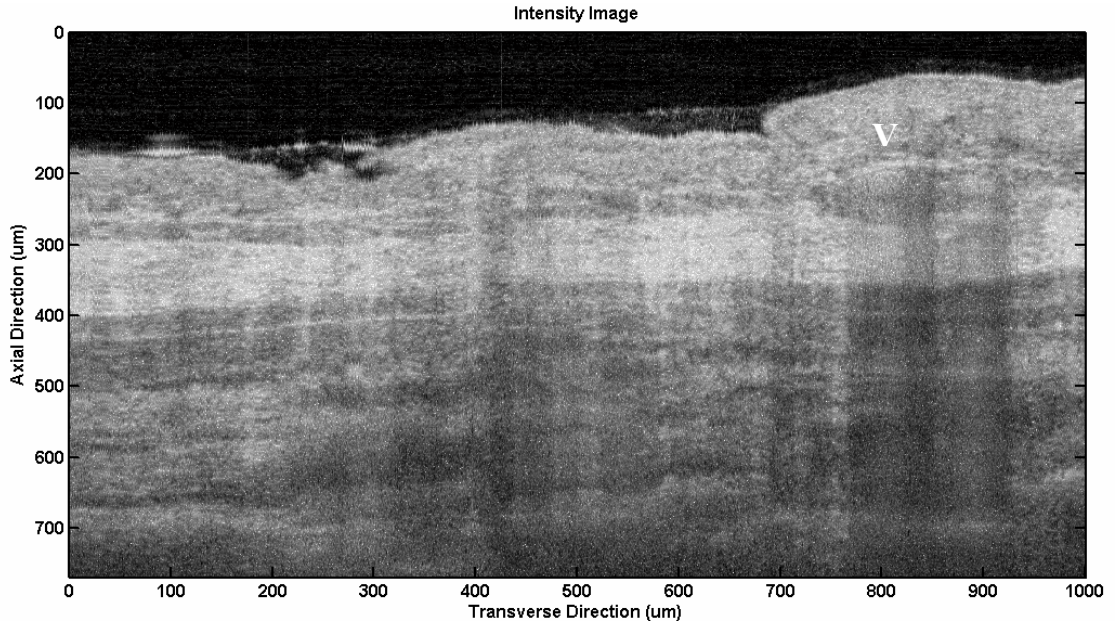

Figure 1. Standard *in vivo* intensity-based OCT image of Syrian golden hamster cheek pouch. Structural features are clearly visualized and blood vessels (V) are visible in upper right portion of image.

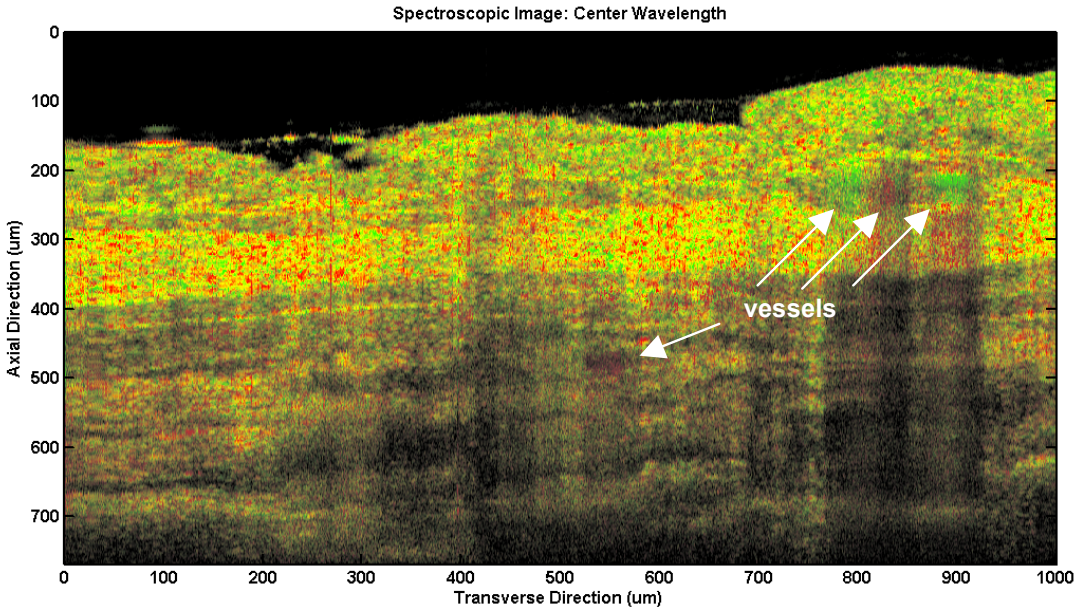

Figure 2. Spectroscopic OCT image of Syrian golden hamster cheek pouch, acquired *in vivo*. Red and green colors indicate red-shifting and blue-shifting of the detected spectra, respectively. Blood vessels are clearly visible under spectroscopic analysis, including a deeply buried vessel not visible with intensity-based OCT imaging.

Spectroscopic analysis based on a calculation of the center wavelength of the detected spectra is useful, but other analysis methods can be used to provide alternative contrast modalities. For example, there is a correlation between the size of biological scattering particles and the spectral modulation observed by interferometry [4-11]. Central to this method is the idea that cellular organelles of epithelial tissue can be considered as spheroidal scatterers whose interactions with light are governed by Mie theory [12,13]. By quantifying the spectral modulation at each pixel in a spectroscopic OCT image, it is possible to differentiate tissue types based on the size of the scattering particles contained in the tissue. Figure 3 shows a standard intensity-based OCT image of a developing Xenopus Laevis (African frog) tadpole. Figure 4 shows the same image after spectroscopic processing, using an analysis of spectral modulation to generate the color overlay. Here, red colors indicate areas of low modulation, while blue colors indicate areas of high modulation. The various tissue types of the tadpole are spectroscopically differentiated based on the scattering particle sizes contained in the tissues. This method may eventually enable the detection of early-stage epithelial cancers, which are characterized by an abnormal proliferation of epithelial basal membrane cells having organelle sizes that differ from surrounding cells.

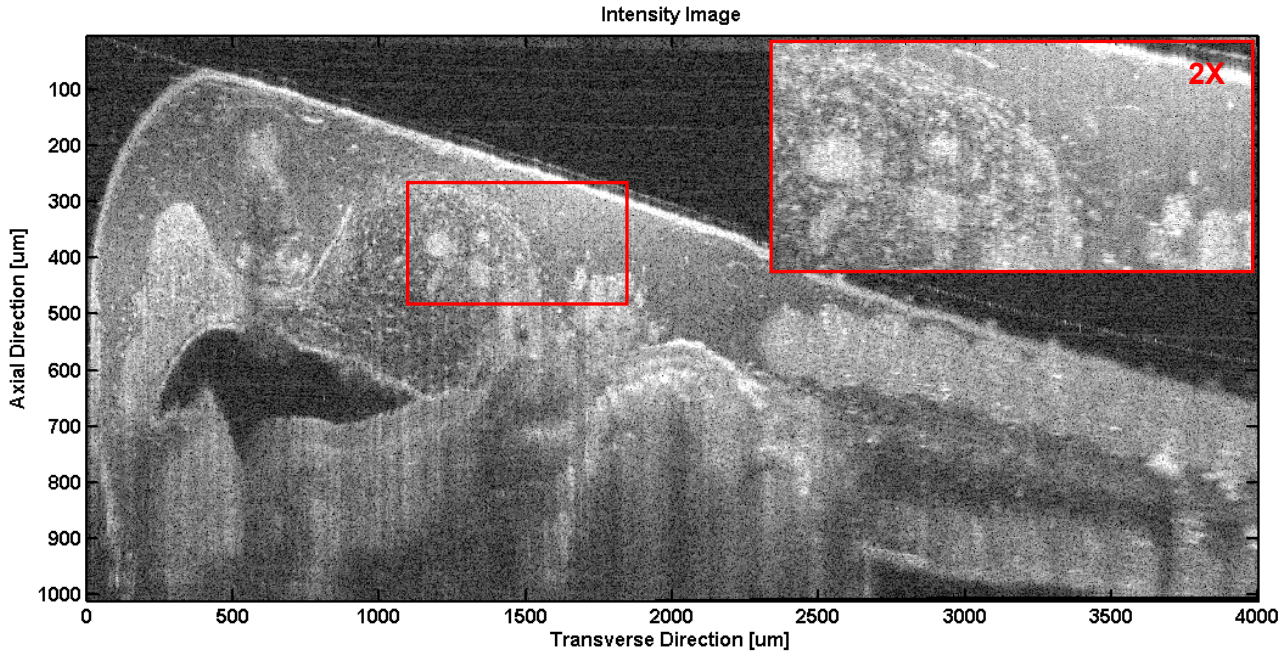

Figure 3. Standard *in vivo* intensity-based OCT image of a developing Xenopus Laevis (African frog) tadpole.

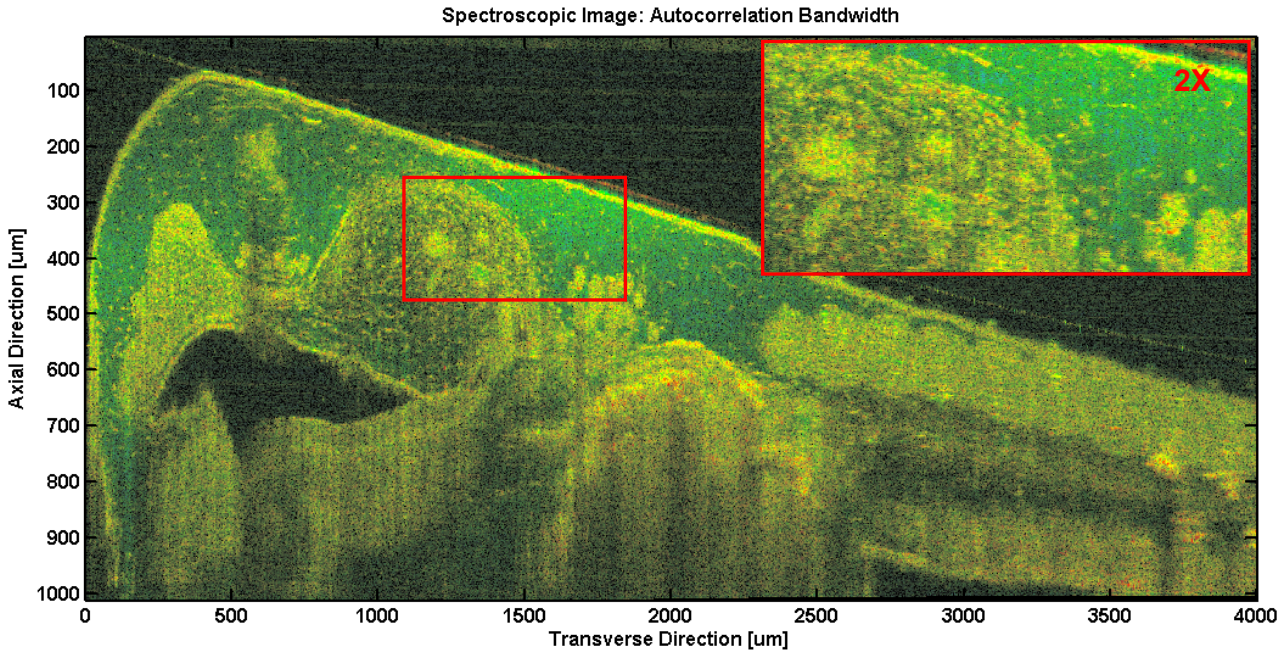

Figure 4. *In vivo* spectroscopic OCT image of a developing Xenopus Laevis (African frog) tadpole, using spectral modulation to generate the color overlay. Red regions indicate low spectral modulation, while blue areas high spectral modulation. Spectroscopic contrast is obtained between the various tissue types of the organism.

Image Enhancement using Wavelet Processing

In any medical imaging technique, it is important to provide the clinician with an image that is as free from noise as possible to maximize the system's utility. This is especially true in OCT, due to the inherently low level of the detected signals compared to the noise background. The ability to reduce noise in an image is also important for the accuracy of quantitative data analysis and image segmentation. With the development of high-speed spectral domain OCT, it is becoming possible to rapidly generate full three-dimensional reconstructions of biological tissue. Segmentation of these 3D reconstructions will provide a valuable tool for the diagnosis of disease, especially in ophthalmic and vascular imaging. A significant reduction in image noise will greatly improve the accuracy of these segmentation techniques. Furthermore, the development of new broadband SLD light sources for OCT may potentially enable the widespread adoption of ultrahigh resolution OCT imaging. These light sources, however, have much lower output power than femtosecond lasers. This decrease in output power leads to a degradation in signal-to-noise ratio (SNR), which must be compensated by image enhancement techniques.

Since OCT is a coherent imaging technique like ultrasound and synthetic aperture radar (SAR), the main source of noise is coherent speckle [14]. Speckle noise is present in an OCT system when the sample contains multiple scattering particles within the active volume of the imaging beam. Speckle appears as localized regions of constructive and destructive interference in the final image, thus giving the image a granular appearance and making it difficult to detect the boundaries between tissue layers.

A significant amount of work has been carried out on speckle reduction in OCT imaging. Several methods based on spatial or angular compounding have been described [14-17] and make use of incoherent averaging over multiple "looks" at the same location in the tissue sample. Since the speckle pattern is uncorrelated at slightly different observation positions or angles, these techniques are capable of reducing the speckle in proportion to the number of data sets acquired. The main drawback to these techniques is that multiple data sets must be acquired for every desired image, and more complicated OCT systems are required for angle-sensitive measurement. The speckle pattern in OCT images is also uncorrelated across optical frequencies, so incoherent averaging over multiple data sets acquired by using sources with different center wavelengths will also reduce speckle noise [14,18]. The drawback is that multiple broadband sources are required, which dramatically increases the system cost and complexity. Time domain filtering techniques based on the rotating kernel transform (RKT) have been investigated for OCT speckle reduction [19,20]. These produce good contrast enhancement of gross image features, but also a significant blurring of edge boundaries.

Wavelet-based denoising techniques are another class of filtering methods capable of reducing coherent speckle noise. They have had widespread application in ultrasound and SAR imaging in recent years due to their excellent noise reduction properties and their capability to maintain image sharpness. Application to OCT speckle reduction has been relatively limited [21,22], with most of the work focused on fairly simple coefficient thresholding schemes that do not take full advantage of the properties of wavelet decompositions. For OCT imaging, a spatially adaptive technique based on the process described by Chang *et al.* [23] was investigated for the noise reduction of UHR-OCT images acquired with a broadband SLD light source [24]. Figure 5 shows a comparison between an unprocessed image of a normal human retina acquired with a broadband SLD light source, and the same image after wavelet processing. The algorithm separates edge features from noise in the wavelet domain, and removes the noise without significantly degrading the edge sharpness. The algorithm can improve the signal-to-noise ratio (SNR) of OCT images by 8 dB, while retaining 95% edge sharpness of the original.

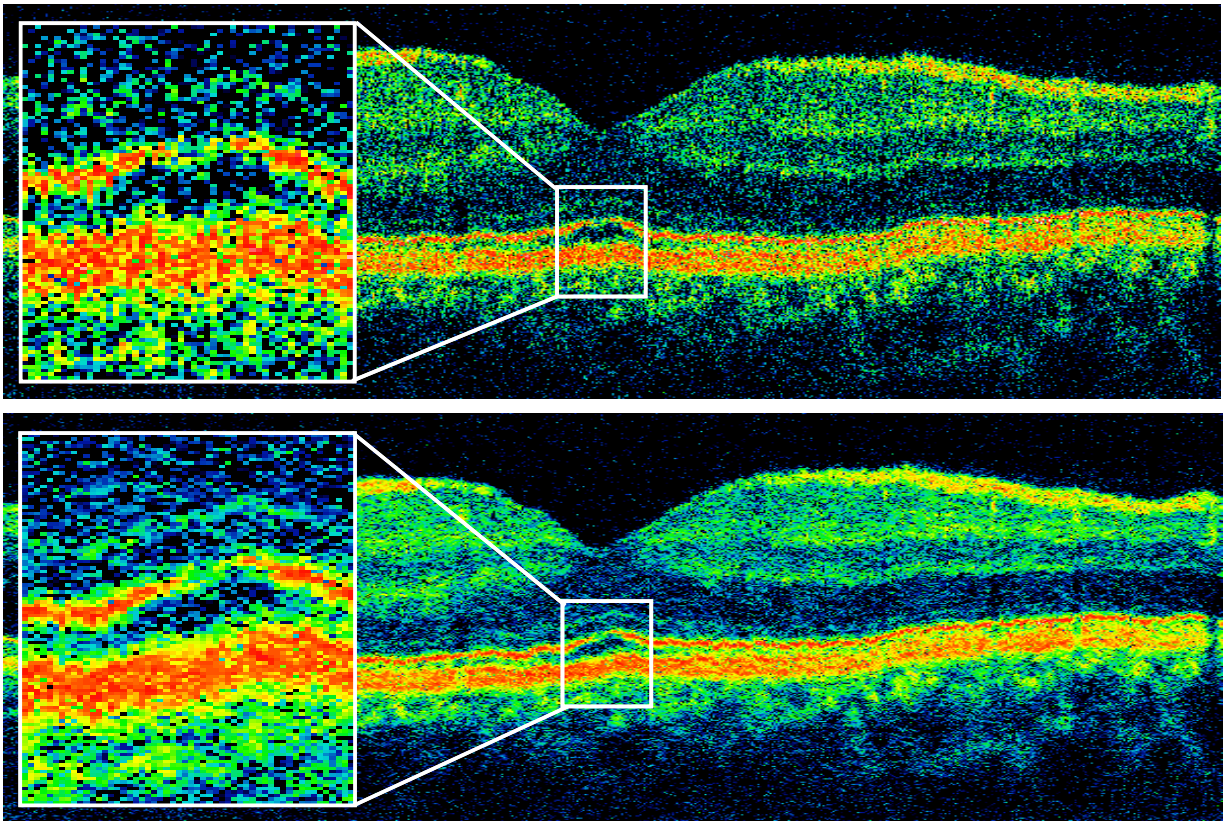

Figure 5. Ultrahigh resolution OCT image of a normal human retina before denoising (a) and after denoising with a spatially adaptive wavelet filter (b). The denoised image has greatly decreased speckle artifacts, with an 8dB improvement in SNR over the original image while maintaining image sharpness to 95% of the original.

The results of spectroscopic processing of OCT images, and wavelet processing for noise reduction of OCT images, illustrate that DSP technology can significantly enhance the functionality and quality of OCT systems. Spectroscopic OCT promises to enable the investigation of alternative contrast modalities, thus differentiating tissue types and potentially identifying diseased areas by using their spectroscopic properties. Wavelet image processing techniques are capable of quantitatively improving OCT image quality and removing speckle noise without significantly affecting the sharpness of features.

References

1. V. Westphal, S. Yazdanfar, A.M. Rollins, and J.A. Izatt, "Real-time, high velocity-resolution color Doppler optical coherence tomography," *Optics Letters* 27(1): 34-6 (2002).
2. S. Yazdanfar, A.M. Rollins, and J.A. Izatt, "In vivo imaging of human retinal flow dynamics by color Doppler optical coherence tomography," *Arch Ophthalmol* 121(2): 235-9 (2003).
3. U. Morgner, W. Drexler, F.X. Kartner, X.D. Li, C. Pitris, E.P. Ippen, and J.G. Fujimoto, "Spectroscopic optical coherence tomography," *Optics Letters* 25(2): 111-13 (2000).
4. L.T. Perelman, V. Backman, M. Wallace, G. Zonios, R. Manoharan, A. Nusrat, S. Shields, M. Seiler, C. Lima, T. Hamano, I. Itzkan, J. Van Dam, J.M. Crawford, and M.S. Feld, "Observation of periodic fine structure in reflectance from biological tissue: a new technique for measuring nuclear size distribution," *Physical Review Letters* 80(January): 627-630 (1998).

5. V. Backman, R. Gurjar, K. Badizadegan, I. Itzkan, R.R. Dasari, L.T. Perelman, and M.S. Feld, "Polarized light scattering spectroscopy for quantitative measurement of epithelial cellular structures in situ," *IEEE Journal of Selected Topics in Quantum Electronics* 5(4): 1019-26 (1999).
6. V. Backman, M. Wallace, L.T. Perelman, J. Arendt, R. Gurjar, M. Muller, Q. Zhang, G. Zonios, E. Kline, T. McGillican, S. Shapshay, T. Valdez, K. Badizadegan, J.M. Crawford, M. Fitzmaurice, S. Kabani, H. Levin, M. Seiler, R.R. Dasari, I. Itzkan, J. Van Dam, and M.S. Feld, "Detection of preinvasive cancer cells," *Nature* 406: 35-36 (2000).
7. M.B. Wallace, L.T. Perelman, V. Backman, J.M. Crawford, M. Fitzmaurice, M. Seiler, K. Badizadegan, S.J. Shields, I. Itzkan, R.R. Dasari, J. Van Dam, and M.S. Feld, "Endoscopic detection of dysplasia in patients with Barrett's esophagus using light-scattering spectroscopy," *Gastroenterology* 119(3): 677-682 (2000).
8. V. Backman, V. Gopal, M. Kalashnikov, K. Badizadegan, R. Gurjar, A. Wax, I. Georgakoudi, M. Mueller, C.W. Boone, R.R. Dasari, and M.S. Feld, "Measuring cellular structure at submicrometer scale with light scattering spectroscopy," *IEEE Journal of Selected Topics in Quantum Electronics* 7(6): 887-93 (2001).
9. R. Gurjar, V. Backman, K. Badizadegan, R.R. Dasari, I. Itzkan, L.T. Perelman, and M.S. Feld, "Imaging human epithelial properties with polarized light scattering spectroscopy," *Nat Med* 7: 1245-1248 (2001).
10. A. Wax, C. Yang, V. Backman, M. Kalashnikov, R. Dasari, and M.S. Feld, "Determination of particle size by using the angular distribution of backscattered light as measured with low-coherence interferometry," *Journal of the Optical Society of America A* 19(4): 737-744 (2002).
11. A. Wax, C. Yang, and J.A. Izatt, "Fourier-domain low-coherence interferometry for light-scattering spectroscopy," *Opt Lett* 28(14): 1230-2 (2003).
12. J. Beuthan, O. Minet, J. Helfmann, M. Herrig, and G. Muller, "The spatial variation of the refractive index in biological cells," *Physics in Medicine and Biology* 41(3): 369-382 (1996).
13. P. Sloot, A. Hoekstra, and C. Figdor, "Osmotic response of lymphocytes measured by means of forward light scattering: theoretical considerations," *Cytometry* 9(6): 636-641 (1988).
14. J.M. Schmitt, S.H. Xiang, and K.M. Yung, "Speckle in optical coherence tomography," *Journal of Biomedical Optics* 4(1): 95-105 (1999).
15. J.M. Schmitt, "Array detection for speckle reduction in optical coherence microscopy," *Physics in Medicine and Biology* 42(7): 1427-39 (1997).
16. M. Bashkansky and J. Reintjes, "Statistics and reduction of speckle in optical coherence tomography," *Optics Letters* 25(8): 545-7 (2000).
17. N. Iftimia, B.E. Bouma, and G.J. Tearney, "Speckle reduction in optical coherence tomography by ""path length encoded"" angular compounding," *Journal of Biomedical Optics* 8(2): 260-3 (2003).
18. M. Pircher, E. Gotzinger, R. Leitgeb, A.F. Fercher, and C.K. Hitzenberger, "Speckle reduction in optical coherence tomography by frequency compounding," *Journal of Biomedical Optics* 8(3): 565-9 (2003).
19. J. Rogowska and M.E. Brezinski, "Evaluation of the adaptive speckle suppression filter for coronary optical coherence tomography imaging," *IEEE Transactions on Medical Imaging* 19(12): 1261-6 (2000).
20. J. Rogowska and M.E. Brezinski, "Image processing techniques for noise removal, enhancement and segmentation of cartilage OCT images," *Physics in Medicine and Biology* 47(4): 641-55 (2002).
21. H. Choi, T.E. Milner, and A.C. Bovik. "Speckle Noise Reduction and Segmentation on Polarization Sensitive Optical Coherence Tomography Images," *Proceddings of the 25th Annual International Conference of the IEEE Engineering in Medicine and Biology Society,* Cancun, Mexico, Sep 17-21, 2003.
22. S.H. Xiang, L. Zhou, and J.M. Schmitt. "Speckle noise reduction for optical coherence tomography," paper presented at the Optical and Imaging Techniques for Biomonitoring III, San Remo, Italy, 1997.
23. S.G. Chang, B. Yu, and M. Vetterli, "Spatially adaptive wavelet thresholding with context modeling for image denoising," *IEEE Transactions on Image Processing* 9(9): 1522-1531 (2000).
24. T.H. Ko, D.C. Adler, D. Mamedov, V. Prokhorov, V. Shidlovski, S. Yakubovich, and J.G. Fujimoto, "Ultrahigh resolution optical coherence tomography imaging with a broadband superluminescent diode light source," *Optics Express*, forthcoming.

2.4 OCT Delivery Devices

The development of medical technologies has had a profound impact on both fundamental biomedical research and clinical patient care. Traditionally, the area of medical imaging has served as a diagnostic tool for the visualization and diagnosis of disease pathologies. While this capability has transformed the medical and healthcare fields, there are incredible opportunities to use imaging technology in increasingly valuable ways. Some of these opportunities include the use of imaging technology for the staging of disease progression, implementation in surgical guidance and for interventional procedures, and as a diagnostic methodology to assess therapeutic conditions both before and after treatment.

One of the enabling factors that have transformed imaging from a purely academic vehicle into a diagnostic, therapeutic, and interventional tool is the development of noninvasive or minimally invasive diagnostic technologies. These technologies include advanced imaging techniques themselves as well as sophisticated diagnostic probes that enable the imaging of internal body organs that would otherwise be inaccessible to various imaging modalities. Such devices are critical for the implementation and realization of OCT as a diagnostic imaging modality, since OCT image penetration is limited to the first several millimeters of a tissue surface. In this section, the design, development, and use of minimally invasive catheter-based probes used in OCT systems will be described.

2.4.1 Micromotor Catheter Probe for Endoscopic Imaging

Sponsors
National Institute of Health – R01-CA75289-06, R01-EY11289-18
National Science Foundation – ECS-01-19452, BES-0119494
Air Force Office of Scientific Research – F49620-01-1-0186, F49620-01-01-0084

Project Staff
Paul R. Herz, Dr. Yu Chen, Aaron D. Aguirre, Karl Schneider, Pei-Lin Hsiung, Professor James G. Fujimoto

Minimally invasive endoscope-catheter imaging probes that can focus and scan a beam inside the body have been an important technology for enabling endoscopic OCT imaging studies. The most common probe design uses a mechanical cable, an optical fiber, and a lens assembly housed in a transparent plastic sheath. The cable within the sheath is either rotated or translated in a push-pull motion to produce a rotary or linear scanning motion of the optics in order to generate a transverse or longitudinal OCT image. However, because the distal optics are actuated from the proximal end of the long probe, this design can result in a nonuniform scanning motion that introduces artifacts in the OCT image. Imaging speeds and duty cycles are limited. In addition, for rotary scan designs, a proximally located rotary optical coupling is required. Forward imaging designs avoid these problems, but scan ranges can be limited. Recent developments in novel MEMS scanning technologies promise distal beam scanning, which would improve the speed and reduce image distortion in endoscopic imaging [1,2]. Despite these advances, previous endoscope-catheter probe designs could not provide focus adjustment during OCT imaging. For this reason, relatively large spot sizes were necessary in order to preserve a sufficient depth of field to enable OCT imaging in intraluminal structures. This limits the transverse image resolution.

We recently developed a new, high resolution, micromotor endoscope-catheter with adjustable focus capability. The mechanical scanning and microoptic components are located at the distal end of the probe, thereby eliminating the need for proximally actuated rotating or translating elements. Distal actuation provides better uniformity of beam scanning with reduced image distortion artifacts and an improved range of image speeds. Standard OCT imaging probes usually require long depth of fields and, therefore, the minimum transverse focused beam sizes are limited. With the ability to independently adjust the optical beam focal position and use higher numerical aperture optics, transverse image resolution can be improved. In addition, an adjustable focus device can enable C-mode OCT imaging (acquiring images with several focal planes and fusing them together) to overcome depth of field

limitations [3]. The micromotor imaging probe also has a larger field of view than conventional OCT endoscope-catheter devices, thereby allowing larger diameter lumens to be more readily visualized.

Figure 1 shows a schematic and photograph of the micromotor endoscope-catheter probe assembly. The probe consists of a distally actuated micromotor and an optical assembly for the beam focusing. The micromotor is a commercially available subsystem (manufactured by Micro Precision Systems AG), which consists of a three-phase brushless DC motor. It has a planetary gearhead design and is configured with a 125:1 gear reduction ratio. A vertical Hall sensor built into the motor is used to accurately control and stabilize the rotation speed with a 5V operating voltage. The optical assembly consists of a GRIN lens collimator and an achromatic focusing lens that move independently of the probe sheath (in a longitudinal direction) in order to adjust the focus position within the tissue.

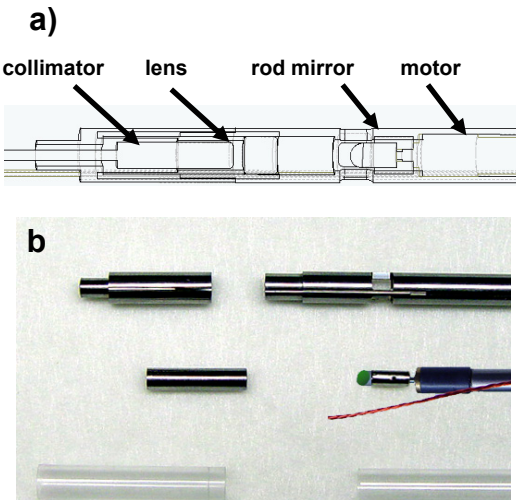

Figure 1. Schematic and photograph of the micromotor catheter assembly and components. a) Wireframe cutaway with fiber collimator, focusing lens, rod mirror, and micromotor enclosed in housing. b) Stainless steel housing and catheter components photographed before assembly. The micromotor is shown with the rod lens attached.

The transverse resolution of the focused optical beam was measured at ~8 μm ($2\omega_0$ spot diameter) by using a knife-edge beam profile technique. The corresponding depth of field or confocal parameter is ~80 μm at a 1250 nm center wavelength. An aluminum-coated rod mirror is mounted onto the motor shaft to direct the focused light onto the tissue and to enable a rotational OCT scan. The motor speed can be adjusted, thus enabling rotation speeds from 1 Hz to 100 Hz. The motor and distal optics fit within a 4.8 mm OD stainless-steel housing, which is enclosed within a 5 mm OD transparent plastic sheath. Control wires to actuate the motor are fed through the tubing to the proximal end of the probe. The fiber collimator and focusing lens are attached to a mechanical speedometer cable, which enables the distal focus to be adjusted by translating the fiber and lens assembly with respect to the fixed scanning motor at the distal end.

The OCT interferometer, which consists of a broadband optical circulator and 90/10 fiber optic beam splitter, transmits 90% of the light into the sample arm and 10% into the reference arm. Dual-channel detection acquired by using polarization diversity is used before digital signal demodulation. A rapid scanning delay line is used in the system reference arm with 2000 axial scans per second. This corresponds to 1000 axial scans per OCT image at a 2 Hz image frame rate. For a probe diameter of 5 mm, this gives a transverse pixel spacing of 15 um/pixel along the probe circumference. A broadband femtosecond Cr:Forsterite laser and nonlinear optical fiber are used as the light source. The measured axial image resolution in air is 5 μm, which corresponds to a resolution of ~3.7 μm in tissue. The imaging scan depth is 4 mm and the axial pixel spacing is 2 μm/pixel. The sensitivity is 92 dB at an incident power of 12 mW.

In order to demonstrate the micromotor endoscope-catheter probe, *in vivo* OCT imaging was performed on an anesthetized New Zealand white rabbit. Animal handling was performed in accordance with protocols approved by the MIT Committee on Animal Care. Imaging was performed on the colon, because the columnar epithelial structure of colonic mucosa provided well-defined tissue morphology for validation of the adjustable focus probe operation. To minimize animal discomfort and to reduce the risk of damaging the colonic mucosa, a sterile bacteriostatic lubricant was used during catheter insertion. Multiple locations within the colon were imaged. At each imaging position, OCT scans were taken at several focus depths to demonstrate the adjustable focusing capability of the probe. The beam focal depth was changed by translating the collimator and focusing lens assembly with respect to the fixed motor assembly.

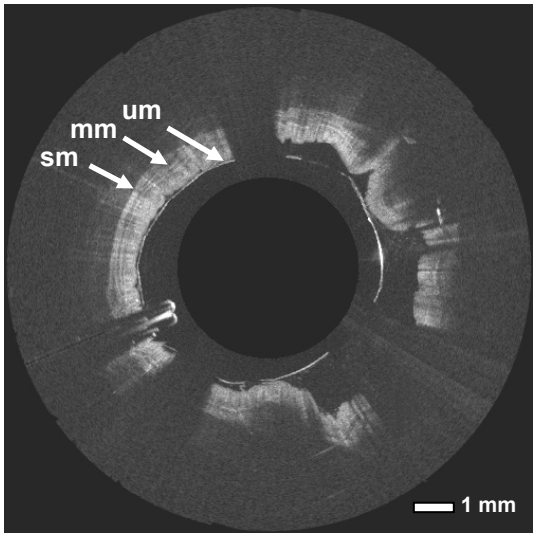

Figure 2. OCT image of rabbit colon *in vivo*. Imaging was performed with < 4 μm axial resolution. Visualization of colonic upper mucosa (um), muscularis mucosae (mm), and submucosa (sm) layers is clear within the colon with > 1 mm image penetration. Shadow regions at the 11 o'clock, 4 o'clock, and 7 o'clock positions indicate areas of housing support struts that occlude approximately 20% of the scan field.

Figure 2 shows an OCT image obtained with the micromotor probe inserted 3 cm inside the colon. The raw image information was converted to polar coordinate display form. Since the axial scans are radially oriented, a bilinear interpolation was performed at larger radii to account for the wider separation of the axial scans. The probe sheath radius is 2.5 mm, while the OCT scan depth extends an additional 2 mm beyond the sheath. The OCT image was able to clearly delineate the upper mucosa (um), muscularis mucosae (mm), and submucosa (sm) regions within the colon. Adjustment of the optical beam focus in real time was also demonstrated. Figures 3 shows enlarged OCT images of a region in the colon with two different beam focus positions. When the focus was set at a shallower position (closer to the probe sheath), it was possible to resolve detailed features near the colonic upper mucosa more clearly (Figure 3a). By focusing deeper inside the tissue, farther from the probe sheath, the visualization of deeper layers improved (Figures 3b). Figure 3c shows two radial A-scans plotted along the dashed lines in the Figure 3a and Figure 3b. A clear difference in the A-scan intensity behavior is observed when the focus is set closer to the tissue surface (Figure 3a), as opposed to deeper in the tissue (Figure 3b).

This micromotor imaging probe design has several attractive features. Adjustable focus enables smaller focused spot sizes and a shorter depth of field than what was previously feasible. The resulting improvement in image resolution could improve the performance of ultrahigh resolution OCT imaging by

enabling a better visualization of tissue pathology. With additional engineering, it should be possible to perform dynamic focusing, where the focal position is adjusted as a function of rotary beam position. This would enable focus tracking in cases where the endoscope-catheter probe was not centered in the lumen. The use of a micromotor for distal actuation reduces the motion nonuniformity that could occur with previous proximally actuated endoscope catheter probes. A wider range of imaging speeds can be achieved with improved duty cycle. Finally, although this prototype imaging probe was 5 mm in diameter, a reduction in probe size is possible with smaller micromotors.

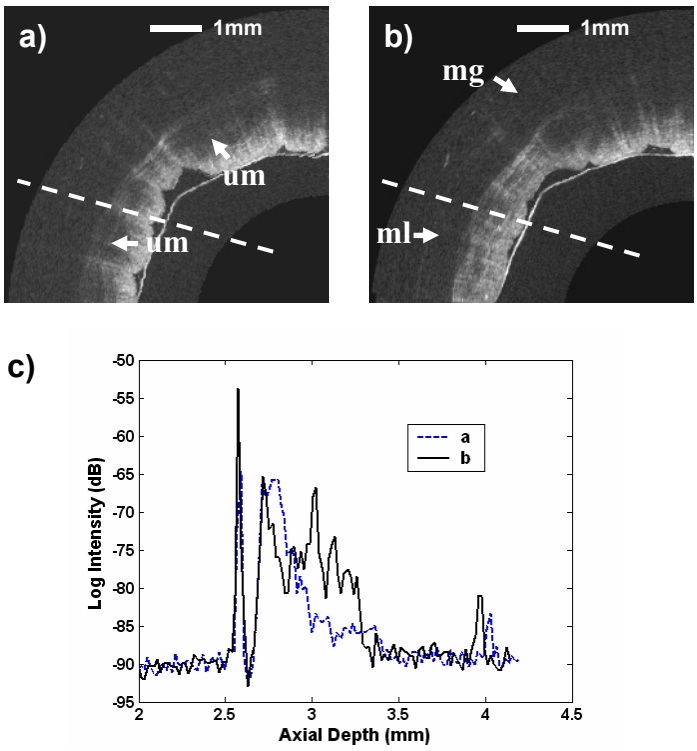

Figure 3. OCT images at two different focus settings. a) Beam focus set near the tissue surface provides a higher contrast within the colonic upper mucosa (um). b) Setting the focus 500 μm deeper enhances the visualization of deeper mucosal layers (ml) and glandular structure (mg). c) Plots of axial scans along the dashed lines for the two focus depth settings (a and b) illustrate the signal enhancement at different depths inside the tissue.

In conclusion, a new micromotor endoscope-catheter imaging probe for OCT has been developed. This device enables focus adjustment and ultrahigh resolution endoscopic imaging. *In vivo* endoscopic imaging was demonstrated in an animal model and ultrahigh resolution imaging with <4 μm axial resolution was demonstrated. This new design promises to improve imaging performance in future endoscopic OCT imaging studies.

References

1. Y. Pan, H. Xie, and G.K. Fedder, "Endoscopic optical coherence tomography based on a microelectromechanical mirror," *Optics Letters* 26(24): 1966-8 (2001).
2. J.M. Zara, S. Yazdanfar, K.D. Rao, J.A. Izatt, and S.W. Smith, "Electrostatic micromachine scanning mirror for optical coherence tomography," *Optics Letters* 28(8): 628-30 (2003).
3. W. Drexler, U. Morgner, F.X. Kartner, C. Pitris, S.A. Boppart, X.D. Li, E.P. Ippen, and J.G. Fujimoto, "In vivo ultrahigh-resolution optical coherence tomography," *Optics Letters* 24(17): 1221-3 (1999).

2.4.2 MEMS Scanner for Endoscopic OCT

Sponsors
National Institute of Health – R01 EY11289-16, R01-CA75289-04
Air Force Office of Scientific Research – F49620-01-1-0186, F49620-01-01-0084
National Science Foundation – BES-0119494

Project Staff
Paul Herz, Aaron D. Aguirre, Dr. Yu Chen, Professor James G. Fujimoto (MIT)
Wibool Piyawattanametha, Li Fan, Shu-ting Hsu, Makoto Fujino, Professsor Ming C. Wu (UCLA)

Optical coherence tomography (OCT) is an emerging technology for high-resolution endoscopic imaging of biological tissues *in situ* and in real time [1]. Endoscopic OCT can distinguish architectural layers *in vivo* and can differentiate normal from tumor lesions within the human gastrointestinal tract. A need for compact, robust scanning devices for endoscopic applications has fueled the development of MEMS scanning mirrors for confocal imaging [2,3] and for optical coherence tomography [4,5]. Demonstrations of MEMS scanning OCT endoscopes, however, have been limited to single-axis scanning. The ability to use two-dimensional (2D) scanners would be an important advance that would permit three-dimensional (3D) imaging *in situ*.

The most important requirement for a MEMS imaging scanner is high resolution. The resolution of an angle scanning device is determined by the angular scan range divided by the angular divergence of the beam that it can scan, commonly known as the number of resolvable spots. To achieve 1000 or more resolvable spots for high resolution imaging, a large optical aperture and a large scan range must be achieved. High scan speed, in the hundred Hz to multiple kHz, is also important for real-time imaging and the footprint of the scanner must be small to allow for easy integration into miniaturized devices. Finally, low power actuation is also necessary to avoid risks to the patient.

To meet the stringent design criteria for a 2D MEMS scanner, we have collaborated with one of the world's leading optical MEMS groups led by Professor Ming Wu at the University of California at Los Angeles (UCLA). The UCLA group was first to demonstrate a two-dimensional surface micromachined scanner [6]. As part of a program sponsored by the National Science Foundation, the UCLA and MIT groups have designed and fabricated novel single- and dual-axis high resolution MEMS scanning mirrors, based on a novel electrostatic angular vertical comb (AVC) drive approach [7]. Figures 1a and 1b show the schematic and SEM of a typical mirror. Comb drive actuators can significantly reduce the scan drive voltage and extend the scan range, as compared to previous parallel-plate scanner designs. The scanner is realized by combining a foundry surface-micromachining process (Multi-User MEMS Processes, MUMPs) with a three-mask deep-reactive-ion-etching (DRIE) post-process. Surface-micromachining provides versatile mechanical design and electrical interconnect, while bulk micromachining offers flat micromirrors and high-force actuators. The actuator uses torsion beams and a gimbal-mounting configuration in order to scan on two axes. Furthermore, our mirror designs implement a large mirror surface area in a small overall form factor that enables large optical aperture and miniaturized device integration.

The 2D MEMS mirror was packaged with imaging optics in a compact aluminum housing to make a miniaturized OCT endoscope. Figure 2 illustrates the package design. The entire device measures < 6 mm in diameter and is compatible with requirements for minimally invasive endoscopic procedures. The housing can be machined for low cost and it allows precise adjustment of optical alignment using tiny set screws. The optics consists of a graded-index fiber collimator followed by an anti-reflection-coated achromat focusing lens that produces a beam diameter (2w) of ~ 13 μm. The mirror is mounted at 45 degrees and directs the beam orthogonal to the endoscope axis in a side-scanning configuration similar to those typically used for endoscopic OCT procedures. Post-objective scanning eliminates off-axis aberration encountered with pre-objective scanning.

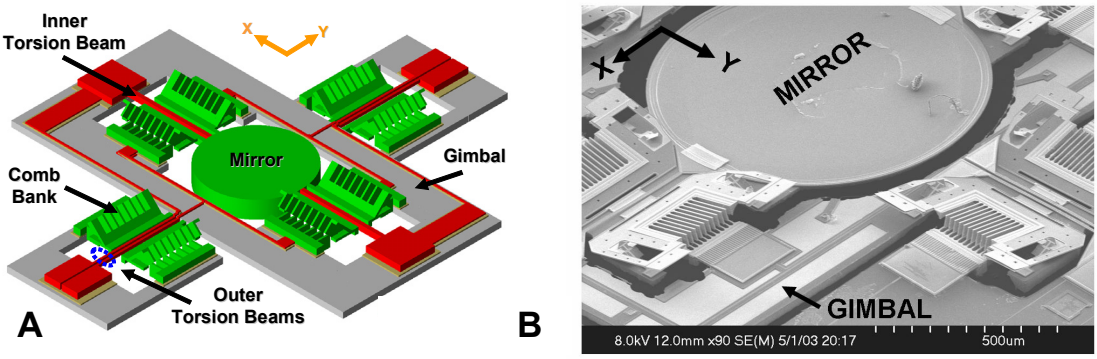

Figure 1. Schematic (A) and SEM (B) of the 2D MEMS scanning mirror. The mirror was realized by a combination of surface-micromachining and deep-reactive-ion-etching (DRIE). It offers a large mirror in a small form factor that enables large optical aperture and miniaturized device integration.

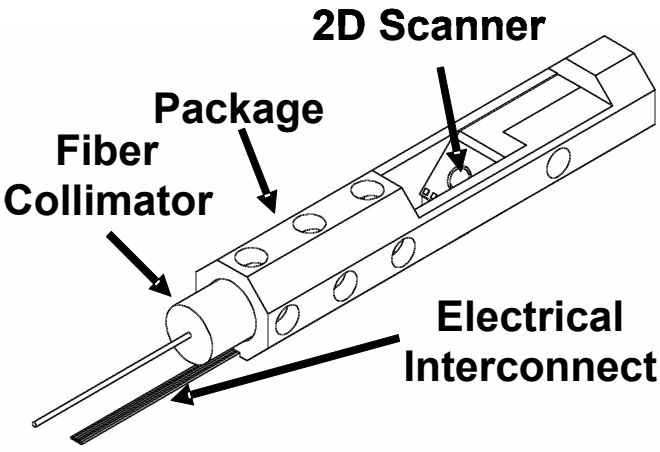

Figure 2. Schematic of packaged MEMS endoscope. The entire device measures less than 6 mm in diameter and can be further reduced in size.

The 2D MEMS scanner can also be used for endoscopic microscopy applications using fast-axis resonant scanning. Figure 3 shows the frequency response for the mirror. High-frequency scan rates up to 1.4 kHz are possible, which should enable real-time microscopy applications.

Preliminary *in vivo* imaging results of human skin were obtained with the MEMS endoscope. A modelocked Cr^{4+}: Forsterite laser centered at 1250 nm with ~ 180 nm bandwidth was used to achieve 5 μm axial resolutions. The transverse resolution was ~ 13 μm. The stratum corneum, epidermis layer, and a spiraling sweat duct are visualized. Figure 3b shows an image of the human nailfold. Good delineation of the nailfold structure can be seen with low image speckle. Acquisition rates ranging from 2 Hz (1000 transverse pixels per image) to 20 Hz (160 transverse pixels per image) were demonstrated. Fast acquisition rates enabled real-time video capture and frame averaging in order to improve image contrast. These results are preliminary and were obtained with uncoated mirror optics. Further improvement in sensitivity should be possible with the next generation of devices.

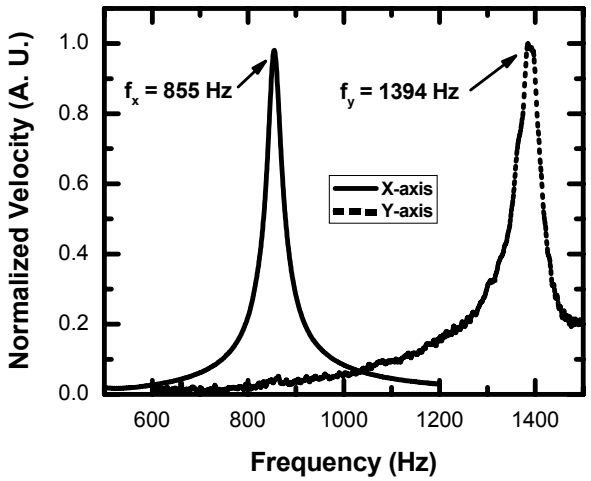

Figure 3. Frequency response of the two-dimensional MEMS scanner. High-speed resonant scanning should enable endoscopic microscopy applications.

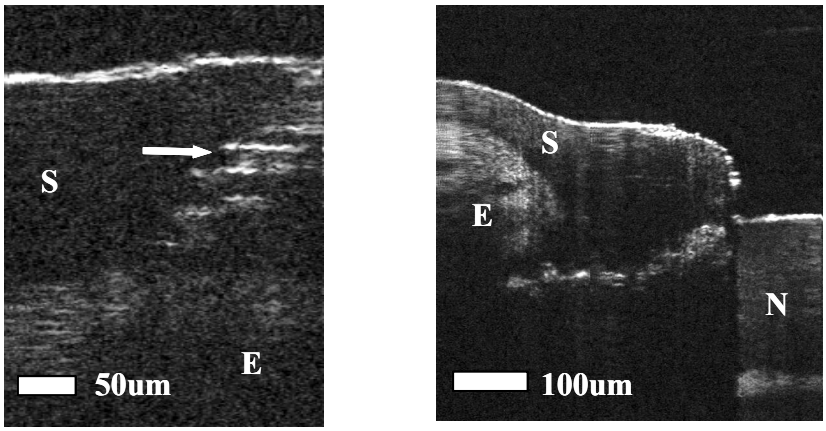

Figure 4. OCT images obtained with the 2D MEMS scanner. (a) *In vivo* image of human skin showing the delineation of stratum corneum (S), epidermis (E), and a spiraling sweat duct (horizontal arrow). (b) Image of human nail fold obtained at 20 frames per second with 4 frame averaging, with stratum corneum (S), epidermis (E), and nail (N) are clearly delineated.

References

1. G.J. Tearney, M.E. Brezinski, B.E. Bouma, S.A. Boppart, C. Pitvis, J.F. Southern, and J.G. Fujimoto, "In vivo endoscopic optical biopsy with optical coherence tomography," *Science* 276(5321): 2037-9 (1997).
2. D.L. Dickensheets and G.S. Kino, "Micromachined scanning confocal optical microscope," *Optics Letters* 21(10): 764-766 (1996).
3. W. Piyawattanametha, H. Toshiyoshi, L. LaCosse, and M.C. Wu. "Surface-micromachined confocal scanning optical microscope," paper presented at the Conference on Lasers and Electro-Optics (CLEO 2000), San Francisco, CA, USA, 2000.
4. Y. Pan, H. Xie, and G.K. Fedder, "Endoscopic optical coherence tomography based on a microelectromechanical mirror," *Optics Letters* 26(24): 1966-8 (2001).

5. J.M. Zara, S. Yazdanfar, K.D. Rao, J.A. Izatt, and S.W. Smith, "Electrostatic micromachine scanning mirror for optical coherence tomography," *Optics Letters* 28(8): 628-30 (2003).
6. L. Fan and M.C. Wu. "Two-dimensional optical scanner with large angle rotation realized by self-assembled micro-elevator," paper presented at the IEEE LEOS Summer Topical Meeting on Optical MEMS, Monterey, CA, 1998.
7. W. Piyawattanametha, P.R. Patterson, D. Hah, H. Toshiyoshi, and M.C. Wu. "A 2D scanner by surface and bulk micromachined angular vertical comb actuators," paper presented at the IEEE/LEOS International Conference on Optical MEMS, HI, USA, 2003.

3. Optical Coherence Microscopy Development

Sponsors
National Institute of Health – R01-EY11289-16, R01-CA75289-04
Air Force Office of Scientific Research – F49620-01-1-0186, F49620-01-01-0084
National Science Foundation – BES-0119494

Project Staff
Aaron D. Aguirre, Pei-Lin Hsiung, Tony H. Ko, Professor James G. Fujimoto

Due to the significant clinical potential for a minimally invasive optical biopsy device, competing techniques have arisen [1]. These include confocal microscopy, multiphoton microscopy, and optical coherence tomography (OCT). These methods differ fundamentally in the means by which they section tissue, and these differences in sectioning method translate into differences in contrast, imaging depth, and available probe technology. None of these technologies has individually met all the needs of an optical biopsy tool. Confocal microscopy can provide high resolution cellular imaging, but it is limited in imaging depth and cannot be easily integrated into miniaturized imaging probes. Multiphoton microscopy also provides cellular resolution and can extend the imaging depth over confocal microscopy, but it is difficult to miniaturize. OCT provides the greatest imaging depth and, by contrast, lends itself to easy integration into miniature devices for widespread clinical application. Standard OCT techniques, however, cannot reliably reach the level of cellular imaging. In order to extend OCT imaging to the cellular level and to address the existing limitations of confocal and multiphoton microscopy, we are developing a method known as optical coherence microscopy (OCM). OCM is a novel extension of OCT and confocal microscopy that allows cellular imaging with superior imaging depth when compared to confocal microscopy alone and it facilitates the design of endoscopic and laparoscopic probes for cellular imaging. OCM promises to extend cellular imaging capability to the vast range of imaging applications previously available only to lower resolution imaging with optical coherence tomography.

OCM combines coherence-gated detection of OCT with confocal rejection of out-of-plane scattered light. These optical sectioning methods complement each other to provide enhanced imaging in highly scattering tissues. To achieve cellular-level imaging, OCM focuses to small spot sizes in tissue, as in confocal microscopy. OCT operates by fixing the focus at a specific depth in tissue and then scanning the coherence gate in the axial direction to generate a cross-sectional image. In order to maintain a sufficient depth of field over the extent of the image, OCT must operate with weaker focusing and lower transverse resolution. OCM is able to overcome this depth of field limitation because it scans an *en face* image plane similar to that of confocal microscopy and multiphoton microscopy. Figure 1 compares the imaging planes for OCM and OCT. In OCM, the position of the coherence gate is precisely matched to the optical focus at a specific depth in tissue and the beam is raster scanned in a two-dimensional *en face* pattern. Because the signal is recorded from a single depth in tissue, and not over a depth scan, a very tight focus can be maintained without the loss of signal that would occur in OCT. In focusing to a smaller spot size, the field of view in OCM must decrease, as in confocal microscopy. A cross-sectional OCT image spans 2-3 mm in each dimension, while a high resolution *en face* OCM image spans only 200-300 micrometers in each dimension, thus it represents only a small range of the OCT image.

OCM has the unique advantage of using two distinct optical sectioning techniques–confocal gating and coherence gating. Generally, the imaging point spread function in an OCM system is determined by the product of the confocal field point spread function $\sqrt{I_C}$ and the source autocorrelation function G, $I_D \propto \sqrt{I_C(z)} \times G(\Delta l)$, where z is the distance of the object from the microscope focus and Δl is the mismatch between the reference arm path length and the path length to the object. The confocal point spread function is entirely determined by the sample arm optics, and in particular, the numerical aperture of the final objective lens. The coherence gate, however, is determined by the light source bandwidth. The degree of confocal rejection of unfocused scattered light can be varied by changing the numerical aperture of the objective lens, while the amount of coherence gated sectioning can be varied by changing the bandwidth of the light source. The multiplicative effect of the two sectioning methods strengthens the overall optical sectioning power, thus allowing increased rejection of unwanted, out-of-focus scattered

light. Studies from our group, as well as others have demonstrated that combined confocal and coherence gating can provide improved imaging depth when compared to confocal gating alone [2-4]. Figure 2a illustrates the imaging depth advantage of OCM. The addition of high-sensitivity coherence-gated detection to confocal detection extends the imaging depth in scattering media to the shot noise quantum limit, thus providing a factor of 2-3 increase over standard confocal microscopy.

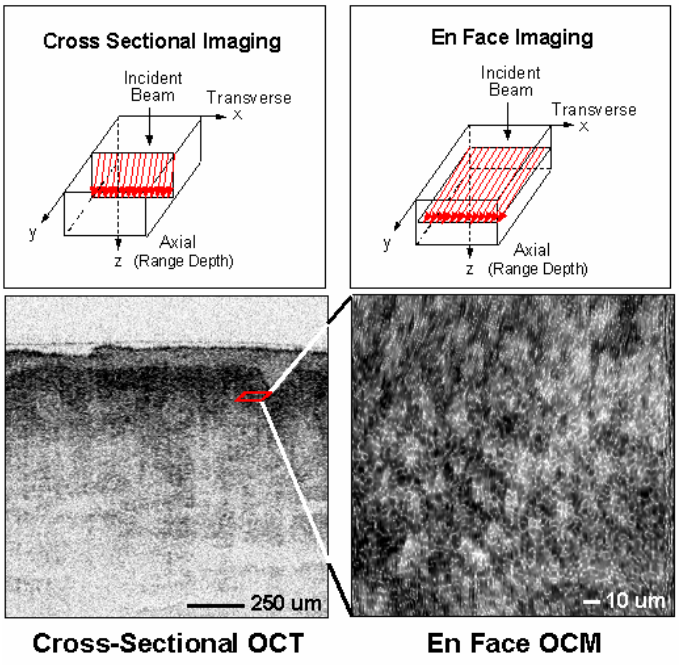

Figure 1. Scan planes for OCT and OCM. OCT scans a cross-sectional image plane and produces images of millimeter dimensions. OCM scans an *en face* image plane and achieves very high transverse resolution over small field of view that spans hundreds of micrometers.

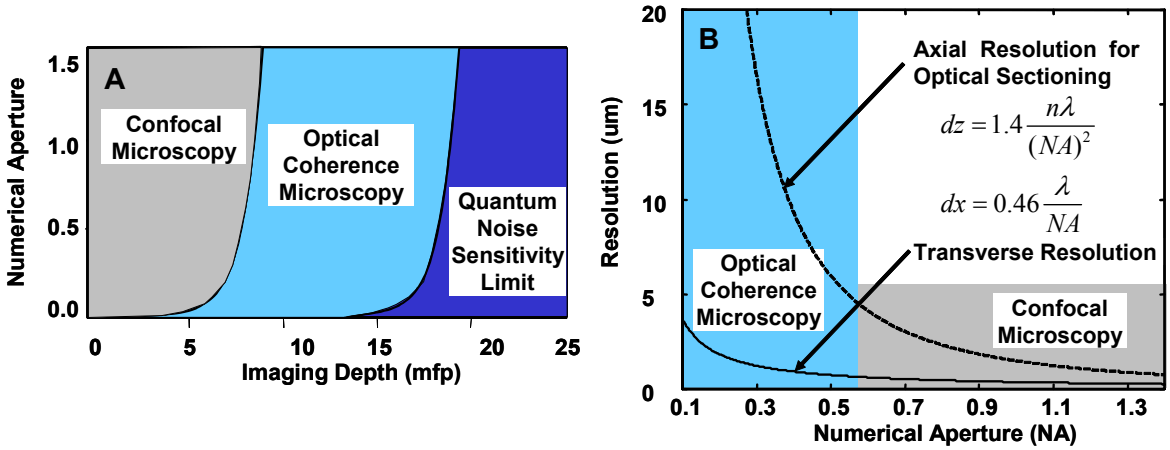

Figure 2. Advantages of OCM when compared to confocal microscopy. OCM can provide increased imaging depth (A). OCM can also image with high transverse resolution at much lower numerical aperture than confocal microscopy, because it does not depend on high axial resolution for optical sectioning (B).

The use of multiple optical sectioning techniques also allows considerable flexibility in system design for achieving high-resolution cellular images. In one limit, high numerical aperture (NA) optics can be used to produce very thin confocal tissue sections, while relatively weak coherence gating can be added to improve rejection of unwanted light. In the other limit, broad-bandwidth light sources as used in ultrahigh

resolution OCT can provide thin optical sectioning via coherence gating, and the confocal sectioning can be relaxed to facilitate development of miniaturized imaging devices. Figure 2b compares the confocal axial and transverse imaging resolution as a function of the numerical aperture of the probe optics in order to demonstrate this operating limit for OCM. The axial section thickness degrades much more quickly than the transverse resolution, and there exists a region where the transverse resolution is sufficient for cellular imaging but the axial resolution is not. Addition of a short coherence gate to provide tissue sectioning can, therefore, make cellular imaging possible with a much lower NA than what is sufficient for confocal microscopy alone. This operating regime for OCM imaging has very important clinical implications, since it promises to allow cellular imaging with small-diameter probes that are compatible with standard endoscopic and laparoscopic procedures.

Recently, we extended previous theoretical work on OCM in order to develop an OCM system suitable for *in vivo* clinical imaging applications [5]. Such a system needs to be capable of high-speed imaging to minimize the amount of motion artifacts in images. In addition, the system should support broad optical bandwidths, as in ultrahigh resolution OCT, to take full advantage of the optical sectioning ability of OCT. Previous attempts at high-speed, high-resolution OCM imaging were limited by the lack of high-speed, broadband phase modulators. Based on previous OCT phase delay scanners [6,7] and femtosecond pulse shaping devices [5,8,9], we designed a novel reflective grating phase modulator capable of performing continuous phase modulation of broadband laser light. Figures 3a and 3b illustrate the phase modulator design in its top and side views. A collimated beam is spectrally dispersed by a grating onto a curved mirror. The curved mirror captures and focuses the diffracted beam onto the galvanometer mirror, which imparts a wavelength-dependent phase shift in the Fourier plane. The modulator is set for double-pass configuration to increase the delay characteristics and to improve backcoupling of the scanned beam. Use of a relatively low dispersion grating and a short focal-length mirror results in zero group delay at a realizable beam offset from the center axis of the scanning mirror. Furthermore, large phase delays of > 1700 radians per degree of mirror rotation can be achieved. Most importantly, the reflective nature of the design allows the modulator to support a large optical bandwidth, thus enabling high resolution OCM imaging.

The imaging system diagram, including the grating phase modulator, is shown in figure 4. Light from a broadband femtosecond laser source is coupled into a fiber optic interferometer, which splits the light equally between the broadband phase modulator and a scanning confocal microscope. Light returning from the phase modulator and from the tissue is recombined at a pair of balanced detectors to produce the image interference signal, which is then demodulated electronically and displayed on a computer screen. The fiber optic geometry makes the system ready for integration with a variety of catheter-based devices for clinical applications. This OCM system is the first system demonstrated that is capable of performing high-speed, high-resolution OCM imaging with broadband femtosecond laser sources.

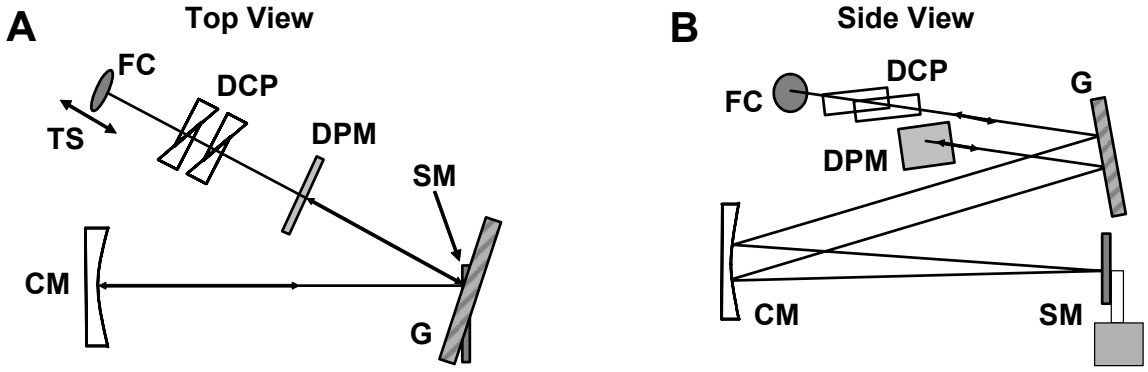

Figure 3. Schematic of reflective grating phase modulator in top (A) and side (B) views. TS, translation stage; FC, fiber collimator; DCP, dispersion compensating prisms; G, grating; CM, curved mirror; SM, scanning mirror; DPM, double-pass mirror. The modulator supports broad optical bandwidths that enable high resolution OCM imaging.

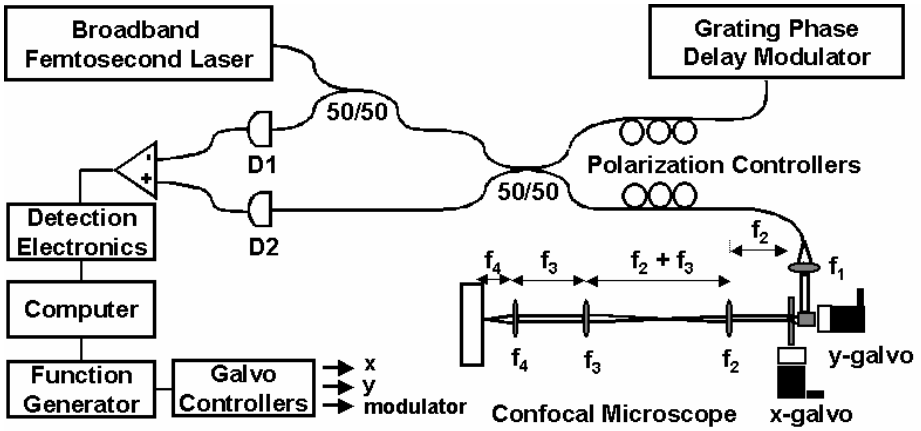

Figure 4. Schematic of broadband, high resolution OCM system.

Using this system, we verified for the first time the ability to use combination coherence gating and confocal gating to image cellular features when confocal micrsocopy alone would be inadequate. In particular, the results show that strong optical sectioning achieved with a short coherence gate can mitigate the need for high numerical aperture confocal optics. Figure 5 demonstrates this concept. A short coherence gate of ~3 μm is combined with a confocal gate of ~30 μm. While this confocal section thickness is nearly six times that of standard histology, a high transverse resolution can still be maintained, as shown by imaging the smallest features of the USAF resolution target, which measures 4.4 μm. The combined gating effects are sufficient for high-resolution *in vivo* imaging of cellular features in various tissues, as demonstrated in Xenopus laevis tadpole and in human skin in Figure 6. In Xenopus tadpole, nuclei (N), cell membranes (CM), and blood cells (BC) inside a vessel (V) are visible, while in human skin, epidermal cells (EC) and a vessel or duct structure (D) in the dermis can be visualized.

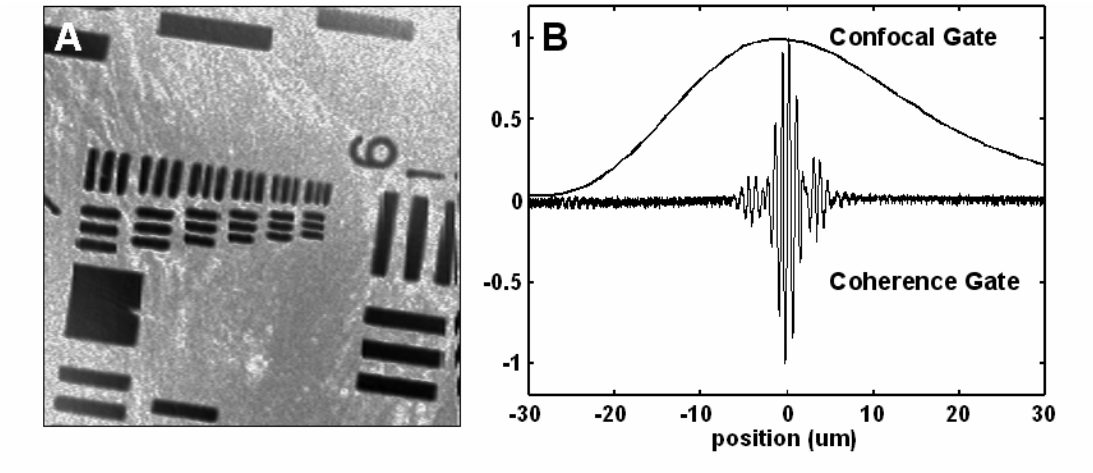

Figure 5. OCM system characterization. A short coherence gate is used to compensate a longer confocal gate, which will moderate probe design constraints on endoscopic imaging. High transverse resolution is maintained, despite weaker confocal sectioning.

Demonstration of this operating limit for OCM marks an important advance because it opens the door for the development of multiple miniaturized OCM imaging probes. Eliminating the need for high NA confocal sectioning will significantly mitigate the design constraints on catheter and rigid endoscope design. Future work will include the demonstration of OCM imaging of multiple tissue types and important pathologies, as well as the development of miniaturized OCM imaging devices for endoscopic and laparoscopic applications.

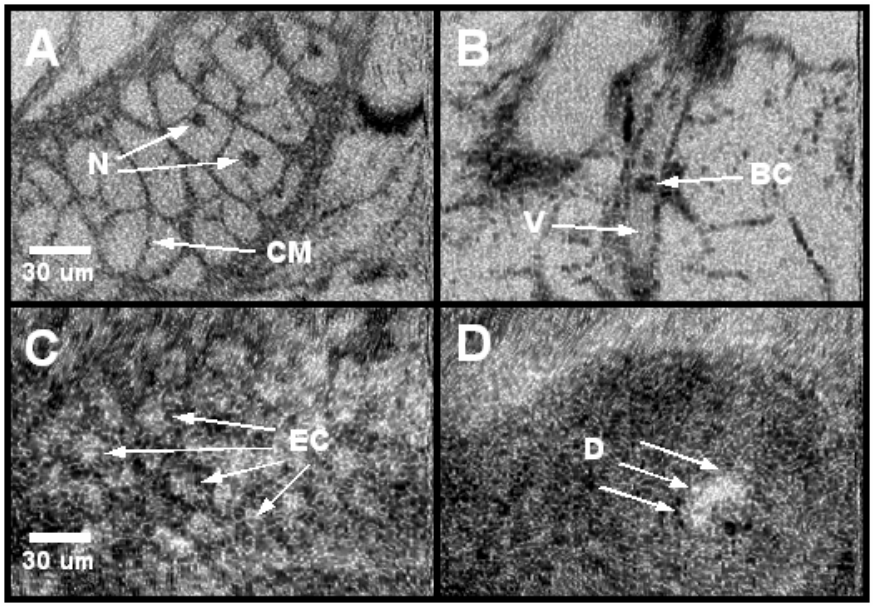

Figure 6. *In vivo* OCM cellular imaging in Xenopus laevis tadpole (A,B) and human skin (C,D). Nuclei (N), cell membranes (CM), and blood cells (BC) inside a vessel (V) are visible in the tadpole images, and epidermal cells (EC) and a vessel or duct structure (D) in the dermis can be seen in the skin images. The images were acquired at 800 nm wavelength at 4 frames per second.

References

1. F. Koenig, J. Knittel, and H. Stepp, "Diagnosing cancer in vivo," *Science* 292(5520): 1401-3 (2001).
2. J.A. Izatt, M.R. Hee, G.M. Owen, E.A. Swanson, and J.G. Fujimoto, "Optical coherence microscopy in scattering media," *Optics Letters* 19(8): 590-2 (1994).
3. M. Kempe, W. Rudolph, and E. Welsch, "Comparative study of confocal and heterodyne microscopy for imaging through scattering media," *J. Opt. Soc. Am. A* 13(1): 46-52 (1996).
4. M. Kempe and W. Rudolph, "Analysis of heterodyne and confocal microscopy for illumination with broad-bandwidth light," *Journal of Modern Optics* 43(10): 2189-2204 (1996).
5. A.D. Aguirre, P. Hsiung, T.H. Ko, I. Hartl, and J.G. Fujimoto, "High-resolution optical coherence microscopy for high-speed, in vivo cellular imaging," *Opt. Lett.* 28(21): 2064-6 (2003).
6. G.J. Tearney, B.E. Bouma, and J.G. Fujimoto, "High-speed phase- and group-delay scanning with a grating-based phase control delay line," *Optics Letters* 22(23): 1811-13 (1997).
7. A.V. Zvyagin and D.D. Sampson, "Achromatic optical phase shifter-modulator," *Optics Letters* 26(4): 187-189 (2001).
8. J.P. Heritage, A.M. Weiner, and R.N. Thurston, "Picosecond pulse shaping by spectral phase and amplitude manipulation," *Optics Letters* 10(12): 609-611 (1985).
9. B.E. Lemoff and C.P.J. Barty, "Quintic-phase-limited, spatially uniform expansion and recompression of ultrashort optical pulses," *Optics Letters* 18(19): 1651-1653 (1993).

4. Optical Biopsy using OCT

Optical Coherence Tomography (OCT) permits the visualization of tissue microstructures *in vivo* and *in situ*, with resolutions of 1-15 μm. Like conventional biopsy and histology, OCT can provide three-dimensional cross-sectional images that may allow differentiation of normal from diseased tissues. However, unlike biopsy, OCT can be performed in real-time and without the need of tissue excision, thus increasing its possible application areas in where the excision biopsy is impossible or undesirable, and potentially allowing the use of OCT in guidance of biopsy or surgery.

We are investigating the use of OCT in imaging a variety of clinically relevant tissue types and pathologies, for application in clinical diagnosis and treatment, and for basic biomedical research. Integration of high resolution OCT into portable systems with various delivering devices described previously offers promise to expand the use of OCT in *in vivo* and *ex vivo* imaging in clinic and pathology lab.

4.1 Ultrahigh Resolution OCT in Ophthalmology

Sponsors
National Institutes of Health – R01 EY11289-16, R01-CA75289-05
U.S. Air Force Office of Scientific Research – F49620-01-01-0084, F49620-01-1-0186
National Science Foundation – ECS-0119452, BES-0119494
The Whitaker Foundation

Project Staff
Tony H. Ko, Desmond C. Adler, Vivek J. Srinivasan, Dr. Maciej Wojtkowski, Professor James G. Fujimoto, Annie Chan (New England Eye Center, NEEC), Dr. Jay S. Duker (NEEC), Dr. Hiroshi Ishikawa (University of Pittsburg Medical Center, UPMC), Dr. Gadi Wallstein (UPMC), Dr. Joel S. Schuman (UPMC)

OCT has perhaps been most widely investigated in ophthalmology, where it is beginning to make a clinical impact in the assessment of retinal diseases such as macular holes, age-related macular degeneration, glaucoma, and diabetic retinopathy [1-5]. Current clinical practice calls for the development of techniques to diagnose ophthalmic disease in its early stages, when treatment is most effective and significant irreversible damage can either be prevented or delayed. Since the introduction of commercial OCT instrumentation for retinal imaging in 1996 by Humphrey Instruments, now Carl Zeiss Meditec, OCT technology has undergone multiple generations of improvement. The introduction of the commercial instrument OCT3 in 2002 achieved a four-fold increase in imaging speed when compared to earlier instruments. The commercial ophthalmic OCT3 system, with ~10 μm axial image resolution, provides more detailed cross-sectional information on retinal pathology than any other ophthalmic diagnostic technique (Figure 1). This system is beginning to achieve widespread acceptance as a standard ophthalmic diagnostic tool and is rapidly becoming available in many ophthalmology clinics. However, the detection of many early changes associated with disease can require a more accurate quantification of retinal structure than what is possible with standard resolution OCT.

Using the broad bandwidth of our ultrahigh resolution (UHR) OCT system, we can image with axial resolutions better than 3 μm in the retina [6], which corresponds to a factor of five-fold improvement when compared to OCT technology that uses conventional superluminescent diode sources. The signal-to-noise ratio for the system is ~95 dB. This system enables a significant improvement in the visualization of intraretinal structures for earlier diagnosis and more precise staging of pathology (Figure 1). Standard resolution OCT3 can visualize major intraretinal morphology such as retinal nerve fiber layer, retinal pigment epithelium, the inner and outer plexiform layers, and the inner and outer nuclear layers. Ultrahigh resolution OCT offers an unprecedented axial resolution to visualize intraretinal morphology such as the external limiting membrane and the photoreceptor inner and outer segments. These intraretinal structures are relevant in a variety of retinal diseases, including age-related macular degeneration, diabetic retinopathy, and glaucoma (the three leading causes of blindness worldwide).

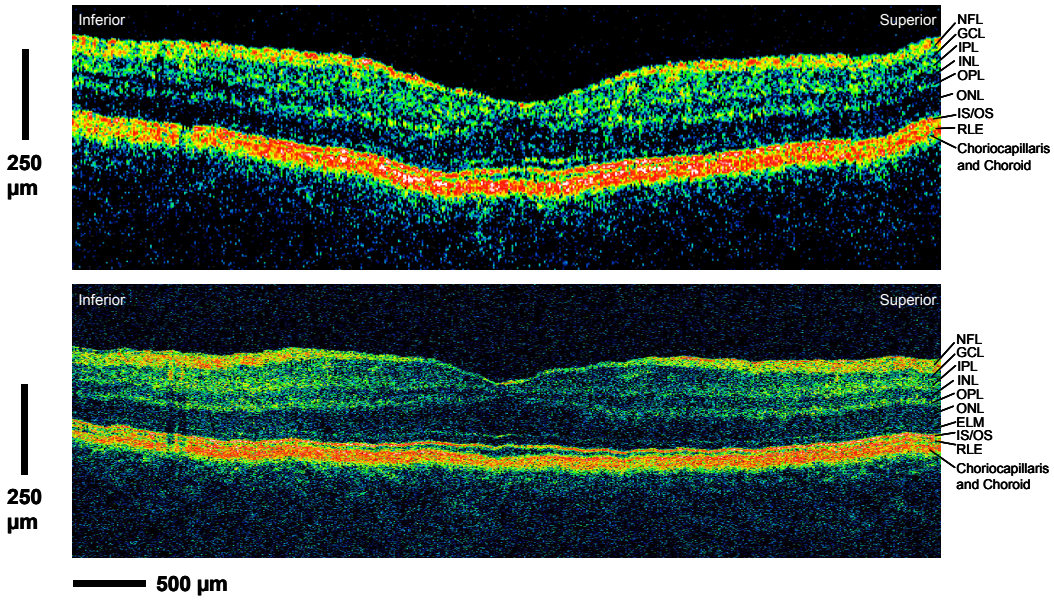

Figure 1. *In vivo* standard resolution OCT3 (top) and ultrahigh resolution (bottom) OCT images of a normal human fovea at approximately the same site. Resolutions were ~10-15 µm (axial) x 15 µm (transverse) and ~3 µm (axial) x 15 µm (transverse), respectively.

In addition to *in vivo* retinal imaging of normal subjects, we have begun clinical studies to compare the performance of the commercial OCT3 instrument and the ultrahigh resolution OCT prototype for the retinal imaging of ophthalmology patients. We have developed a compact, low-threshold Ti:Sapphire laser that is robust and portable and can be used in the ophthalmology clinic [7]. The imaging study was performed in collaboration with Drs. Jay S. Duker and Joel S. Schuman. The diagnosis of retinal pathology was performed using standard methods, including fundus examination, fundus photography, and/or fluorecein angiography. A total of more than 550 patients have been imaged so far at the Tufts-New England Eye Center. Figure 2 illustrates OCT scans of a patient with macular hole Stage I. Ultrahigh resolution OCT provides unprecedented axial resolution to visualize the intraretinal morphology of retinal diseases. It promises to provide additional information that can be used to understand retinal disease morphology, pathogenesis, and management.

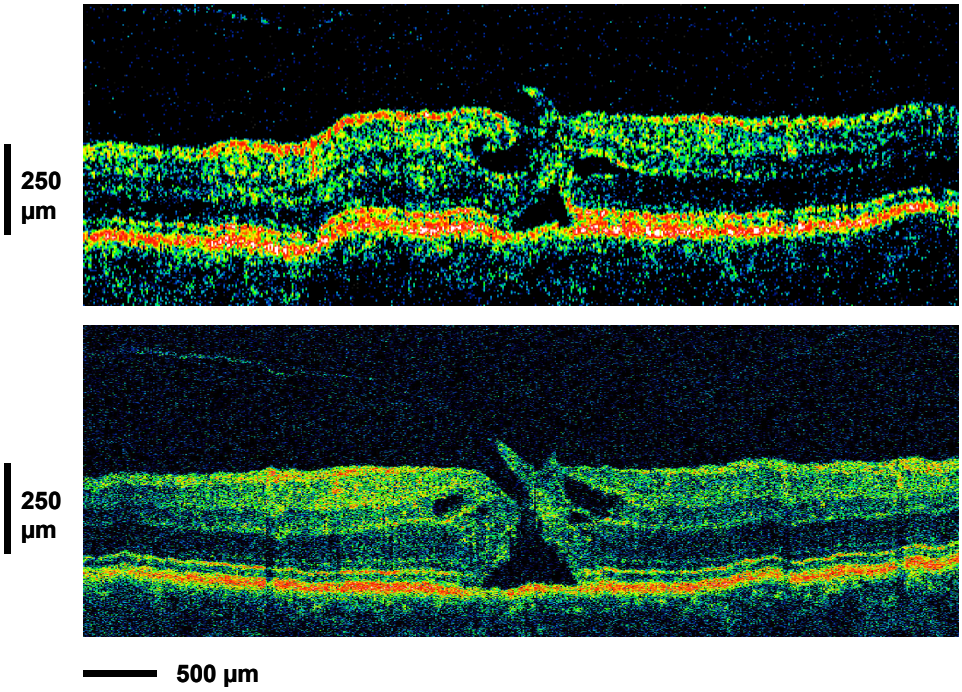

Figure 2. *In vivo* standard resolution OCT3 (top) and ultrahigh resolution (bottom) OCT images at approximately the same site of a patient with stage I macular hole. Resolutions were ~10-15 µm (axial) x 15 µm (transverse) and ~3 µm (axial) x 15 µm (transverse), respectively.

The visualization and quantification of retinal and intraretinal layers should serve as a valuable clinical tool for the early assessment of ophthalmic disease. This concept has already been demonstrated in a mouse retinal disease model, which allows us to follow and track different retinal diseases in this animal. Using the ultrahigh resolution OCT system, we have imaged and identified the many intraretinal layers of the mouse retina. Figure 5 illustrates the ability for ultrahigh resolution OCT to visualize the intraretinal layers of a normal mouse retina *in vivo*. When compared with histology taken from the same animal, the ultrahigh resolution OCT image corresponds well with the layers identified in the histology.

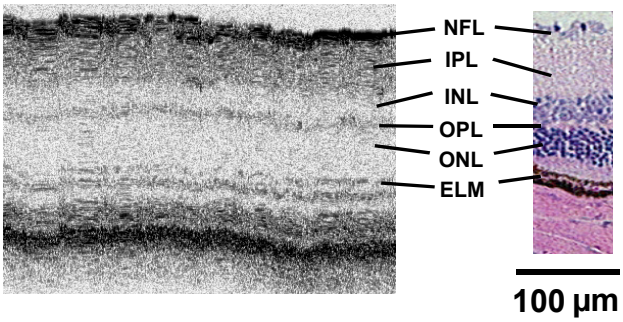

Figure 3. In vivo ultrahigh resolution OCT image of a normal mouse retina and its corresponding histology. The layers identified in the OCT images correspond well with the layers in the histology.

In the rhodopsin knockout mouse, the outer plexiform and outer nuclear layers undergo degeneration three months postpartum. Figure 6 illustrates the differences between the *in vivo* OCT images of a normal mouse retina and a rhodopsin knockout mouse retina. At 5 months of age, the outer plexiform layer and the outer nuclear layer of the rhodopsin knockout mouse retina would have undergone degeneration. When comparing the knockout mouse retina with the normal wild-type mouse retina, the OCT image clearly demonstrates this degeneration in the knockout mouse. The *in vivo* ultrahigh resolution OCT images clearly depict the degeneration of the outer plexiform and the outer nuclear layer in the rhodopsin knockout mouse retina.

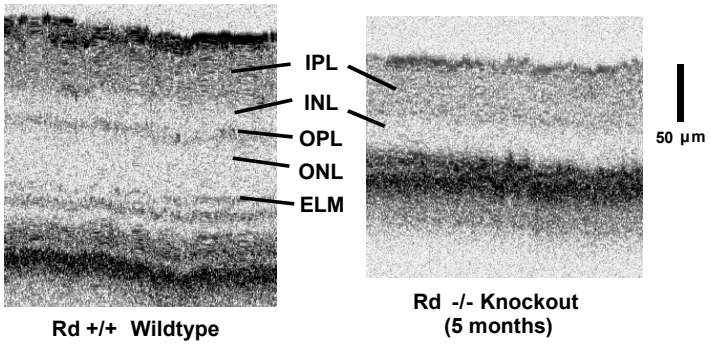

Figure 4. *In vivo* ultrahigh resolution OCT image of a normal mouse retina (Rd +/+ wild type) and a rhodopsin knockout mouse retina (Rd -/-). OCT has the ability to quantify the thickness of the different intraretinal layers as well as track disease progression in a noninvasive manner.

References

1. D. Huang, E.A. Swanson, C.P. Lin, J.S. Schuman, W.G. Stinson, W. Chang, M.R. Hee, T. Flotte, K. Gregory, C.A. Puliafito, and J.G. Fujimoto, "Optical coherence tomography," *Science* 254(5035): 1178-81 (1991).
2. M.R. Hee, J.A. Izatt, E.A. Swanson, D. Huang, C.P. Lin, J.S. Schuman, C.A. Puliafito, and J.G. Fujimoto, "Optical coherence tomography of the human retina," *Arch Ophthalmol* 113: 325-332 (1995).
3. C.A. Puliafito, M.R. Hee, J.S. Schuman, and J.G. Fujimoto, *Optical coherence tomography of ocular diseases* (Thorofare, NJ: Slack Inc., 1996).
4. C.A. Puliafito, M.R. Hee, C.P. Lin, E. Reichel, J.S. Schuman, J.S. Duker, J.A. Izatt, E.A. Swanson, and J.G. Fujimoto, "Imaging of macular diseases with optical coherence tomography," *Ophthalmology* 102(2): 217-29 (1995).
5. J.S. Schuman, M.R. Hee, C.A. Puliafito, C. Wong, T. Pedut-Kloizman, C.P. Lin, E. Hertzmark, J.A. Izatt, E.A. Swanson, and J.G. Fujimoto, "Quantification of nerve fiber layer thickness in normal and glaucomatous eyes using optical coherence tomography," *Arch Ophthalmol* 113(5): 586-96 (1995).
6. W. Drexler, U. Morgner, F.X. Kartner, C. Pitris, S.A. Boppart, X.D. Li, E.P. Ippen, and J.G. Fujimoto, "In vivo ultrahigh-resolution optical coherence tomography," *Optics Letters* 24(17): 1221-3 (1999).
7. A.M. Kowalevicz, T.R. Schibli, F.X. Kartner, and J.G. Fujimoto, "Ultralow-threshold Kerr-lens mode-locked Ti:Al_2O_3 laser," *Optics Letters* 27(22): 2037-2039 (2002).

4.2 Ultrahigh Resolution OCT Imaging in the Pathology Laboratory

Sponsors
U.S. Army Medical Research Material Command – DAMD 17-01-1-156
National Institutes of Health – R01-CA75289-05
National Science Foundation – ECS-01-19452
Air Force Office of Scientific Research – F49620-01-1-0186
Poduska Family Foundation Fund for Innovative Research in Cancer
Philanthropy of Mr. Gerhard Andlinger

Project Staff
Pei-Lin Hsiung, Paul R. Herz, Tony H. Ko, Dr. Stephane Bourquin, Karl Schneider, Professor James G. Fujimoto (MIT)
Dr. Liron Pantanowitz, Dr. James Connolly (Beth Israel Deaconess Medical Center, Harvard Medical School)

Advances in OCT technology have enabled the development of portable ultrahigh resolution, high-speed OCT technology, which has image resolutions of 4.5 μm, a factor of two to three times finer than standard OCT imaging systems. Imaging in the pathology laboratory setting allows access to fresh surgical specimens, enables the control of imaging parameters, and allows the accurate registration of OCT images with histology, which is difficult to achieve with *in vivo* OCT imaging. In order to preserve diagnostic integrity, specimens often cannot be removed from the hospital. The capability of performing ultrahigh resolution imaging in the pathology lab setting enables access to tissues that were previously inaccessible and is especially important as a research tool. The purpose of this study is to provide a basis for interpreting future *in vivo* endoscopic and laparoscopic OCT studies using ultrahigh resolution imaging. This study is being conducted in collaboration with Dr. Liron Pantanowitz and Dr. James Connolly at Beth Israel Deaconess Medical Center and Harvard Medical School.

For this study, we used a novel compact solid-state Cr^{4+}:Forsterite laser operating at a center wavelength of 1260 nm. Tissue scattering and absorption are minimized by using light in the near infrared (1200 to 1300 nm) range, thus permitting OCT imaging to be performed at 1-2 mm depths in most tissues. Using this laser light source, it was possible to achieve an axial resolution of ~4.5 μm in tissue, a factor of two to three times higher than conventional OCT systems previously used to image scattering tissues *in vivo*. The transverse image resolution was determined by the focused spot size of the optical beam, which is related to the numerical aperture of the focusing lens and the wavelength of the light source, as in conventional microscopy. The transverse spot size diameter for the OCT system used in this study was approximately 18 μm. Imaging was performed by using a surgical imaging probe (measuring 1 cm in diameter and 15 cm in length) that was mounted on a precision stage to provide controlled displacements of the light beam orientation and position. Imaging was performed at 2-4 frames per second, enabling real-time visualization and the ability to adjust the imaging plane. Imaging was performed without contact with the tissue in order to prevent alterations in scattering and brightness due to the pressure of the probe on the tissue.

Studies were performed on freshly excised surgical specimens in the pathology laboratory of Beth Israel Deaconess Medical Center. Normal and diseased tissues from surgical resections were imaged within two hours of excision. Since the OCT source light was in the near infrared and invisible to the naked eye, tissue registration was performed with a visible green light guiding beam that was coincident with the OCT imaging beam. When necessary, the irrigation of specimens with isotonic saline was used to prevent dehydration during imaging. Specimens were marked at the beginning and end of each OCT scan with microinjections of ink to designate the orientation of the OCT imaging plane. Tissue specimens were then placed in 10% buffered formalin, routinely processed, and paraffin embedded. Multiple serial tissue sections of 5 μm thickness were obtained and stained with hematoxylin and eosin. Samples were sectioned in the same plane as the OCT imaging plane. The OCT images recorded in this study were acquired at 2-4 frames per second with 1.84 mm (axial) x 2 mm (transverse) dimension and 940 (axial) x 1000 (transverse) pixels. Images were scaled by a factor of 1.3x to correct for index of refraction. Digital two-dimensional OCT images and histology sections corresponding to the imaged areas were compared.

Minor discrepancies between histology and OCT imaging can be attributed to tissue fixation, processing, and sectioning artifacts.

Colorectal cancer (CRC) is a common and lethal disease. Approximately 148,000 new cases of large bowel cancer are diagnosed each year in the United States, and approximately one in three people who develop CRC die of this disease. CRC is the second leading cause of cancer death, accounting for 10-11% of cancer deaths overall [1]. The majority of colon and rectal cancers are endoluminal adenocarcinomas that arise from the mucosa. Therefore, there is significant interest in the development of diagnostic techniques that can detect early stage colorectal disease.

Optical coherence tomography has the advantage of a higher resolution than current clinical ultrasound without the need for tissue contact or imaging through a transducing medium. Since OCT can be incorporated into a variety of endoscopic and laparoscopic imaging devices [2,3], it has the particular advantage of enabling the visualization of microscopic mucosal and submucosal architectural features that are not visible by using clinically available imaging methods. Endoscopic OCT has also been shown to provide complementary information to endoscopic ultrasound for potential applications in the staging of endoscopic tumor resection [4]. Because of these advantages, there is significant interest in using OCT to improve current endoscopic diagnostic techniques for detecting early stage disease.

The goal of this study was to investigate the feasibility of using ultrahigh resolution OCT for imaging pathologies of the gastrointestinal tract and to provide a basis for interpreting future endoscopic OCT studies using ultrahigh resolution imaging. In this study, a total of 52 areas of the lower gastrointestinal tract from 18 adult patients were scanned. The diseased tissues that were imaged included inflammatory bowel disease and neoplasia, with one submucosal lipoma, one tubulovillous adenoma involving the duodenum, three sites of invasive adenocarcinoma involving the transverse colon, and one squamous cell carcinoma in the anorectal region. Grossly normal as well as ulcerated and scarred lesions were also imaged.

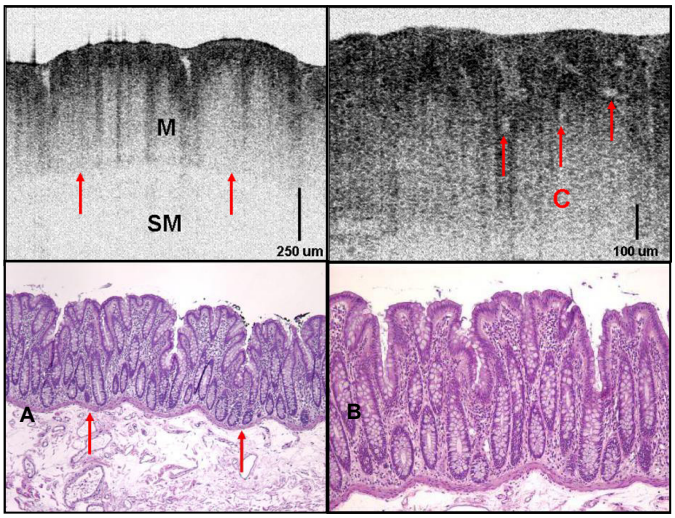

Figure 1. (A) OCT image of the normal colon. Mucosa (M) is clearly delineated from underlying submucosa (SM) by a scattering band that corresponds to the thin muscularis mucosa (arrows). Mucosal folds and crypts are visible. The submucosa is shown as a loose and less optically scattering layer. (B) Higher magnification shows individual colonic crypts (arrows). (OCT top; histology bottom, H&E, A: 40x; B:100x)

Figure 1 shows normal colon specimens imaged with OCT. The imaging of the normal colon produced distinct images of the mucosa, including the muscularis mucosa and submucosa characteristic of normal colonic microstructure. Full thickness mucosa of the colon is visible. High scattering bands as thin as 25

μm, which corresponds to the muscularis mucosa, could be visualized in OCT images. This corresponds to what is seen in the histology; delineating the mucosa from the underlying stroma. The submucosa appears as a pale and less optically scattering layer. Figure 1B shows a higher magnification image where individual crypts are visible.

Images of chronic colitis due to ulcerative colitis and Crohn's disease are shown in Figures 2A and 2B. Ulceration and erosion of the epithelium is evident. Irregular and distorted glands that are characteristic of chronic inflammatory bowel disease were clearly visible. In addition, the markedly increased inflammatory cells within the supporting lamina propria were noted and appeared as highly scattering. Figure 2C shows an image of invasive adenocarcinoma. Highly scattering and irregular invasive glands were visible in OCT images of adenocarcinoma. OCT images of invasive carcinoma revealed a complete loss of normal mucosal architecture and invasion of the submuscosa. OCT images also identified areas within the carcinomas of ulceration with overlying fibrinopurulent exudate.

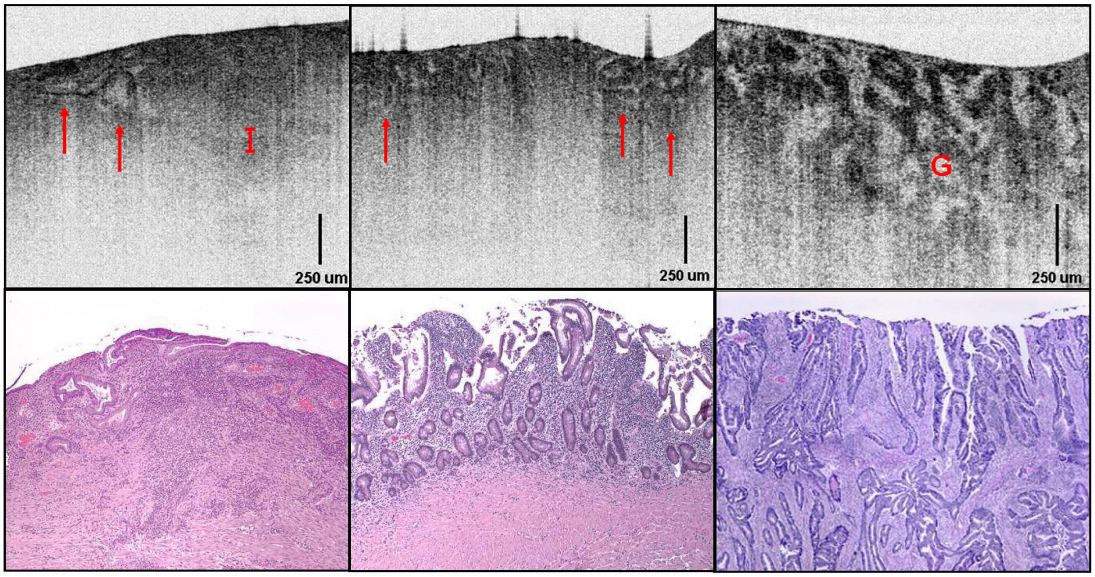

Figure 2. (A) OCT image of severe ulcerative colitis showing surface ulceration, architectural distortion of glands (arrows) and a dense chronic inflammatory infiltrate within the lamina propria (I). (B) Chronic colitis due to Crohn's disease showing branching irregular glands (arrows) and a dense inflammatory infiltrate in the lamina propria. (C) Well differentiated adenocarcinoma. Highly irregular invasive glands (G) are visible in a desmoplastic stroma. (top: OCT; bottom: histology, H&E; 40x)

These preliminary results demonstrate the feasibility of ultrahigh resolution OCT imaging by using a portable system in a pathology laboratory environment. Additional studies are in progress to evaluate the ability of OCT to differentiate normal and pathologic conditions in the upper gastrointestinal tract and other tissues. Spectroscopically resolved OCT using broadband light sources also promises to improve tissue differentiation and image contrast. The ability to visualize tissue pathology *in situ* and in real-time on tissues that were previously inaccessible promises to be an important research tool that will improve diagnosis and therapy.

References

1. A. Jemal, R.C. Tiwari, T. Murray, A. Ghafoor, A. Samuels, E. Ward, E.J. Feuer, and M.J. Thun, "Cancer statistics, 2004," *CA Cancer J. Clin.* 54(1): 8-29 (2004).

2. G.J. Tearney, M.E. Brezinski, B.E. Bouma, S.A. Boppart, C. Pitvis, J.F. Southern, and J.G. Fujimoto, "In vivo endoscopic optical biopsy with optical coherence tomography," *Science* 276(5321): 2037-9 (1997).
3. A.M. Sergeev, V.M. Gelikonov, G.V. Gelikonov, F.I. Feldchtein, R.V. Kuranov, N.D. Gladkova, N.M. Shakhova, L.B. Snopova, A.V. Shakov, I.A. Kuznetzova, A.N. Denisenko, V.V. Pochinko, Y.P. Chumakov, and O.S. Streltzova, "In vivo endoscopic OCT imaging of precancer and cancer states of human mucosa," *Optics Express* 1(13): 432 (1997).
4. A. Das, M.V. Sivak, Jr., A. Chak, R.C. Wong, V. Westphal, A.M. Rollins, J. Willis, G. Isenberg, and J.A. Izatt, "High-resolution endoscopic imaging of the GI tract: a comparative study of optical coherence tomography versus high-frequency catheter probe EUS," *Gastrointest. Endosc.* 54(2): 219-24 (2001).

4.3 Endoscopic Imaging of Barrett's Esophagus and Gastrointestinal Cancer

Sponsors
National Institute of Health – R01-CA75289-06, R01-EY11289-18
National Science Foundation – ECS-0119452, BES-0119494
U.S. Air Force Office of Scientific Research – F49620-01-01-0084, F49620-01-01-0186

Project Staff
Paul Herz, Dr. Yu Chen, Pei-Lin Hsiung, Aaron D. Aguirre, Professor James G. Fujimoto (MIT)
Dr. Hiroshi Mashimo, Dr. Saleem Desai, Dr. Mihr Wagh (Veteran Administration Medical Center)
Amanda Koski, Dr. Joseph Schmitt (LightLab Imaging)

Epithelial cancers of the gastrointestinal tract, reproductive tract, and the respiratory tract comprise the majority of cancers encountered in internal medicine. Many epithelial cancers are preceded by pre-malignant changes, such as dysplasia. Conventional screening methods often rely on the gross morphological characteristics of tissues. Biopsy and histopathology are the standard for the diagnosis of dysplasia or carcinoma, but they can suffer from sampling errors and are cumbersome for screening and surveillance applications. Our hypothesis is that OCT can function as a form of "optical biopsy", which can perform microstructural imaging of tissue morphology *in situ* without excision. We have examined the use of OCT for the identification of early neoplastic changes and tissue abnormalities that have a predisposition to malignancy. The aim of this work is to perform imaging of architectural morphology of the human upper gastrointestinal tract to explore the feasibility of OCT for the identification of morphologies that are characteristic of early neoplastic changes.

Previous data has demonstrated that OCT can image features of architectural morphology that are relevant for the diagnosis and monitoring of early neoplastic tissue changes. We have performed *in vitro* survey imaging and histopathologic correlations of normal as well as abnormal human tissue pathologies, including Barrett's esophagus, adenocarcinoma of the esophagus, ulcerative colitis, colonic dysplasia, adenomatous polyps, colorectal carcinoma, cervical intraepithelial neoplasia, cervical carcinoma, uterine dysplasia, and endometrial carcinoma, in order to evaluate the ability of OCT to differentiate early neoplastic changes and other tissue abnormalities with a predisposition to malignancy. We have performed imaging of normal tissue by using OCT endoscope-catheters in an *in vivo* rabbit animal model. Survey imaging studies were performed on the gastrointestinal, urinary, reproductive, and respiratory tracts and correlated with histology. We also performed endoscopic imaging of patients with Barrett's esophagus. OCT imaging demonstrates the ability to differentiate changes in the esophageal architectural morphology associated with the development of Barrett's esophagus.

The identification of early malignant changes remains a central objective of clinical medicine since, once widely metastatic, most neoplasms become incurable. In addition to biochemical methods, excisional biopsy, with subsequent histologic processing, remains a cornerstone of early diagnostics. However, in many instances, diagnostics based on excisional biopsy are ineffective because of sampling errors. A technology capable of performing optical biopsy (i.e., imaging at a resolution comparable to histopathology without the need for tissue removal) could significantly improve the ability of clinicians to identify malignancies at curable stages [1-5]. Large areas could be screened in real time with an imaging system that is high resolution and relatively low cost. High-resolution imaging of architectural morphology may allow the *in situ* assessment of early neoplastic changes such as dysplasia. If successful, this technology could be coupled with excisional biopsy in order to reduce sampling errors and false-negative rates. We have investigated the feasibility of optical biopsy with OCT to identify early neoplastic changes. Although we believe that micron-scale imaging has the potential to be a general diagnostic in most, if not all, organ systems, this study will emphasize one clinical scenario where current methods of excisional screening are plagued with serious limitations: the problem of early neoplastic diagnosis in Barrett's esophagus.

Barrett's esophagus is the replacement of the squamous epithelium of the distal esophagus with columnar epithelium [6]. It is believed to be caused by chronic gastroesophageal reflux. Several well-designed studies have demonstrated that Barrett's esophagus is associated with a 30-40x increased risk

of developing adenocarcinoma. The prevalence of Barrett's esophagus within the US population is between 0.3% and 2% [7]. Among patients with reflux, the prevalence is 8-14% [8,9]. The incidence of progression to adenocarcinoma in Barrett's esophagus is approximately 7-9% [10]. For this reason, endoscopic surveillance of Barrett's epithelium every 6-18 months is recommended. Endoscopic screening currently involves random biopsies every 2 cm. However, sampling errors exist and may miss small foci of carcinoma [11,12]. Because of the imprecision and high cost associated with screening, new methods are required to identify high risk patients.

An important technology that is necessary in order to apply OCT to the imaging of internal organ systems is a catheter-endoscope, which is capable of delivering, focusing, scanning, and collecting a single spatial mode optical beam. We have developed, tested, and applied a prototype transverse scanning OCT catheter that is suitable for luminal imaging [13]. The OCT catheter consists of an optical coupling element at its proximal end, a single-mode fiber running the length of the catheter, and optical focusing and beam directing elements at the distal end. The catheter is designed to scan the beam in a circumferential or longitudinal pattern in order to cross-sectionally image through the lumen (or other biological structures) into which it is inserted. A single-mode optical fiber lies within a flexible speedometer cable that is rotated with a motor drive unit at the proximal end. The distal end contains a graded index (GRIN) lens to focus the imaging beam and a right-angle microprism to direct the beam at a 90-degree angle with respect to the axis of the catheter. The entire assembly is housed in a transparent plastic sheath that can be disinfected prior to use and is discarded after use.

The development and application of OCT has been made possible by the vertically integrated structure of our research program at the Massachusetts Institute of Technology, which combines fundamental physical studies, engineering, biomedical studies, and clinical applications. We have recently increased the image acquisition speed for OCT to achieve subsecond acquisition times [14]. This permits tissue microstructure to be viewed in real-time, thus making possible a wide range of potential, new clinical applications ranging from *in vivo* optical biopsy to intraoperative monitoring of surgery. In order to achieve the high powers and short coherence lengths necessary for high resolution, high speed imaging, a Cr:Forsterite laser is used as the light source. This laser generates short pulses in the 1200-1350 nm wavelength regime. The Cr:Forsterite laser has a coherence length of 15 microns. However, because it generates short pulses, the output bandwidth can be increased by using nonlinear effects in optical fibers to yield coherence lengths of 5 microns or less. Nonlinear techniques such as these are well established in laser engineering and research, and they have been used for many applications including pulse compression and signal processing [15-18].

Our group, as well as others, have performed investigations of *in vivo* endoscopic OCT imaging in human subjects [19-22]. In the previous study, we performed endoscopic OCT to evaluate scanning techniques and to demonstrate the ability to discern changes in architectural morphology associated with Barrett's esophagus [19]. We have established a clinical study at the Veterans Affairs Medical Centers of the Boston Healthcare system to perform ultrahigh resolution imaging of patients who are diagnosed with Barrett's esophagus and who have a predisposition to the presence of dysplasia or adenocarcinoma of the esophagus. Figure 1 shows an OCT image of normal columnar epithelium in the stomach. Pit architecture within the gastric (gp) is visible as regular vertical regions of high backscattering intensity. Small pockets of mucosal secretion below the surface are also visualized as weakly scattering regions that are circular in geometry and have approximate diameters of 50-100 μm.

Figure 1 also shows an OCT image of a normal esophagus with squamous epithelium. The OCT image illustrates the relatively homogeneous epithelium (ep), the high-backscattering region (appears brighter) of the lamina propria (lp), The low-backscattering muscularis mucosa (mm), the high-backscattering submucosa (sm), and the low-backscattering and thick muscularis propria (mp). The solid horizontal line noted above the mucosal surface is from the transparent plastic sheath of the OCT catheter.

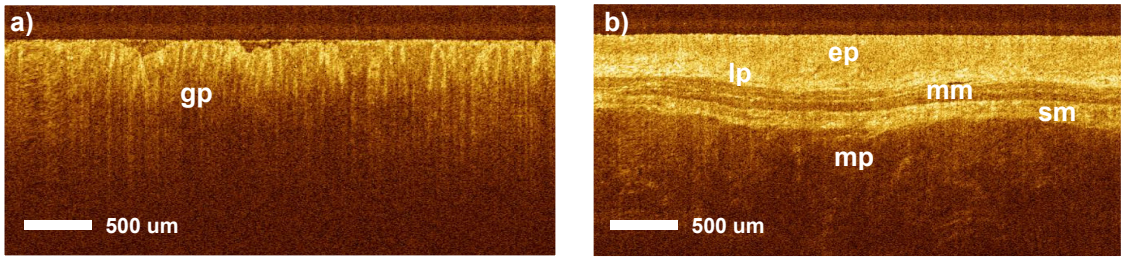

Figure 1. a) Ultrahigh resolution OCT image of gastric mucosa. Gastic pits (gp) are clearly visible as vertical regions of high backscattering (bright) intensity. b) Ultrahigh resolution OCT image of normal esophagus. Layered structure of the esophagus is well defined with a homogeneous epithelium (ep) above a highly backscattering lamina propria (lp). Deeper layers of the muscularis mucosa (mm), submucosa (sm), and muscularis propria (mp) are also visualized.

Images were also acquired from regions of Barrett's epithelium in the same patient. Figure 2 shows an OCT image of an abnormal esophageal region and an endoscopic video image of the area. The video image reveals both normal regions of the esophagus and finger-like projections of abnormal epithelium that are indicative of Barrett's esophagus. The OCT image shows clear differences in the tissue architecture of the Barrett's region, when compared to squamous epithelium of normal esophagus. The uniformly layered structure is disrupted by the presence of multiple crypt- and gland-like structures and is highly heterogeneous.

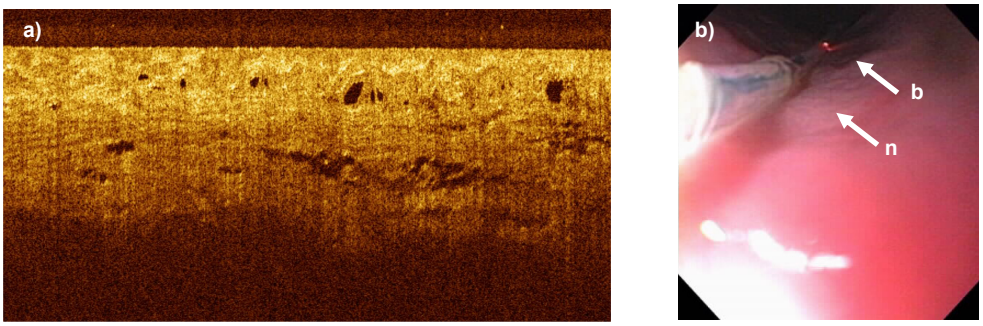

Figure 2. a) Ultrahigh resolution OCT image of Barrett's esophagus. Architectural disruption and glandular features are highly distinct and can be differentiated well from OCT images of the normal esophagus. b) Endoscopic view of a patient's esophagus and the OCT catheter. Regions of Barrett's esophagus (b) are seen as finger-like projections consisting of a darker hue than the normal pink esophageal tissue (n). The red aiming beam of the OCT catheter is also visible, which indicates the area being imaged.

The ability of OCT to differentiate between normal and pathologic tissue has been demonstrated by our group and others [19-23]. The image resolution of OCT has enabled the visualization of architectural morphology features, such as the normal, layered structure of the epithelium, as opposed to the glandular and crypt structures associated with Barrett's esophagus. Because pinch biopsies were obtained, it was not possible to exactly orient the sectioning plane of the histology, as with *in vitro* imaging studies. The correspondence of OCT with histology was evaluated, based on the presence or absence of architectural morphology, which indicates normal as opposed to Barrett's esophagus.

It has been demonstrated that endoscopic OCT resolution can differentiate between normal and Barrett's epithelium in real-time, based on differences in epithelial architecture. Crypt-like and gland-like structures that disrupted the relatively uniform layers of squamous epithelium are readily identified, thus enabling the

differentiation between normal and Barrett's epithelium. The ability to differentiate between normal and Barrett's epithelium suggests that the OCT could be used for screening applications. These findings are consistent with other investigations [19-22]. In the surveillance of patients with Barrett's esophagus for high-grade dysplasia and adenocarcinoma, the most intriguing application of OCT would be to direct excisional biopsy in order to reduce sampling errors. One can envision new OCT imaging probes that integrate OCT imaging with pinch biopsy in order to provide a real-time "first look" at pathology prior to the excision and processing of a specimen. If successful, this technology could be used to help guide excision biopsy in order to reduce sampling errors and false-negative rates. This could improve the sensitivity of diagnosis, reduce the cost of surveillance, and provide enhanced diagnosis and treatment decisions.

References

1. T.J. Romer, J.M. Fitzmaurice, R.M. Cothren, R. Richards-Kortum, R. Petras, J. Sivak, M. V., and J.R. Kramer, "Laser-induced fluorescence microscopy of normal colon and dysplasia in colonic adenomas: implications for spectroscopic diagnosis," *American Journal of Gastroenterology* 90: 81-87 (1995).
2. T. Vo Dinh, M. Panjehpour, B.F. Overholt, C. Farris, F.P. Buckley, and R. Sneed, "*In vivo* cancer diagnosis of the esophagus using differential normalized fluorescence (DNF) indices," *Lasers Surg Med* 16: 41-47 (1995).
3. G. Bottiroli, A.C. Croce, D. Locatelli, R. Marchesini, E. Pignoli, S. Tomatis, C. Cuzzoni, S. Di Palma, M. Dalfante, and P. Spinelli, "Natural fluorescence of normal and neoplastic human colon: a comprehensive," *Lasers Surg Med* 16: 48-60 (1995).
4. M. Panjehpour, B.F. Overholt, J.L. Schmidhammer, C. Farris, and P.F. Buckley, "Laser-induced fluorescence spectroscopy: somewhere over the rainbow," *Gastroenterology (selected summaries)* 110: 643-645 (1996).
5. P.T.T. Wong, R.K. Wong, T.A. Caputo, T.A. Godwin, and B. Rigas, "Infrared spectroscopy of exfoliated human cervical cells: evidence of extensive structural changes during carcinogenesis," *Proceedings of the National Academy of Science* 88: 10988-10992 (1991).
6. R.W. Phillips and R.K.H. Wong, "Barrett's esophagus: natural history, incidence, etiology, and complications," *Gastro. Clinics of North America* 20: 791-815 (1991).
7. A.L. Taylor, "The epithelial heterotopias of the alimentary tract," *J. Pathol. Bacteriol.* 30: 415-449 (1927).
8. M.J. Sarr, S.R. Hamilton, and G.C. Marrone, "Barrett's esophagus: its prevalence and association with adenocarcinoma in patients with symptoms of gastroesophageal reflux," *American Journal of Surgery* 149: 187-194 (1985).
9. A.P. Naef, M. Savary, and L. Ozzello, "Columnar-lined lower esophagus: an acquired lesion with malignant predisposition. Report on 140 cases of Barrett's esophagus with 12 adenocarcinomas," *J. Thorac. Cardiovasc. Surg.* 70: 826-834 (1975).
10. A.J. Cameron, B.J. Ott, and W.S. Payne, "The incidence of adenocarcinoma in columnar-lined (Barrett's)esophagus," *New England Journal of Medicine* 313: 857-859 (1985).
11. P. Rozen, M. Baratz, F. Fefer, and T. Gilat, "Low incidence of significant dysplasia in a successful endoscopic surveillance program of patients with ulcerative colitis," *Gastroenter.* 108: 1361-1370 (1995).
12. A. Axon, "Cansurveillance in ulcerative colitis - letter on article," *Gut* 35: 801 (1994).
13. G.J. Tearney, S.A. Boppart, B.E. Bouma, M.E. Brezinski, N.J. Weissman, J.F. Southern, and J.G. Fujimoto, "Scanning single-mode fiber optic catheter-endoscope for optical coherence tomography," *Optics Letters* 21(7): 543-5 (1996).
14. G.J. Tearney, B.E. Bouma, S.A. Boppart, B. Golubovic, E.A. Swanson, and J.G. Fujimoto, "Rapid acquisition of in vivo biological images using optical coherence tomography," *Optics Letters* 21(September): 1408-1410 (1996).
15. M.T. Asaki, C.P. Huang, D. Garvey, J.P. Zhou, H.C. Kapteyn, and M.M. Murnane, "Generation of 11-fs pulses from a self-mode-locked Ti-Sapphire laser," *Optics Letters* 18(12): 977-979 (1993).
16. J.P. Heritage, A.M. Weiner, and R.N. Thurston, "Picosecond Pulse Shaping by Spectral Phase and Amplitude Manipulation," *Optics Letters* 10(12): 609-611 (1985).

17. C.W. Hillegas, J.X. Tull, D. Goswami, D. Strickland, and W.S. Warren, "Femtosecond Laser-Pulse Shaping by Use of Microsecond Radiofrequency Pulses," *Optics Letters* 19(10): 737-739 (1994).
18. G.J. Tearney, B.E. Bouma, and J.G. Fujimoto, "High-speed phase- and group-delay scanning with a grating-based phase control delay line," *Optics Letters* 22(23): 1811-13 (1997).
19. X.D. Li, S.A. Boppart, J. Van Dam, H. Mashimo, M. Mutinga, W. Drexler, M. Klein, C. Pitris, M.L. Krinsky, M.E. Brezinski, and J.G. Fujimoto, "Optical coherence tomography: advanced technology for the endoscopic imaging of Barrett's esophagus," *Endoscopy* 32(12): 921-30 (2000).
20. S. Brand, J.M. Poneros, B.E. Bouma, G.J. Tearney, C.C. Compton, and N.S. Nishioka, "Optical coherence tomography in the gastrointestinal tract," *Endoscopy* 32(10): 796-803 (2000).
21. G. Zuccaro, N. Gladkova, J. Vargo, F. Feldchtein, E. Zagaynova, D. Conwell, G. Falk, J. Goldblum, J. Dumot, J. Ponsky, G. Gelikonov, B. Davros, E. Donchenko, and J. Richter, "Optical coherence tomography of the esophagus and proximal stomach in health and disease," *Am. J. Gastroenterol.* 96(9): 2633-9 (2001).
22. J. Poneros, S. Brand, and B. Bouma, "Diagnosis of specialized intestinal metaplasia by optical coherence tomography," *Gastroenterology* 120: 7-12 (2001).
23. C. Pitris, C. Jesser, S.A. Boppart, D. Stamper, M.E. Brezinski, and J.G. Fujimoto, "Feasibility of optical coherence tomography for high-resolution imaging of human gastrointestinal tract malignancies," *J Gastroenterol.* 35(2): 87-92 (2000).

Publications

Journal Articles, Published

V. Guedes, J.S. Schuman, E. Hertzmark, G. Wollstein, A. Correnti, R. Mancini, D. Lederer, S. Voskanian, L. Velazquez, H.M. Pakter, T. Pedut-Kloizman, J.G. Fujimoto, and C. Mattox, "Optical coherence tomography measurement of macular and nerve fiber layer thickness in normal and glaucomatous human eyes," *Ophthalmology* **110**, 177-189, January 2003.

P.L. Hsiung, X. Li, C. Chudoba, I. Hartl, T.H. Ko, and J.G. Fujimoto, "High-speed path-length scanning with a multiple-pass cavity cell delay line," *Appl. Opt*. **42**, 640-648, February 2003.

S.D. Martin, N.A. Patel, S.B. Adams, Jr., M.J. Roberts, S. Plummer, D.L. Stamper, M.E. Brezinski, and J.G. Fujimoto, "New technology for assessing microstructural components of tendons and ligaments," *Intl. Orthop.* **27**, 184-189, February 2003.

N.A. Patel, X. Li, D.L. Stamper, J.G. Fujimoto, and M.E. Brezinski, "Guidance of aortic ablation using optical coherence tomography," *Intl. J. Cardiovasc. Imaging* **19**, 171-178, April 2003.

J.S. Schuman, G. Wollstein, T. Farra, E. Hertzmark, A. Aydin, J.G. Fujimoto, and L.A. Paunescu, "Comparison of optic nerve head measurements obtained by optical coherence tomography and confocal scanning laser ophthalmoscopy," *Am. J. Ophthalmol.* **135**, 504-512, April 2003.

W. Drexler, H. Sattmann, B. Hermann, T.H. Ko, M. Stur, A. Unterhuber, C. Scholda, O. Findl, M. Wirtitsch, J.G. Fujimoto, and A.F. Fercher, "Enhanced visualization of macular pathology in the use of ultrahigh-resolution optical coherence tomography," *Arch. Ophthalmol.* **121**, 695-706, May 2003.

D.E. Lederer, J.S. Schuman, E. Hertzmark, J. Heltzer, L.J. Velazques, J.G. Fujimoto, and C. Mattox, "Analysis of macular volume in normal and glaucomatous eyes using optical coherence tomography," *Am. J. Ophthalmol*., **135**, 838-843, June 2003.

A. Ayedin, G. Wollstein, L.L. Price, J.G. Fujimoto, and J.S. Schuman, "Optical coherence tomography assessment of retinal nerve fiber layer thickness changes after glaucoma surgery," *Ophthalmology* **110**, 1506-1511, August 2003.

J.G. Fujimoto, "Optical coherence tomography: Principles and applications," *Rev. of Laser Engin.*, **31**, 635-642, October 2003.

M.J. Roberts, S.B. Adams, Jr., N.A. Patel, D.L. Stamper, M.S. Westmore, S.D. Martin, J.G. Fujimoto, and M.E. Brezinski, "A new approach for assessing early osteoarthritis in the rat," *Anal. Bioanal. Chem.* **377**, 1003-1006, October 2003.

A.D. Aguirre, P. Hsiung, T.H. Ko, I. Hartl, and J.G. Fujimoto, "High-resolution optical coherence microscopy for high-speed, in vivo cellular imaging," *Opt. Lett.* **28**, 2064-2066, November 2003.

J.G. Fujimoto, "Optical coherence tomography for ultrahigh resolution in vivo imaging," *Nat. Biotechnol.*, **21**, 1361-1367, November 2003.

E. Lai, G. Wollstein, L.L. Price, L.A. Paunescu, P.C. Stark, J.G. Fujimoto, and J.S. Schuman, "Optical coherence tomography disc assessment in optic nerves with peripapillary atrophy," *Ophthalmic Surg. Lasers Imaging* **34**, 498-504, November/December 2003.

S. Bourquin, A.D. Aguirre, I. Hartl, P. Hsiung, T.H. Ko, and J.G. Fujimoto, "Compact broadband light source for ultrahigh resolution optical coherence tomography imaging using a femtosecond Nd:Glass laser and a nonlinear fiber," Opt. Exp., 11, 3290-3297, December 2003.

L. Pantanowitz, P.L. Hsiung, T.H. Ko, K. Schneider, P.R. Herz, J.G. Fujimoto, S. Raza, and J.L. Connolly, "High-resolution imaging of the thyroid gland using optical coherence tomography," Head and Neck 26: 425-434, April 2004.

J. Rogowska, N.A. Patel, J.G. Fujimoto, and M.E. Brezinski, "Optical coherence tomographic elastography technique for measuring deformation and strain of atherosclerotic tissues," Heart 90: 556-562, May2004.

T.H. Ko, D.C. Adler, J.G. Fujimoto, D. Mamedov, V. Prokhorov, V. Shidlovski, and S. Yakubovich, "Ultrahigh resolution optical coherence tomography imaging with broadband superluminescent diode light source," *Optics Express* 12: 2112-2119, May 2004.

M. Wojtkowski, V.J. Srinivasan, T.H. Ko, J.G. Fujimoto, J.S. Duker, and A. Kowalevicz, "Ultrahigh resolution, high speed, Fourier domain optical coherence tomography and methods for dispersion compensation," *Optics Express*12: 2404-2422, May 2004.

Journal Articles, Accepted for Publication

J.S. Schuman, T. Pedut-Kloizman, E. Hertzmark, M.R. Hee, L. Pieroth, N. Wang, W. C. Kiernan, J.G. Fujimoto, W. Drexler, and R. Ghanta, "Quantitation of nerve fiber layer thickness loss over time in the glaucomatous monkey model using optical coherence tomography," *Arch. Ophthalmol.*, forthcoming.

W.P. Roach, C.P. Cain, C.D. DiCarlo, R. Birngruber, J.G. Fujimoto, and C.A. Toth, "The retinal response of macacca mulatta to picosecond laser pulses of varying energy and spot-size," *J. Biomed. Opt.*, forthcoming.

T.H. Ko, J.G. Fujimoto, J.S. Schuman, L.A. Paunescu, A.M. Kowalevicz, I. Hartl, W. Drexler, G. Wollstein, J.S. Duker, and H. Ishikawa, "Comparison of ultrahigh and standard resolution optical coherence tomography for imaging of macular pathology," *Arch. Ophthalmol*., forthcoming.

T.H. Ko, J.G. Fujimoto, J.S. Duker, L.A. Paunescu, W. Drexler, C.R. Baumal, C. Mattox, E. Reichel, A.H. Rogers, and J.S. Schuman, "Comparison of ultrahigh and standard optical coherence tomography for imaging macular hole pathology and repair," *Ophthalmology*, forthcoming.

Journal Articles, Submitted for Publication

X.D. Li, H. Gold, N. Weissman, K. Saunders, C. Pitris, J.G. Fujimoto, and M.E. Brezinski, "Optical coherence tomography guided stent deployment: a comparison with IVUS in an in vivo rabbit model," submitted to *J. Am. Coll. Cardiol.*

L.A. Paunescu, J.S. Schuman, L.L. Price, P.C. Stark, S. Beaton, H. Ishikawa, G. Wollstein, and J.G. Fujimoto, "Reproducibility of nerve fiber thickness, macular thickness and optic nerve head measurements using StratusOCT optical coherence tomography," submitted to *Invest. Ophthalmol. and Vis. Sci.*

N. Patel, J. Zoeller, D.L. Stamper, J.G. Fujimoto, and M.E. Brezinski, "Monitoring osteoarthritis in the rat model using optical coherence tomography, submitted to *IEEE Trans. Med. Imaging.*

P.L. Hsiung, L. Pantanowitz, T.H. Ko, S. Bourquin, J.L. Connolly, and J.G. Fujimoto, "Ultra-high-resolution imaging of lower GI pathology using optical coherence tomography, submitted to *Gastrointestinal Endoscopy*.

E. Ergun, B. Hermann, M. Wirtisch, A. Unterhuber, T. Ko, H. Sattmann, C. Scholda, J.G. Fujimoto, A.F. Fercher, M. Stur, and W. Drexler, "Assessment of central visual function in Stargardt's Disease/Fundus

flavimaculatus with ultrahigh resolution optical coherence tomography," submitted to *Invest. Ophthal. and Vis. Sci.*
M.G. Wirtitsch, E. Ergun, B. Hermann, A. Unterhuber, M. Stur, C. Scholda, H. Sattmann, T.H. Ko, J.G. Fujimoto, A.F. Fercher, and W. Drexler, "Ultrahigh resolution optical coherence tomography in macular dystrophy," submitted to *Arch. Ophthalmol*.

X. Li, S. Martin, C. Pitris, R. Ghanta, M. Harman, D.L. Stamper, J.G. Fujimoto, and M.E. Brezinski, "High-resolution optical coherence tomographic imaging of osteoarthritis cartilage during open knee surgery," submitted to *Arthritis Research and Therapy*.

P.R. Herz, Y. Chen, A. Aguirre, P. Hsiung, K. Schneider, J.G., Fujimoto, H. Mashimo, J. Schmitt, A. Koski, J. Goodnow, and C. Petersen, "High resolution optical biopsy with endoscopic optical coherence tomography," submitted to *Optics Express*.

P. Hsiung, Y. Chen, T.H. Ko, and J.G. Fujimoto, "Continuous-wave, high-power, Raman continuum light source for optical coherence tomography, submitted to *Opt. Lett.*

A. Chan, J.S. Duker, T.H. Ko, J.G. Fujimoto, and J.S. Schuman, "Normal macular thickness measurements in healthy eyes using Stratus optical coherence tomography (OCT3)," submitted to *Arch. Ophthal.*

A. Chan, J.S. Duker, J.S. Schuman, and J.G. Fujimoto, "Stage zero macular holes: observations by optical coherence tomography," submitted to *Ophthal*.

S.G. Schuman, E. Hertzmark, J.G. Fujimoto, and J.S. Schuman, "Wavelength independence and interdevice variability of optical coherence tomography," submitted to *Ophthal. Lasers Surg. and Imaging*.

Book/Chapters in Books

J.G. Fujimoto, M. Brezinski, W. Drexler, I. Hartl, F. Kärtner, X. Li, and M. Morgner, "Optical coherence tomography," in *Ultrafast Lasers*, Eds. M.E. Fermann, A. Galvanauskas, and G. Sucha (New York: Marcel Dekker, 2003).

J.G. Fujimoto, "Optical coherence tomography," In *Encyclopedia of Optical Engineering*, Ed., R. Driggers (New York: Marcel Dekker, 2003).

J.G. Fujimoto and M.E. Brezinski, "Optical coherence tomography imaging," in *Biomedical Photonics Handbook*, Ed. T. Vo-Dinh, (Boca Raton, Florida: CRC Press, 2003).

J.S. Schuman, Z.Y. Williams, J.G. Fujimoto, and L.A. Paunescu, "Imaging in ophthalmology," in *Lasers in Ophthalmology—Basic, Diagnostic and Surgical Aspects*, Eds. F. Fankhauser and S. Kwasniewska (The Hague, The Netherlands: Kugler Publications, 2003).

J.S Schuman, C.A Puliafito, and J.G. Fujimoto, *Optical Coherence Tomography of Ocular Diseases*, 2nd edition (Thorofare, New Jersey: SLACK, Inc., 2004).

Meeting Papers

S. Bourquin, I. Hartl, A. D. Aguirre, P. Hsiung, T. H. Ko, J. G. Fujimoto, T. A. Birks, W. J. Wadsworth, U. Buenting, D. Kopf, "Portable broadband light sources using a femtosecond Nd:Glass laser and nonlinear fiber for ultrahigh resolution OCT imaging," SPIE International Biomedical Optics Symposium, BIOS'2003, San Jose, California, January 25-31, 2003, paper 4956-03.

P. Hsiung, K. Schneider, P. R. Herz, S. Bourquin, T. H. Ko, X. Li, J. G. Fujimoto, M. E. Weinstein, M. S. Hirsch, A. D'Amico, J. Richie, "Ultrahigh resolution OCT of prostate pathology in the clinic using a portable Cr:forsterite laser," SPIE International Biomedical Optics Symposium, BIOS'2003, San Jose, California, January 25-31, 2003, paper 4956-16.

P. R. Herz, S. Martin, P. Hsiung, T. H. Ko, X. Li, N. A. Patel, J. G. Fujimoto, M. E. Brezinski, "Arthroscopic optical coherence tomography for minimally invasive assessment of osteoarthritic cartilage," SPIE International Biomedical Optics Symposium, BIOS'2003, San Jose, California, January 25-31, 2003, paper 4958-16.

W. Drexler, H. Sattmann, B. Hermann, T. H. Ko, A. Unterhuber, M. Stur, C. Scholda, O. Findl, J. G. Fujimoto, and A. F. Fercher, "Evaluation of clinical feasibility of ultrahigh resolution ophthalmic optical coherence tomography," SPIE International Biomedical Optics Symposium, BIOS'2003, San Jose, California, January 25-31, 2003, paper 4951-32.

T.H. Ko, W. Drexler, L.A. Paunescu, I. Hartl, R.K. Ghanta, J.S. Schuman, and J.G. Fujimoto, "Ultrahigh resolution optical coherence tomography for enhanced visualization of retinal pathology, SPIE International Biomedical Optics Symposium, BIOS'2003, San Jose, California, January 25-31, 2003, paper 4656-12.

L.A. Paunescu, T.H. Ko, W. Drexler, H. Ishikawa, I. Hartl, R.K. Ghanta, J.G. Fujimoto, and J.S. Schuman, "Optic nerve head imaging: Comparison between ultrahigh resolution OCT, standard OCT, and HRT," SPIE International Biomedical Optics Symposium, BIOS'2003, San Jose, California, January 25-31, 2003, paper 4951-35.

J.G. Fujimoto, "Optical coherence tomography: a new method for in vivo imaging," Keystone Symposia on Molecular and Cellular Biology, Optical Imaging: Applications to Biology and Medicine, Taos, NM, February 11-16, 2003, invited talk.

J.G. Fujimoto, "Optical coherence tomography," SPIE International Symposium on Medical Imaging, San Diego, California, February 14-20, 2003, invited plenary talk.

H. Ishikawa, G. Wollstein, L.A. Paunescu, J.G. Fujimoto, and J.S. Schuman, "Evaluation of OCT 3 border detection algorithms, American Glaucoma Society Annual Meeting, San Francisco, California, March 7-9, 2003.

J.S. Schuman, T.H. Ko, J.G. Fujimoto, C. Mattox, L. Paunescu, H. Ishikawa, G.Wollstein, W. Drexler, A.M. Kowalevicz, I. Hartl, "Comparative study of glaucoma using ultrahigh resolution and standard optical coherence tomography," Association for Research in Vision and Ophthalmology, ARVO, Fort Lauderdale, Florida, May 4-9, 2003, paper 976.

W. Drexler, B. Hermann, A. Unterhuber, M. Wirtitsch, M. Stur, E. Ergun, E.M. Anger, T. Ko, P.K. Ahnelt, and J.G. Fujimoto, "Investigation of photoreceptor layer impairment in macular pathologies using ultrahigh resolution ophthalmic optical coherence tomography" Association for Research in Vision and Ophthalmology, ARVO, Fort Lauderdale, Florida, May 4-9, 2003, board B511.

M.G. Wirtitsch, E. Ergun, B. Hermann, A. Unterhuber, H. Sattmann, M. Stur, T. Ko, O. Findl, J.G. Fujimoto, and W. Drexler, "Ultrahigh resolution optical coherence tomography in macular dystrophy," Association for Research in Vision and Ophthalmology, ARVO, Fort Lauderdale, Florida, May 4-9, 2003, board B513.

L.A. Paunescu, L.L. Price, P.C. Stark, S. Beaton, H. Ishikawa, G. Wollstein, J.G. Fujimoto, and J.S. Schuman, "OCT 3 measurement reproducibility of nerve fiber layer thickness, macula thickness map and optic nerve head analysis on normal subjects," Association for Research in Vision and Ophthalmology, ARVO, Fort Lauderdale, Florida, May 4-9, 2003, board B12.

T.H. Ko, J.S. Schuman, J.G. Fujimoto, L.A. Paunescu, A.M. Kowalevicz, I. Hartl, W. Drexler, J. Duker, G. Wollstein, and H. Ishikawa, "Comparison of ultrahigh resolution and standard optical coherence tomography for imaging retinal pathologies," Association for Research in Vision and Ophthalmology, ARVO, Fort Lauderdale, Florida, May 4-9, 2003, paper 3277.

H. Ishikawa, R. Hariprasad, G. Wollstein, L.A. Paunescu, L.L. Price, P.C. Stark, J.G. Fujimoto, and J.S. Schuman, "New quality assessment parameters for OCT 3," Association for Research in Vision and Ophthalmology, ARVO, Fort Lauderdale, Florida, May 4-9, 2003, board B61.

G. Wollstein, J.S. Schuman, L.L. Price, A. Aydin, L.A. Paunescu, P.C. Stark, J.G. Fujimoto, and H. Ishikawa, "Relationship between optical coherence tomography (OCT) macular and peripapillary measurements and automated visual fields," Association for Research in Vision and Ophthalmology, ARVO, Fort Lauderdale, Florida, May 4-9, 2003, board B72.

C.D. Scholda, M. Wirtitsch, B. Hermann, A. Unterhuber, H. Sattmann, M. Stur, T. Ko, O. Findl, J.G. Fujimoto, and W. Drexler, "Macular hole imaging using ultrahigh resolution optical coherence tomography," Association for Research in Vision and Ophthalmology, ARVO, Fort Lauderdale, Florida, May 4-9, 2003, board B339.

S. Beaton, H. Ishikawa, G. Wollstein, L.A. Paunescu, J.G. Fujimoto, and J.S. Schuman, "Alternate color scheme for OCT images: A pilot study," Association for Research in Vision and Ophthalmology, ARVO, Fort Lauderdale, Florida, May 4-9, 2003, board B94.

A.J. Correnti, H. Ishikawa, G. Wollstein, L.A. Paunescu, L.L. Price, P.C. Stark, J.G. Fujimoto, and J.S. Schuman, "Evaluation of two OCT 3 border detection algorithms," Association for Research in Vision and Ophthalmology, ARVO, Fort Lauderdale, Florida, May 4-9, 2003, board B97.

E. Ergun, M. Wirtitsch, B.Hermann, A. Unterhuber, H. Sattmann, M. Stur, C. Scholda, J. Fujimoto, A. Fercher, and W. Drexler, "Ultrahigh resolution optical coherence tomography in Stargardt's disease," Association for Research in Vision and Ophthalmology, ARVO, Fort Lauderdale, Florida, May 4-9, 2003, board B767.

J.G. Fujimoto, T.H. Ko, J.S. Schuman, J. Duker, L.A. Paunescu, A.M. Kowalevicz, I. Hartl, W. Drexler, H. Ishikawa, and G. Wollstein, "Comparative study of macular holes using ultrahigh resolution and standard optical coherence tomography," Association for Research in Vision and Ophthalmology, ARVO, Fort Lauderdale, Florida, May 4-9, 2003, board B520.

S. Bourquin, P. Hsiung, I. Hartl, A. Aguirre, T.H. Ko, J.G. Fujimoto, T.A. Birks, W.J. Wadsworth, U. Buenting, and D. Kopf, "Compact ultrahigh resolution OCT system for real-time in vivo imaging," Conference on Lasers and Electro-Optics, CLEO, June 1-6, 2003, Baltimore, Maryland, paper CMU1.

P.R. Herz, P. Hsiung, S. Bourquin, T.H. Ko, K. Schneider, H. Ishikawa, and J.G. Fujimoto, "Micro-motor endoscope with adjustable focus for ultrahigh resolution OCT," Conference on Lasers and Electro-Optics, CLEO, June 1-6, 2003, Baltimore, Maryland, paper CMU2.

S.B. Adams, Jr., M.J. Roberts, N.A. Patel, S. Plummer, J. Rogowska, D.L. Stamper, J.G. Fujimoto, and M.E. Brezinski, "The use of polarization sensitive optical coherence tomography and elastography to assess connective tissue," Conference on Lasers and Electro-Optics, CLEO, June 1-6, 2003, Baltimore, Maryland, paper CTuM48.

A.D. Aguirre, P. Hsiung, T.H. Ko, S. Bourquin, K. Schneider, I. Hartl, and J.G. Fujimoto, "Alternate scanning modalities for high resolution optical coherence tomography," Conference on Lasers and Electro-Optics, CLEO, June 1-6, 2003, Baltimore, Maryland, paper CTuM49.

P. Hsiung, A.D. Aguirre, T.H. Ko, S. Bourquin, K. Schneider, I. Hartl, and J.G. Fujimoto, “Transverse priority scanning and microscopy for high resolution optical coherence tomography,” European Conference on Biomedical Optics, Munich, Germany, June 22-25, 2003, 5140-20.

T.H. Ko, A.M. Kowalevicz, Jr., A. Paunescu, J.S. Schuman, W. Drexler, I. Hartl, F. Kaertner, and J.G. Fujjimoto, “Ultrahigh resolution OCT imaging of retinal pathology in the ophthalmology clinic,” European Conference on Biomedical Optics, Munich, Germany, June 22-25, 2003, 5140-26.

B. Hermann, A. Unterhuber, H. Sattmann, M. Stur, M. Wirtisch, M. Glosman, C. Schubert, C. Scholda, O. Findl, T.H. Ko, P. Ahnelt, and J. Fujimoto, “Investigation of photoreceptor layer impairment in macular pathologies, European Conference on Biomedical Optics, Munich, Germany, June 22-25, 2003, 5140-27.

P.R. Herz, S. Adams, Jr., J. Roberts, S. Bourquin, P. Hsiung, T. Ko, N. Patel, D. Stamper, S. Martin, K. Schneider, J.G. Fujimoto, and M. Brezinski, “Imaging of cartilage degeneration progression in vivo,” European Conference on Biomedical Optics, Munich, Germany, June 22-25, 2003, 5140-30.

S. Bourquin, A.D. Aguirre, I. Hartl, P. Hsiung, T.H. Ko, and J.G. Fujimoto, “Real-time ultrahigh resolution OCT systems for in vivo imaging,” European Conference on Biomedical Optics, Munich, Germany, June 22-25, 2003, 5140-31.

T. H. Ko, A. Paunescu, I. Hartl, A. Kowalevicz, J. Duker, J. Schuman, W. Drexler, A. Rogers, C. Baumal, E. Reichel, L.P. Aiello, S. Bursell, J. Fujimoto, “Comparing ultrahigh resolution optical coherence tomography and StratusOCT imaging of retinal pathologies,” SPIE International Biomedical Optics Symposium, BIOS’2004, San Jose, California, January 24-29, 2004, paper 5314-22.

W. Drexler, B. Hermann, A. Unterhuber, H. Sattmann, T.H. Ko, M. Wirtitsch, M. Stur, C. Scholda, E. Ergun, E. Anger, P. Ahnelt, J.G. Fujimoto, and A.F. Fercher, “Quantification of photoreceptor layer thickness in different macular pathologies using ultrahigh resolution optical coherence tomography,” SPIE International Biomedical Optics Symposium, BIOS’2004, San Jose, California, January 24-29, 2004, paper 5314-27.

T.H. Ko, A. Paunescu, A. Kowalevicz, I. Hartl, J. Schuman, J. Duker, W. Drexler, L.P. Aiello, S. Bursell, J. Fujimoto, “Ultrahigh resolution optical coherence tomography for imaging retinal pathology,” SPIE International Biomedical Optics Symposium, BIOS’2004, San Jose, California, January 24-29, 2004, paper 5316-02.

J.G. Fujimoto, Y. Chen, D. Adler, A. Aguirre, P. Herz, P. Hsiung, T. Ko, and M. Wojtkowski, “Ultrahigh resolution imaging using optical coherence tomography,” OSA Biomedical Optics Topical Meetings, Miami Beach, Florida, April 14-17, 2004, paper FD1.

B.K. Courtney, A.L. Robertson, Jr., F.P. Chan, Y. Honda, P.G. Yock, P.J. Fitzgerald, P.R. Herz, T.H. Ko, J.G. Fujimoto, D.L. Stamper, S.B. Adams, M.J. Roberts, and M.E. Brezinski, “Attentuation measurements of optical coherence tomographic signals for the assessment of vascular tissue composition,” OSA Biomedical Optics Topical Meetings, Miami Beach, Florida, April 14-17, 2004, paper FD3.

D.C. Adler, T.H. Ko, J.G. Fujimoto, D. Mamedov, V. Prokhorov, V. Shidlovski, and S. Yakubovich, “Ultrahigh resolution optical coherence tomography using broadband superluminescent diodes,” OSA Biomedical Optics Topical Meetings, Miami Beach, Florida, April 14-17, 2004, paper SE2.

Y. Chen, P.R. Herz, P. Hsiung, K. Schneider, J.G. Fujimoto, K. Madden, J. Schmitt, A. Koski, J. Goodnow, and C. Petersen, “Endoscopic imaging in rabit gastrointestinal tract with high resolution optical coherence tomography,” OSA Biomedical Optics Topical Meetings, Miami Beach, Florida, April 14-17, 2004, paper SE4.

P. Hsiung, Y. Chen, N. Nishizawa, P.R. Herz, T.H. Ko, J.G. Fujimoto, C.J.S. de Matos, S.V. Popov, J.R. Taylor, J. Broeng, V.P. Gapontsev, “All-fiber, continuous wave, Raman continuum sources for optical

coherence tomography," OSA Biomedical Optics Topical Meetings, Miami Beach, Florida, April 14-17, 2004, paper SE7.

T.H. Ko, A.M. Kowalevicz, M.S. Wojtkowski, D. Adler, J.S. Duker, J.S. Schuman, W. Drexler, V. Shidlovski, S. Yakubovich, and J.G. Fujimoto, "Advances in ultrahigh resolution optical coherence tomography imaging of retinal pathology," 2nd Annual International Society for Imaging in the Eye Meeting, ISIE, Ft. Lauderdale, Florida, April 23-24, 2004, poster B647.
M. Wojtkowski, V.J. Srinivasan, T.H. Ko, J.S. Duker, J.S. Schuman, and A. Kowalczyk, "Video rate ultrahigh resolution optical coherence tomography for retinal imaging," 2nd Annual International Society for Imaging in the Eye Meeting, ISIE, Ft. Lauderdale, Florida, April 23-24, 2004.

A. Chan, J.S. Duker, and J.G. Fujimoto, "Stage Zero Macular Holes: Observations by Optical Coherence Tomography," Association for Research in Vision and Ophthalmology, ARVO, Fort Lauderdale, Florida, April 25-29, 2004, poster 1967/B778.

B. Hermann, A. Unterhuber, M. Wirtitsch, M. Stur, E. Ergun, C. Scholda, T. Ko, J.S. Schuman, J.G. Fujimoto, and W. Drexler, "Quantification Of Photoreceptor Layer Thickness Using Ultrahigh Resolution Optical Coherence Tomography, Association for Research in Vision and Ophthalmology, ARVO, Fort Lauderdale, Florida, April 25-29, 2004, poster 2373/B8.

J.G. Fujimoto, T.H. Ko, D.C. Adler, D. Mamedov, V. Prokhorov, V. Shidlovski, S .Yakubovich, M.D. Wojtkowski, J.S. Duker, and J.S. Schuman, "New Technology for Ultrahigh Resolution Optical Coherence Tomography Imaging Using Diode Light Sources," Association for Research in Vision and Ophthalmology, ARVO, Fort Lauderdale, Florida, April 25-29, 2004, poster 3002/B637.

M. Wojtkowski, T.H. Ko, J.G. Fujimoto, T. Bajraszewski, I. Gorczynska, P. Targowski, A. Kowalczyk, J.S. Schuman, and J.S. Duker, "Ultrahigh Speed, Ultrahigh Resolution Optical Coherence Tomography Using Spectral Domain Detection," Association for Research in Vision and Ophthalmology, ARVO, Fort Lauderdale, Florida, April 25-29, 2004, poster 3009/B644.

T.H. Ko, J.G. Fujimoto, J.S. Duker, L.A. Paunescu, A. Chan, W. Drexler, A.H. Rogers, C.R. Baumal, E. Reichel, and J.S. Schuman, "Ultrahigh Resolution Optical Coherence Tomography Imaging of Architectural Morphology in Retinal Diseases," Association for Research in Vision and Ophthalmology, ARVO, Fort Lauderdale, Florida, April 25-29, 2004, poster 3012/B647.

H. Ishikawa, G. Wollstein, M. Aoyama, D. Stein, S. Beaton, J.G. Fujimoto, and J.S. Schuman, "Stratus OCT Image Quality Assessment," Association for Research in Vision and Ophthalmology, ARVO, Fort Lauderdale, Florida, April 25-29, 2004, poster 3317/B952.

G. Wollstein, H. Ishikawa, S. Beaton, D.M. Stein, M. Aoyama, J.G. Fujimoto, and J.S. Schuman, "Pointwise relationship between OCT nerve fiber layer thickness and visual field threshold level," Association for Research in Vision and Ophthalmology, ARVO, Fort Lauderdale, Florida, April 25-29, 2004, poster 3329/B964.

C. De Matos, S.V. Popov, J.R. Taylor, P. Hsiung, Y. Chen, N. Nishizawa, P.R. Herz, T.H. Ko, J.G. Fujimoto, J. Broeng, and V. P. Gapontsev, "Continuous wave, all-fibre broad-band sources for optical coherence tomography," Conference on Lasers and Electro-Optics, CLEO, San Francisco, California, May 16-21, 2004, paper CWJ1.

W. Piyawattanametha, L. Fan, S. Hsu, M. Fujino, M.C. Wu, P.R. Herz, A.D. Aguirre, Y. Chen, and J.G. Fujimoto, "Two-dimensional endoscopic MEMS scanner for high resolution optical coherence tomography," Conference on Lasers and Electro-Optics, CLEO, San Francisco, California, May 16-21, 2004, paper CWS2.

P.R. Herz, Y. Chen, K. Schneider, P. Hsiung, J.G. Fujimoto, K.A. Madden, J.M. Schmitt, A. Koski, J. Goodnow, and C.L. Petersen, "Ultrahigh resolution optical coherence tomography for in vivo endoscopic

imaging of the rabbit," Conference on Lasers and Electro-Optics, CLEO, San Francisco, California, May 16-21, 2004, paper CWS3.

T.-M. Liu, S.-W. Chu, S.-P. Tai, C.-K. Sun, F.X. Kärtner, and J.G. Fujimoto, "Compact self-started femtosecond Cr:forsterite laser for non-linear optical microscopy," Conference on Lasers and Electro-Optics, CLEO, San Francisco, California, May 16-21, 2004, paper CThFF4.